NASA TECHNICAL REPORT

NASA TR R-286

NASA TR R-286

TEST SECTIONS FOR SMALL THEORETICAL WIND-TUNNEL-BOUNDARY INTERFERENCE ON V/STOL MODELS

by Ray H. Wright

Langley Research Center

Langley Station, Hampton, Va.

NATIONAL AERONAUTICS AND SPACE ADMINISTRATION • WASHINGTON, D. C. • AUGUST 1968

NASA TR R-286

TEST SECTIONS FOR SMALL THEORETICAL WIND-TUNNEL-BOUNDARY INTERFERENCE ON V/STOL MODELS

By Ray H. Wright

Langley Research Center
Langley Station, Hampton, Va.

NATIONAL AERONAUTICS AND SPACE ADMINISTRATION

For sale by the Clearinghouse for Federal Scientific and Technical Information
Springfield, Virginia 22151 – CFSTI price $3.00

TEST SECTIONS FOR SMALL THEORETICAL WIND-TUNNEL-BOUNDARY INTERFERENCE ON V/STOL MODELS

By Ray H. Wright
Langley Research Center

SUMMARY

A wind-tunnel test section with closed upper wall, slotted side walls, and open lower boundary was found theoretically to produce zero tunnel-boundary lift interference on a small wing with horizontal wake mounted at the center of the test section. For this test section the variation of the interference with angle of the vortex wake behind a high-lift-coefficient model was not large. Because of the small slot widths required for zero interference and of the effects of boundary layer, the theory is regarded as unreliable for predicting the slot widths required; however, the variation of the interference with the slot width for widths somewhat greater than those needed for zero interference was found to be small. The interference in the region likely to be occupied by the tail of a model was investigated in some detail and was found to change with slot width and with wake angle more strongly than did the interference at the lifting element. A limited investigation of the lift interference in a test section with closed upper wall and slotted side and lower boundaries was made to obtain the theoretically indicated slot width required for zero lift interference at a center-mounted wing with the wake horizontal.

INTRODUCTION

Wind-tunnel test-section configurations designed to minimize the boundary interference on the flow over test models have been in use for many years. (See, for example, ref. 1.) For high-speed models the interference of greatest concern is that due to solid blockage, because this type of interference increases strongly as the test Mach number increases toward unity. On the other hand, for testing models of high-lift-coefficient vehicles, such as vertical-take-off and vertical-landing craft (VTOL) and short-take-off-distance and short-landing-distance craft (STOL), which generally operate at relatively low Mach numbers, the lift interference is of first importance. With these high-lift-coefficient models the problem is complicated by the fact that the wake associated with the lift may vary from approximately line vortices extending almost horizontally downstream from the model to a jet extending vertically below, or even upstream from, the

model. The wind-tunnel-boundary interference associated with idealizations of helicopter wakes in the presence of several configurations of open and of closed vertical and horizontal boundaries has been treated in references 2 and 3.

Some insight into the lift interference with high-lift-coefficient test models can be obtained by examining the calculated interference correction factors for helicopter rotors presented in reference 3. For most test-section configurations, the interference varies widely, depending on the angle made by the wake of vorticity with the vertical. However, as may be seen from figures 18 to 21 of reference 3, if only an open lower boundary is present, this variation (with the model some distance from the open boundary) is small. The calculated interference due to lift is greatest for the wake extending vertically below the rotor; however, it is believed that for this vertical wake, the calculations of reference 3 are unreliable, because the wake, which for this condition is in the form of a jet, might be expected to break through the open boundary of the stream rather than to follow along its edge as assumed. In a wind tunnel with boundaries not completely open, as the jet approaches the vertical and the tunnel stream velocity approaches zero, the interference velocity at the rotor must be an upwash (for positive lift) because any solid boundary restricts the flow. The open-lower-boundary condition can be approximated with a many-slotted bottom wall, and the multiple-slotted bottom wall might be preferable to the completely open lower boundary in order to stabilize the flow.

The purpose of the present investigation is to extend the small-disturbance theory of wind-tunnel lift interference on high-lift-coefficient models, such as reported in references 2 and 3, to some test-section configurations that might be expected to minimize the theoretical lift interference for the general class of high-lift-coefficient models over their operating ranges. The configurations investigated are of the mixed (open and closed) boundary type. First to be treated is a test section with top and side walls closed and lower boundary open. The model, assumed to be mounted on the vertical center line of the test section, is represented by a vortex doublet trailing horizontally downstream. A vortex doublet is the limit as two rectilinear parallel line vortices of equal-magnitude but opposite-sense circulation approach each other, the product of circulation with their distance apart remaining constant. This product is called the strength of the doublet. Representation of the wing by a trailing-vortex doublet omits the bound part of the vortex system, but the interference at the lifting element is not affected by this omission. The results are therefore valid for a small, lightly loaded wing. Calculations of the interference are made for rectangular test sections having height-width ratios of 1 and 1.5.

The second configuration treated is like the first except that the side walls are slotted with four equispaced slots. Added flexibility is thereby available for obtaining desirable interference characteristics.

In order to remove the limitation of small lift loading, this second test-section configuration with height-width ratio of 1.5 and slot width corresponding to small downwash interference at the model is investigated with a helicopter rotor mounted at the center. As in references 2 and 3, the rotor wake is represented by a source-sink doublet distribution. This representation again implies the small-model assumption. Even with a small model, the small-disturbance assumption is violated over part of the open lower boundary, because the now-no-longer-horizontal wake approaches and even penetrates that boundary. The validity of the theory may be expected to be degraded progressively with expansion of the region of the boundary over which the small-disturbance assumption is seriously violated. The small-model assumption therefore takes on added importance. On the other hand, provided the small-model assumption is satisfied, the lift-interference theory for the helicopter applies also for other high-lift-coefficient models, and for a horizontal wake it is exactly equivalent to the interference theory for a small, lightly loaded wing. Moreover, if the wake is deflected slightly below the horizontal, it intersects the open lower boundary so far from the model that the violation of the assumed boundary conditions near the intersection region can have little effect on the interference in the vicinity of the model. The helicopter interference theory should therefore be valid for calculating the lift interference on general small high-lift-coefficient models with wake deflected not too much from the horizontal. The wake deflection can be measured as part of the tests or it may be estimated from the lift, the area and geometry of the rotor or lifting surface, and the tunnel stream velocity. (For a short discussion of this problem, see ref. 4.) Unfortunately, although a separate solution is obtained for an exactly horizontal wake, the general solution of the helicopter rotor interference with deflected wake involves nonuniformly convergent integrals; thus, in the calculations the convergence problem becomes increasingly severe as the wake approaches the horizontal.

As an effort toward completeness and toward provision of some theoretical results for comparison with experiment, several other test-section configurations are considered for which the theoretical lift interference on wings (small deflection of the wake) may be reduced to zero. These configurations include the interference of the model for small wings centered over solid lower boundaries with top and side boundaries open and height-width ratios of 0.5, 0.66, 1.0, and 1.5. The possibility of reducing to zero the lift interference of small wings by means of slots in all four walls is also mentioned and appropriate references are given. Finally, the lift interference is calculated for a lightly loaded center-mounted wing spanning 0.58 of the width of a test section of height-width ratio 1.432, with closed top and with sides and bottom slotted with four equispaced slots each. The wing is represented by line vortices trailing downstream from the tips. The calculations are made for a range of slot widths including that width for which the interference of the model is theoretically zero.

Of these several theoretical developments only that for the helicopter rotor is applicable for calculating the interference at the tail. Several studies are therefore made in order to understand the various contributions to the upwash interference at the tail and to obtain a qualitative estimation of that interference for the test section with solid top and slotted sides and bottom. These studies include consideration of the tail interference corresponding to the trailing vortices, investigation of the effect of below-center position of the trailing vortices in the closed-top slotted-side-wall and slotted-bottom configuration, and qualitative consideration of the tail interference of solid top and open bottom and of slotted side walls in the presence of the bound vortex. Finally, the helicopter theory is adapted to calculate first, the effects of infinite parallel slotted side walls and second, the effects of the closed top, open bottom, and slotted side-wall configuration on the upwash interference downstream from the model. For the first of these the calculations are made for walls slotted to produce zero interference of the lifting element. For the second the calculations are made for two configurations of slotted walls, one for zero interference at the lifting element and the other corresponding to a small downwash interference.

In addition to the restrictions imposed by small-model and small-disturbance assumptions, unavoidable uncertainties in boundary conditions limit the applicability of the theoretical treatment such as the possibility, with very high lift, of separation from the upper wall. Because of such uncertainties, experiments are required to check the theory and to determine the desirable slot widths. The theory should nevertheless furnish useful guidance for experimental investigations directed toward developing test sections to reduce the tunnel-boundary interference on high-lift-coefficient models. Since accurate corrections for the interference do not seem likely, such mixed-boundary test sections are believed to hold little promise for increasing the model size that can be satisfactorily tested in a test section of given cross section. (For some discussion of the model-size problem, see refs. 4 to 7.) The more likely benefits are the elimination of all corrections with properly small models and possibly an improvement in the uniformity of the effective test flow in the region of the models.

SYMBOLS

Symbols pertinent to text and figures are given in this list. Appendixes A to D have separate symbol lists.

A	area of helicopter rotor disk
$\overline{A}$	vector area of rotor disk
b	width of test section

C	cross-sectional area of test section
C_L	lift coefficient of test model, positive for upward lift
g	distance from model position to lower boundary of test section
h	height of test section
l	restriction constant (defined by eq. (B2))
P	field point
r_0	ratio of slot width to distance between centers of panels of a slotted wall
$\bar{r}$	vector distance from element of surface enclosed by vortex ring
S	model area on which C_L is based
s	distance from rotor disk to vortex ring
u	streamwise interference velocity, positive in tunnel stream direction
V	tunnel stream velocity
v	upwash interference velocity, positive upward
w_0	velocity at rotor disk induced by the lifting rotor (taken positive for positive lift)
X,Y,Z	rectangular Cartesian coordinate axes
x,y,z	rectangular Cartesian coordinates
α	angle of attack of helicopter rotor-tip-path plane
Γ	circulation, positive for positive lift
δ_w	upwash interference factor for wings
$\delta_{R,x}$	streamwise interference factor for helicopter rotor
$\delta_{R,z}$	upwash interference factor for helicopter rotor
θ	polar angle

μ strength of vortex doublet

ρ density of test medium

χ angle between axis of helicopter rotor disk and axis of cylindrical vortex sheet extending from rotor, designated skew angle (positive counterclockwise)

TEST SECTIONS

Top and Side Walls Closed; Lower Boundary Open; Horizontal Trailing Vortex Doublet

The boundary conditions for closed top and side walls and open lower boundary are simply satisfied by means of images as in reference 8. Figure 1 indicates the required arrangement of line doublets extending downstream from the position of the test model. The original lifting doublet at the position of the model is included in the figure. In figure 1, b is the width of the test section, h is its height, and g is the distance of the model from the open lower boundary. The model is located on the vertical center line of the tunnel. An equation for calculation of the boundary-induced upwash velocity v at the position of the model is developed in appendix A. In this and other equations developed in this investigation, no account has been taken of compressibility effects because in tests of V/STOL models, the speed of the test stream is normally so small that such effects would be negligible.

It is convenient to express the interference in terms of the interference upwash factor δ_w, where δ_w is related to the upwash interference velocity v by

$$\tan \Delta\alpha = \frac{v}{V} = \frac{C_L S}{C} \delta_w \tag{1}$$

where

v upwash velocity, positive upward

V tunnel stream velocity

C cross-sectional area of test section

C_L lift coefficient of model, positive for upward lift

S area on which C_L is based

$\Delta\alpha$ effective change of angle of attack due to upwash velocity

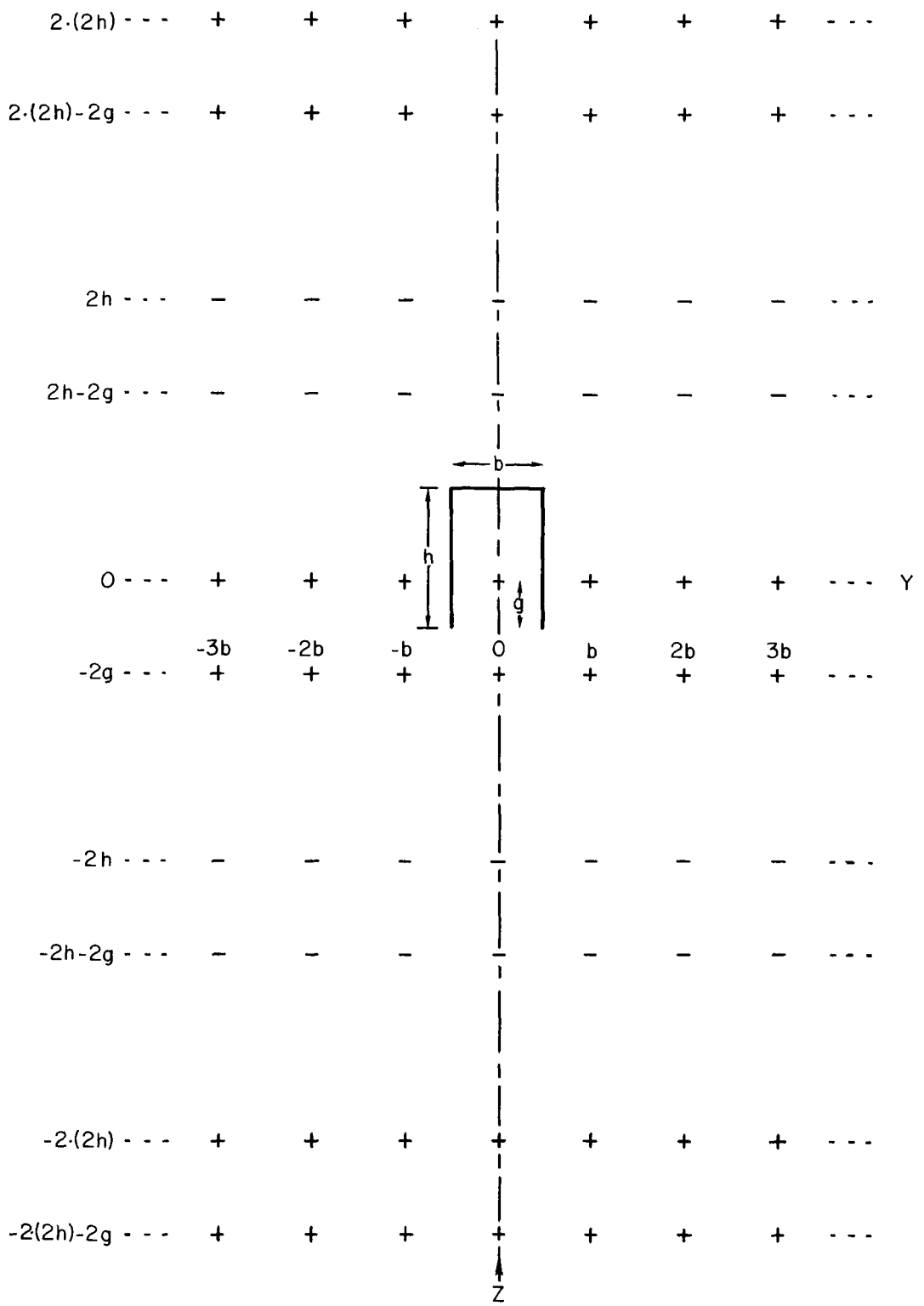

Figure 1.- Arrangement of vortex doublets satisfying boundary conditions for tunnel closed at top and on sides and open on bottom. +, doublet with upward lift; -, doublet with downward lift.

In order to express δ_w in terms of the doublet strength μ instead of in terms of C_L, note that

$$VC_LS = 2\mu$$

and

$$C = hb$$

so that equation (1) gives

$$\delta_w = \frac{hb}{2\mu} v \tag{2}$$

Use of equation (A14) in equation (2) shows that the interference upwash factor δ_w is a function of the test-section height-width ratio h/b and of the ratio of model height above the lower boundary to the tunnel width g/b.

The interference upwash factor δ_w has been computed by use of equations (2) and (A14) for the square test section $\frac{h}{b} = 1$ and for a rectangular test section with $\frac{h}{b} = 1.5$ with several values of g/b. The computed values of δ_w are shown plotted against g/b in figure 2.

Figure 2 shows that with the model near the center of the tunnel, the interference δ_w is approximately the same as that in the closed tunnel, that is, $\delta_w = 0.137$ for the square test section. On the other hand, if both top and bottom boundaries had been open,

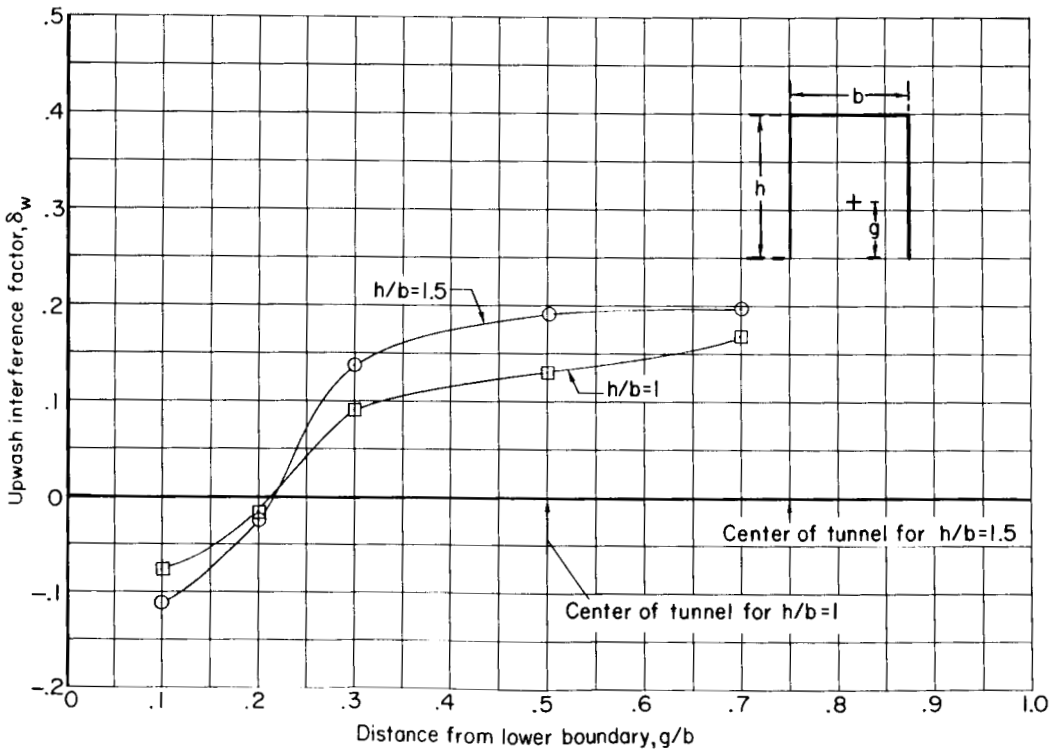

Figure 2.- Interference upwash factor δ_w for vortex doublet in wind tunnel with top and side walls closed and bottom open. Vortex doublet on vertical center line; wake horizontal.

the interference would have been $\delta_w \approx -0.137$ for the square test section, as can be seen from figure 8(a) of reference 9. This effect of opening the top as well as the bottom is due to the fact that with this configuration, the whole tunnel stream is deflected downward. This behavior shows the importance of preventing separation from the upper wall, since the interference factor might then approach the open-tunnel value.

Figure 2 shows that in order to obtain zero interference in a test section with closed top and side walls and open lower boundary, the model must be placed relatively close to the open boundary in a region where the interference varies strongly with model position. In addition, it is to be expected that the interference varies strongly in the region surrounding a model placed in this position. This situation is unsatisfactory. Since the interference at the center is an upwash and since experience indicates that slots produce an interference effect of the opposite sign, slotted side walls to reduce the interference to zero for the model mounted at the center of the test section are suggested.

Top Wall Closed; Side Walls Slotted; Lower Boundary Open; Horizontal Trailing Vortex Doublet

A lifting model of small span mounted on the vertical center line of the rectangular test section is again replaced for the purpose of calculating the boundary-induced interference by a vortex doublet trailing horizontally downstream. The top is again solid and the bottom open, but the side walls are slotted with four equispaced slots so arranged that the center of a (solid) panel intersects the horizontal center line and a half-panel adjoins each corner. (See sketches in figs. 3 and 4.) The top and bottom boundary conditions are again satisfied by images arranged above and below the model as in figure 1, but the side-wall-slotted boundary condition cannot be satisfied by the b-interval repetition of vortex images of the same sign, which was effective for satisfying the solid-boundary condition. Instead, the variable in the vertical direction is eliminated by taking the exponential integral

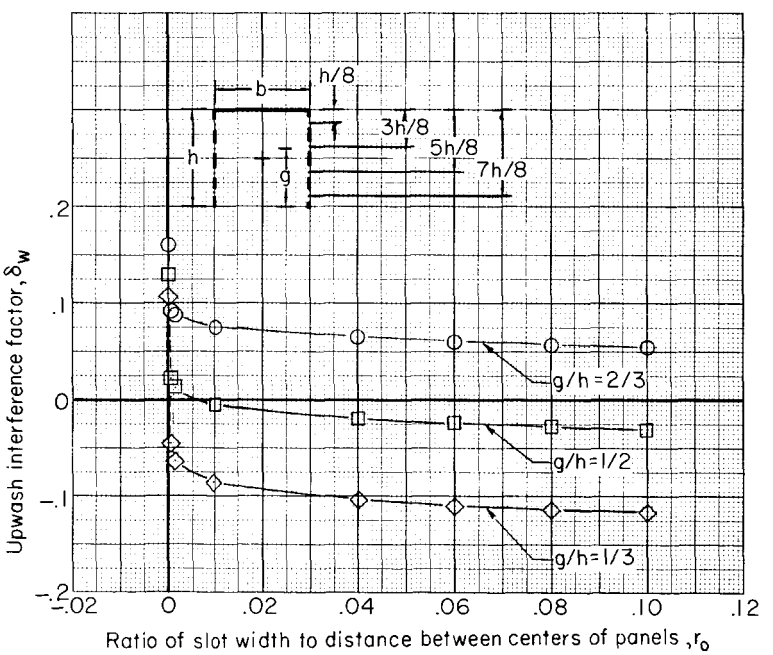

Figure 3.- Upwash interference factor δ_w for vortex doublet in wind tunnel with top wall closed, bottom wall open, and side walls slotted, each with four equispaced slots. Vortex doublet on vertical center line; h/b = 1; wake horizontal.

Fourier transform of the original disturbance potential, of the governing Laplace equation, and of the average (homogeneous) boundary condition. Solution of the transformed system and inversion of the solution give the potential function for the doublet in the presence of the slotted walls. The total interference potential is obtained by summation, and from this potential, the upwash interference factor δ_w is derived. The complete development is given in appendix B.

The upwash interference factor δ_w at the position of the lifting model has been computed from equation (B15) for the square test section and for a rectangular test section with $\frac{h}{b} = 1.5$ for three heights g/h of the model above the lower boundary and is shown in figures 3 and 4 as a function of the ratio of open to closed area of the slotted sides r_0. The slotted side walls are seen to be effective in reducing the upwash interference to zero for a model located near the center of the test section; that is, for $\frac{g}{h} = \frac{1}{2}$. Moreover, in the range of r_0 values corresponding to $\delta_w = 0$, the interference for the centered model is seen to be relatively insensitive to slot width. These characteristics for the small model with vortex wake trailing horizontally downstream are regarded as favorable. Next to be investigated is the behavior in this test section of a high-lift model, a helicopter rotor, for which the vortex wake may not trail approximately horizontally downstream.

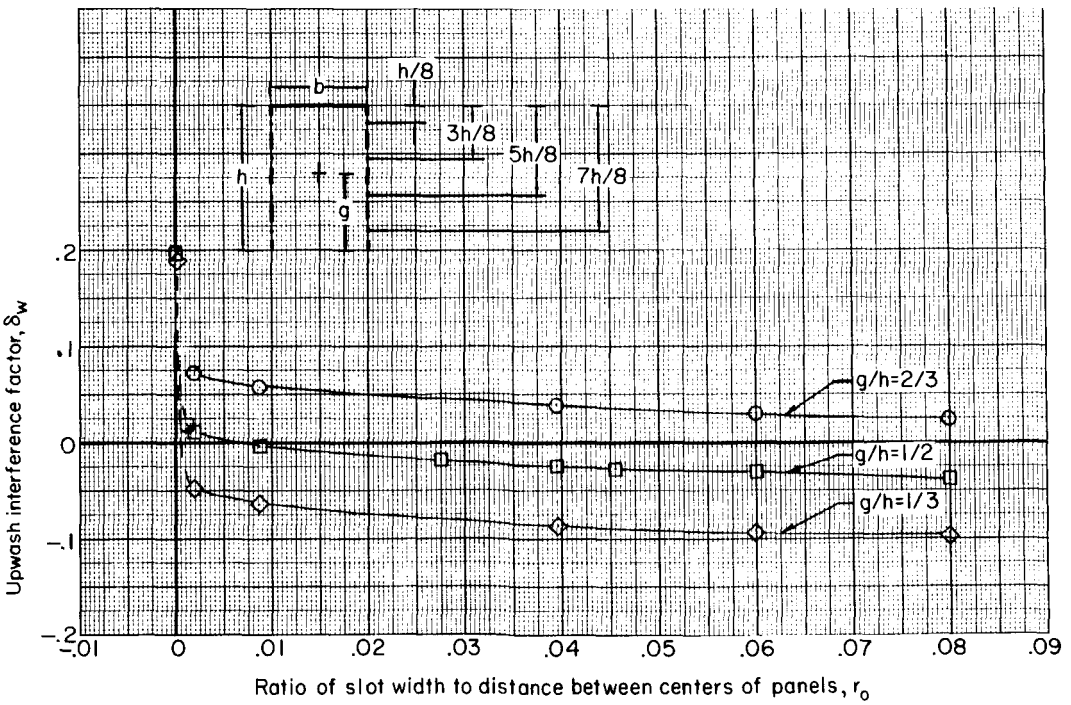

Figure 4.- Upwash interference factor δ_w for vortex doublet in wind tunnel with top wall closed, bottom wall open, and side walls slotted, each with four equispaced slots. Vortex doublet on vertical center line; $h/b = 1.5$; wake horizontal.

Top Wall Closed; Side Walls Slotted; Lower Boundary Open; Helicopter at Center of Test Section

The helicopter rotor is assumed to be mounted at the center of the test section and as in references 2, 10, and 11, its disturbance is represented by a straight elliptic cylindrical vortex sheet extending from the rotor. The rotor disk makes an angle of attack α with the oncoming wind-tunnel stream velocity V as indicated in figure 5, and the vortex cylinder is swept downstream by the skew angle χ; thus, the axis of the vortex cylinder makes an angle $\chi - \alpha$ with the downward-drawn vertical. Note that χ is here measured from the downward-drawn normal to the rotor disk rather than from the negative Z-axis as in references 2 and 3. As in the preceding treatment of the wing, the model is assumed to be small. This assumption permits the simplification of replacing the vortex cylinder by a source-sink doublet line. The calculations of reference 3 show that as the vortex wake is swept back toward the horizontal, that is, $\chi - \alpha = 90^{\circ}$, the boundary-induced upwash with the helicopter rotor approaches that for the wing producing the same lift. It is therefore unnecessary to investigate the interference on the helicopter rotor for values of $\chi - \alpha$ approaching 90°. This investigation is therefore mainly confined to values of the angle for which the vortex wake intersects the lower boundary within the test section. The vortex wake, which now resembles a jet, is assumed to break through

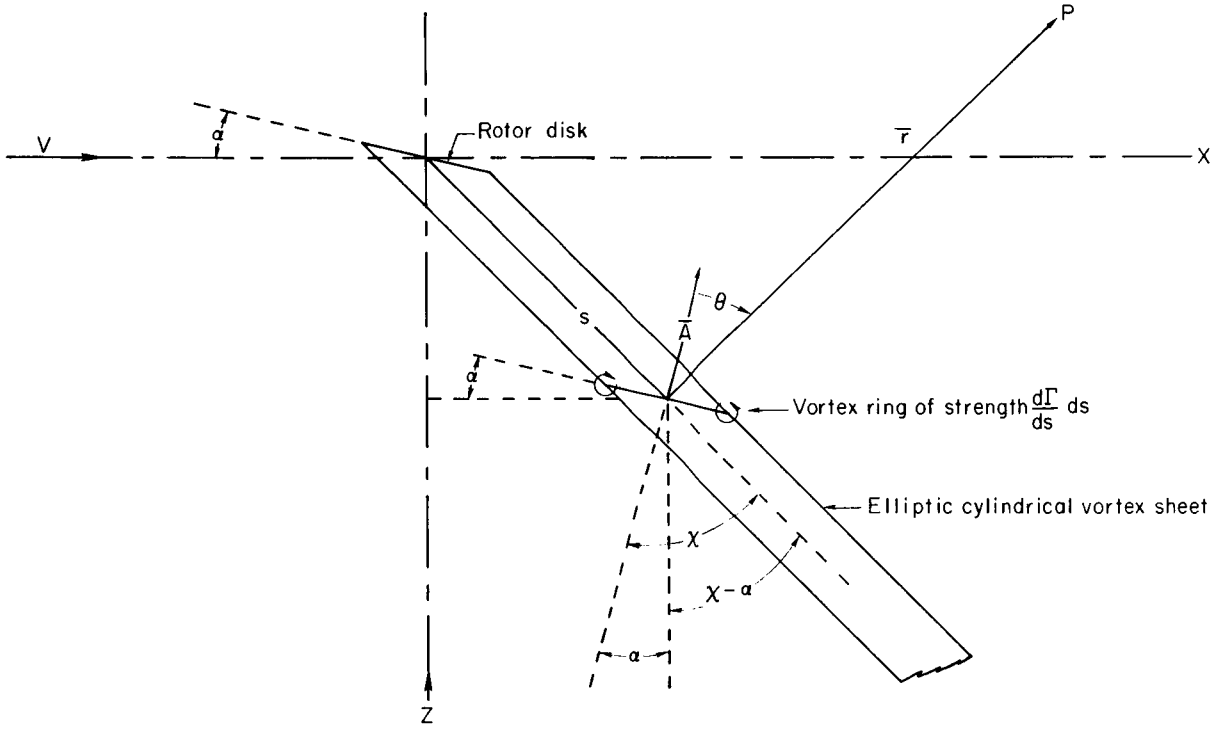

Figure 5.- Elliptic cylindrical vortex sheet representing disturbance due to helicopter rotor. Vector area of vortex ring is taken equal to vector area $\bar{A}$ of rotor disk.

the lower (open) boundary and to have no further influence on the flow about the test model. This assumption seems reasonable if the dimensions of the open space surrounding the test section are large in comparison with the diameter of the rotor. It is not, of course, correct if the wake intersects the closed wall of the diffuser, but the equations herein derived should, even in this case, give a reasonable approximation to the boundary-induced interference provided the diffuser entrance is sufficiently far downstream, as it should be, to exert small influence on the flow about the test model.

The boundary conditions assumed are essentially those of the preceding section, namely zero velocity normal to a solid wall and zero pressure increment at an open boundary. Even for a wing the boundary condition at an open boundary is uncertain, largely because the position of the boundary is unknown. For a helicopter with wake approaching the open lower boundary, it is obviously far less certain, and with the tunnel stream velocity V approaching zero (and $\chi \to 0$), the assumed boundary condition at the open lower boundary becomes completely invalid. The lift-interference theory for the helicopter is therefore generally less reliable than that for the small, lightly loaded wing. Nevertheless, it should furnish useful indications, even for the $\chi \to 0$ condition, provided the helicopter rotor is not too close to the open lower boundary.

Equations for computing the interference factors $\delta_{R,x}$ and $\delta_{R,z}$ for the helicopter rotor in the test section with closed top, slotted side walls, and open lower boundary are derived in appendix C. Here

$$\delta_{R,x} = \frac{u}{w_0}\frac{C}{A} \tag{3}$$

and

$$\delta_{R,z} = \frac{v}{w_0}\frac{C}{A} \tag{4}$$

where

u boundary-induced interference velocity in tunnel stream direction

v boundary-induced interference velocity in vertical direction, positive upward

w_0 average velocity induced by lifting rotor at rotor disk

C cross-sectional area of test section

A area of rotor disk

In this paper the interference velocity components u and v are derived from a single potential rather than being considered separately as in references 2 and 3. Thus the

drag terms of these references are already included. (Note that w_0 is the resultant induced velocity at the rotor disk and at $\alpha = 0$ it is the negative of the corresponding quantity used in refs. 2 and 3.) If the helicopter is operating at considerable forward velocity, its lift is approximately $2\rho V w_0 A$ whereas the lift of the wing is $\frac{1}{2}\rho V^2 C_L S$. If for this operating condition the ratio of upwash interference velocity v to total lift is the same as that of the wing, it therefore follows from equations (1) and (4) that

$$\delta_{R,z} = 4\delta_w$$

In the expression for the lift, ρ is the density of the test medium.

Interference factors for the helicopter rotor at the center of the test section with closed top, slotted side walls, and open lower boundary and with height-width ratio h/b equal to 1.5 have been computed from the equations of appendix C by use of an IBM 7094 electronic data processing system. For this calculation a homogeneous boundary condition on the side walls corresponding to the four equispaced slots in each wall with an open ratio r_0 of 0.0455 was assumed. Because of a mistake in calculations, this value of r_0 was originally believed to correspond to zero interference on the small wing model mounted at the center of the test section (this incorrect result has been quoted in ref. 4); but as seen from figure 4, it actually corresponds to $\delta_w = -0.026$. The calculation was made for angles of attack α of -10°, 0°, 10°, and 20° and for several values of the skew angle χ. The streamwise interference factor $\delta_{R,x}$ was computed at the position of the test model $\frac{x}{h} = 0$ only. The upwash interference factor $\delta_{R,z}$ was computed at the model position $\frac{x}{h} = 0$ and at the downstream positions $\frac{x}{h} = 0.1$, 0.3, and 0.5. The calculated interference factors are shown in figure 6 as functions of the angle $\chi - \alpha$ between the wake axis and the downward-drawn vertical. The values are, in general, not completely negligible, but every curve approaches or crosses zero for some value of $\chi - \alpha$ and the variation does not seem to be unreasonable. For instance, with $\alpha = 0$, $\frac{x}{h} = 0$, an upwash interference $\delta_{R,z} \approx 0.104$ occurs at $\chi = 0$. Such an upwash interference is required, because any boundary other than a completely open boundary places a constraint on the flow for this hovering mode of operation. As χ increases, the value of $\delta_{R,z}$ at $\frac{x}{h} = 0$ decreases, becomes negative, and then appears to be tending back toward zero as it should if for values of $\chi - \alpha$ approaching 90° the interference factor on the helicopter rotor is to approach $\delta_{R,z} = -0.104$ corresponding to $\delta_w = -0.026$ for the wing. It is believed that with the open ratio $r_0 = 0.0073$ needed for zero interference at a small wing, the variation of $\delta_{R,z}$ at $\frac{x}{h} = 0$ with χ at $\alpha = 0$ would be less than that shown in figure 6, since the variation is between 0.145 at $\chi = 0$ and 0 at $\chi = 90^\circ$. Because of the image arrangement used to satisfy the assumed boundary conditions, which with $\chi = 0$, $\alpha = 0$ are no longer valid at the open boundaries, the values calculated at $\chi = 0$, $\alpha = 0$ are believed to be slightly larger than would have been obtained if correct boundary conditions had been used. The value of $\delta_{R,x}$ at $\frac{x}{h} = 0$ and $\alpha = 0$ is zero for the

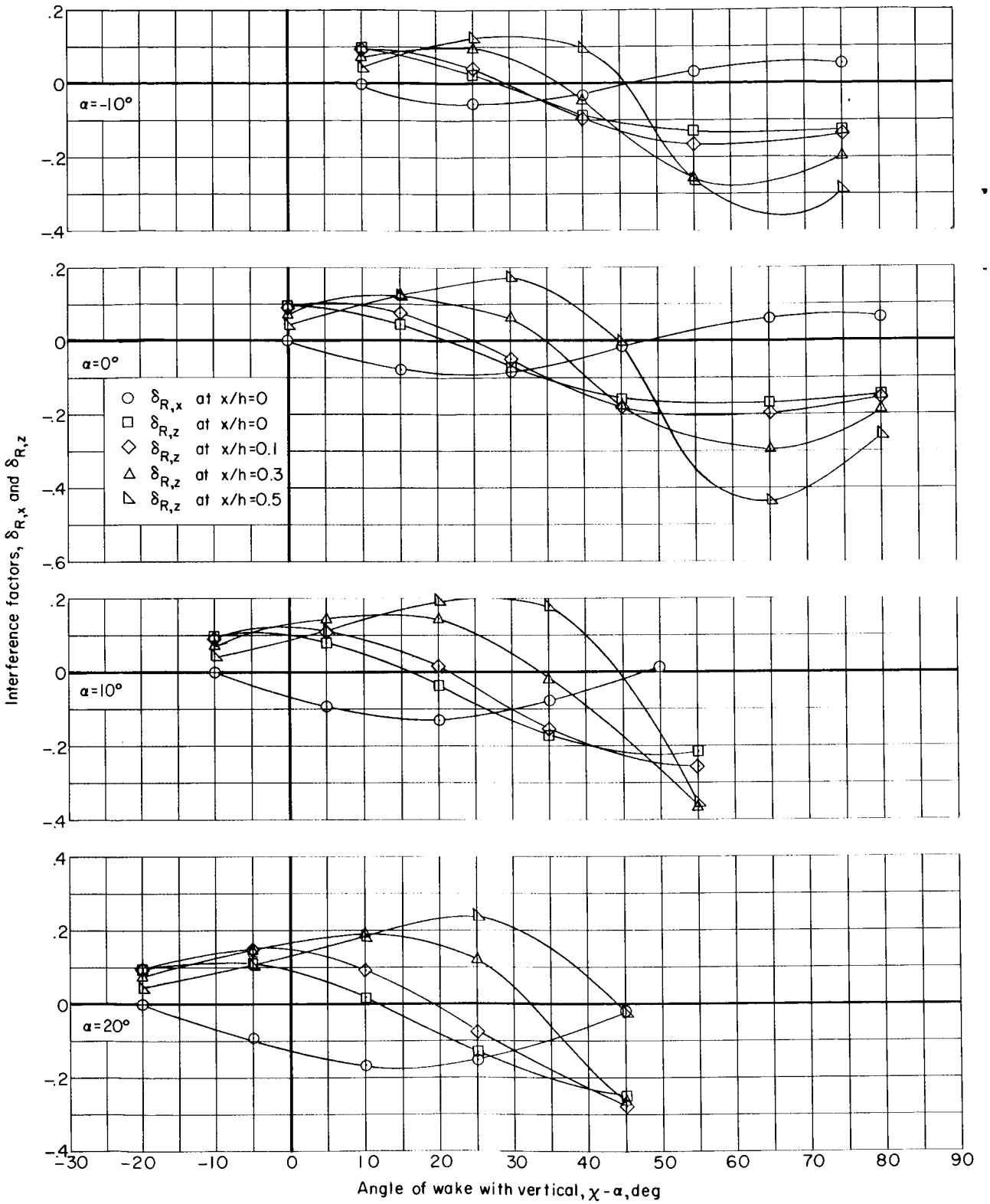

Figure 6.- Interference factors for small helicopter at center of test section with top wall closed, sidewalls slotted, and lower boundary open. h/b = 1.5; r_0 = 0.0455.

hovering condition $\chi = 0$ as it obviously must be. The fact that with $\frac{x}{h} = 0$ and $\chi = 0$, $\delta_{R,x}$ is very close to zero for nonzero values of α is a little surprising, but no reason could be found to doubt the correctness of these calculated results.

Although the skew angle χ is treated as a parameter in the presentation of the calculated values of the interference factors, it may not be arbitrarily chosen, but depends theoretically through equation (C6) on the velocities V and w_0 and on the angle α; and it increases toward 90^o with increase in the stream velocity V more strongly than indicated by that equation because of the tendency of the wake to roll up into two trailing vortices like the vortex wake of a wing. Thus, reference 4 shows that for most operating conditions, the deflection of the wake from the horizontal is only about half that calculated by use of equation (C6).

This behavior means that the uncertainty of the boundary conditions in the region of penetration of the open boundary by the helicopter wake can seriously affect the calculated interference in the neighborhood of the model only for a small range of stream velocities V near zero, where also χ approaches 0. An indication of the variation with skew angle χ of the possible error arising from this uncertainty is seen in the contributions to the interference factors $\delta_{R,z}$ and $\delta_{R,x}$ at $\alpha = 0$ due to subtraction of the part of the helicopter wake below the open lower boundary. Figure 7 shows that for the helicopter rotor mounted at the center of a test section with height-width ratio of 1.5, the effect of any such error becomes negligible at the rotor for $\chi - \alpha$ greater than about 45^o. At the tail the effect becomes negligible for $\chi - \alpha$ somewhat greater than 45^o. With height-width ratio less than 1.5, or otherwise with the rotor closer to the open lower boundary, the region for necessarily small error would be shifted to greater values of $\chi - \alpha$.

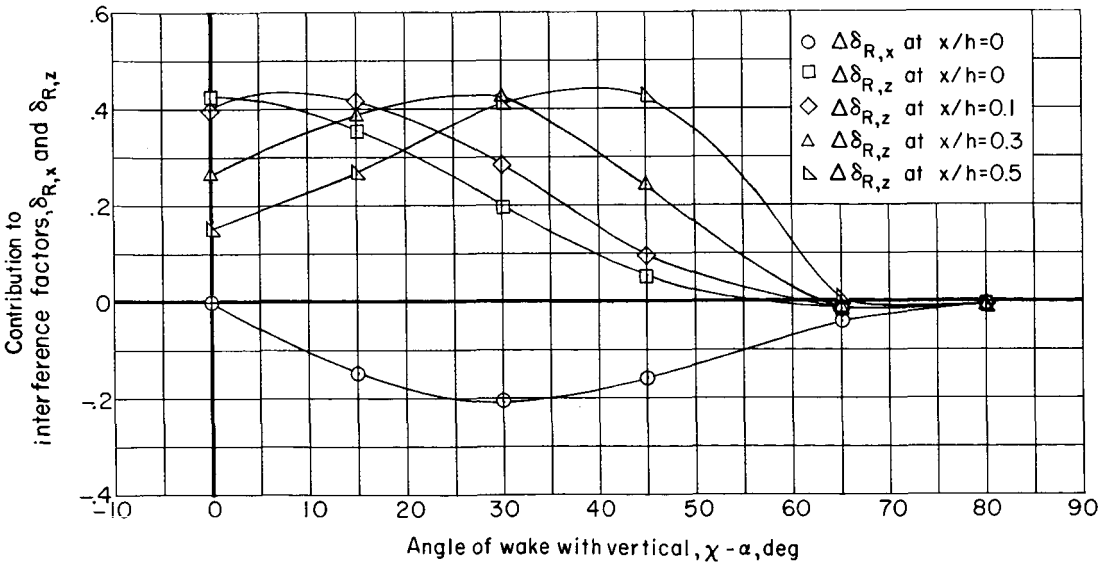

Figure 7.- Contribution to interference factors $\delta_{R,z}$ and $\delta_{R,x}$ due to subtracting part of helicopter wake below the open lower boundary. $\alpha = 0$.

An investigation of the interference with a lifting jet in the test section closed on top, slotted on the sides, and open on the bottom was originally intended, but upon examination, this problem did not seem to differ sufficiently from the helicopter interference problem to justify the additional labor of separate treatment. The essential difference is that the jet issues from the nozzle at some given angle α between its cross section and the tunnel test stream and with skew angle χ equal to zero, but it is then swept downstream and thus the skew angle becomes a function of distance along the jet axis. The path of the jet could be estimated and segments of the jet could be represented by lengths of vortex cylinders at different skew angles to calculate the interference in a manner similar to the calculation for the helicopter. However, it is believed that the nature of the interference would be essentially the same as that of the helicopter and that the interference would in most of the operating range be not much different from that calculated for the helicopter at some average effective angle. This conclusion is partially substantiated by calculations given in reference 12.

Other Configurations

If the requirement for small variation of the interference with decreasing skew angle is relaxed (as it may be if the lift loading is small enough to prevent the wake being greatly deflected from the horizontal), the class of test-section configurations available for reducing the interference is considerably broadened. One which has been suggested, and which has the practical advantage of easy access to the test section, has completely open top and sides and solid bottom. For theoretically zero interference in a given test section, the model must be placed at a fixed distance from the solid wall. Appropriate distances above the lower boundary for zero interference $\left(\delta_{R,z} = 0\right)$ can be read from figure 8 for various ratios of height to width of the rectangular test section h/b. The

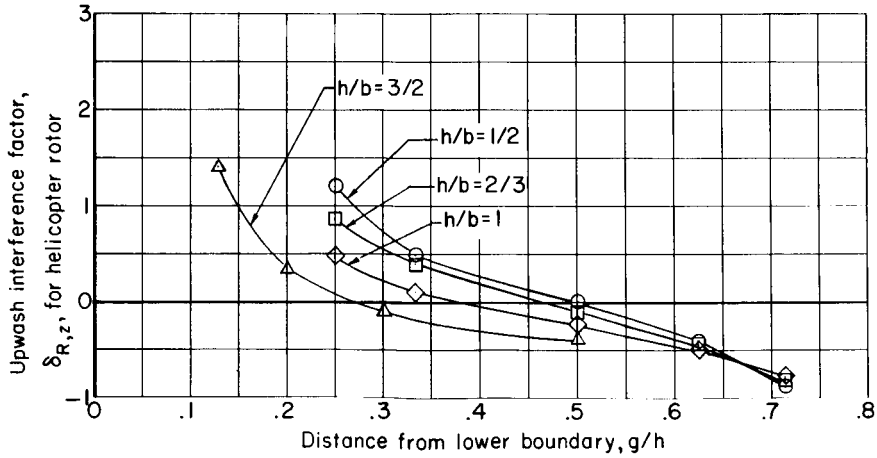

Figure 8.- Interference factor $\delta_{R,z}$ for small rotor on vertical center line of test section of height h and width b with open top and sides and closed bottom as function of nondimensional distance g/h of rotor above bottom boundary. Wake horizontal.

values for h/b equal to 0.5, 0.66, and 1.0 have been derived from figures 14(a), 14(b), and 14(c), respectively, of reference 3 for the condition $\chi - \alpha = 90^{\circ}$. For $\frac{h}{b} = 1.5$, the wing interference factor δ_w was computed as in equation (2) from the upwash velocity v for a lifting doublet computed as in appendix A except for the change in boundary conditions corresponding to replacement of the closed boundaries with open boundary and replacement of the open bottom with closed boundary. The rotor interference factor may then be computed from the relation

$$\delta_{R,z} \approx 4\delta_w$$

From figure 14 of reference 3 it is seen that the interference varies markedly with the skew angle χ; thus, to maintain zero interference, the position of the model would have to be different for different values of χ. Such variation of model position would somewhat complicate model testing procedures.

In wind-tunnel tests of lifting models for which the vortex wake is not deflected much ($\chi - \alpha \approx 90^{\circ}$), the tunnel-boundary-interference problem is essentially that usually treated for lifting wings, and the interference velocity at the model can be reduced to zero by means of slots in all four walls as shown, for instance, in references 9 and 13. Such a configuration might be expected theoretically to produce more nearly uniform flow in the region surrounding the model than would the previously discussed test section with closed top, open bottom, and slotted side walls; but some concern might be felt regarding the danger of malfunction of the slots in the top wall because of the inflow of low-speed air in that region. Because of the panels in the bottom, the interference in this configuration should be more sensitive to skew angle for $\chi - \alpha$ near zero than would that in the configuration with completely open bottom.

In an experimental investigation carried out by the NASA Langley Research Center using a high-lift wing, a test-section configuration with top closed and sides and bottom slotted seemed to produce more nearly uniform flow in the region of the model, particularly in the critical region of the tail, than did the previously suggested configuration with bottom actually or effectively (screened or many-slotted) open. This configuration was therefore investigated theoretically. Since a three-dimensional solution such as was previously obtained for the helicopter in the test section with open bottom would, with the slotted bottom, be mathematically complicated and time consuming to calculate, the two-dimensional method of reference 13 was applied. This method yields the interference velocity at the position of a wing (for $\chi - \alpha = 90^{\circ}$), but not that at the tail. Since this application of the theory of reference 13 is somewhat involved and since a part of the application to be made requires a small extension of that theory, the equations for calculation of the upwash interference factor δ_w are developed in appendix D.

Equation (D23) was used to compute the upwash interference factor δ_w at the center of a center-mounted wing represented by trailing vortices spaced 0.58 of the

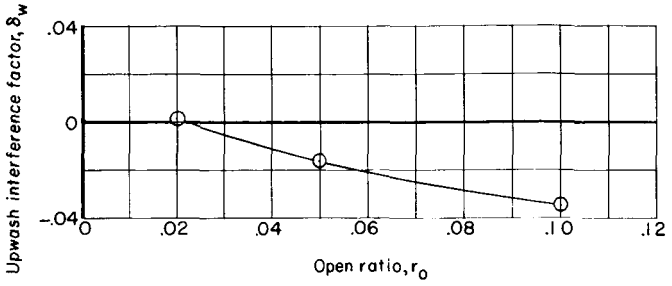

Figure 9.- Upwash interference factor for center-mounted wing spanning 0.58 of width of rectangular test section having height 1.432 times width. Top wall solid; side walls and bottom slotted with four equispaced slots each; trailing vortices horizontal.

test-section width in a rectangular test section with height 1.432 times the width, with closed top, with side walls and bottom having four equispaced slots each, and with (solid) panels cutting the axes through the test-section center. The upwash interference factor is plotted in figure 9 against ratio of open area to total area of the slotted walls r_0. The interference at the center of the wing is indicated to be zero for an open ratio r_0 of about 2.2 percent. In the previously mentioned experiments approximately zero interference at the model was obtained with 10 percent open ratio in the sides and 15 percent open ratio distributed over six slots (close to an effectively open condition) in the bottom. The interference was still approximately zero when the bottom boundary was completely open. Thus, experimentally, approximately zero interference is obtained with slot openings more than four times as wide as indicated theoretically. This apparent divergence from theory may be at least partly due to the insensitivity of the theoretical interference to slot width in the range of width near to but greater than that width required for theoretically zero interference, but it also seems reasonable to suppose that with the narrow slots required for zero lift interference, viscous effects at the edges (and perhaps other departures from the assumptions, such as violation of the small-disturbance assumption) may result in boundary conditions approximately corresponding in the theory to slot widths smaller than those actually being used. It is therefore suggested that not only should slot widths be experimentally designed to produce approximately zero interference for the types and sizes relative to the test section of models to be tested, but also consideration should be given to the possibility of Reynolds number effects on the slot performance. It is a fortunate circumstance that, because of the aforementioned insensitivity to width in the range of interest, slots that are wider than required, as they may be if they are designed in model-tunnel tests at relatively small Reynolds number, may still correspond to approximately zero interference. Moreover, this insensitivity to slot width favors compromise to obtain near-zero blockage interference, for which the zero-interference conditions require wider slots than required for zero lift interference.

UPWASH INTERFERENCE AT THE TAIL

It is evidently not very difficult, at least for a given model configuration, to design a test section for essentially zero upwash interference at the center of the wing, although

the open ratio r_0 of the slotted sides may be different from that theoretically obtained. A much more difficult problem is to design a test section producing only small upwash interference throughout the region occupied by the test model. The upwash interference in the region of the tail is of particular importance.

Because of the aforementioned mathematical complexity and time-consuming calculations required, even with a large machine-computing system, the upwash interference at the tail has not been computed for the test section slotted on sides and bottom. However, some enlightening qualitative considerations can be made. For this test section the upwash interference at the wing was computed as half the interference due to the interaction of the boundaries on the horizontal trailing vortex system at the far-downstream (Trefftz) plane. Since for the horizontal trailing-vortex system, the velocities (zero far upstream) increase monotonically in the downstream direction, it follows that if the interference due to the trailing-vortex system without consideration of the boundary vortex is zero at the wing, it is zero also at the tail, provided the tail lies in the horizontal center plane of the test section. Some interference might result if the tail lies above or below the center plane, but this interference should be small in this type of test section because of the small vertical gradient of upwash velocity in the region near the horizontal center plane. Of greater concern is the effect of the downward deflection of the wake.

In order to obtain a qualitative estimate of this effect, the two-dimensional theory of appendix D was used to calculate the upwash interference factor at the center of the test section for the wing displaced various amounts below the center. Such an estimate applies practically for relatively small wake deflection. For large wake deflection, for which the wake may even approach and penetrate the slots in the lower wall, a theory comparable to the previously presented helicopter theory would be required. For this closed-top slotted-side-wall slotted-bottom configuration, the open ratio r_0 was 2.2 percent, which is seen from figure 9 to correspond theoretically to zero interference at the center of the test section for the wing mounted at the center. From figure 10 it is seen that (as expected) movement of the wing (or rather of the trailing-vortex pair representing the wing) toward the slotted lower boundary results in a downwash interference at the center of the test section. Downstream at the position of the tail of a center-mounted model, the downwash

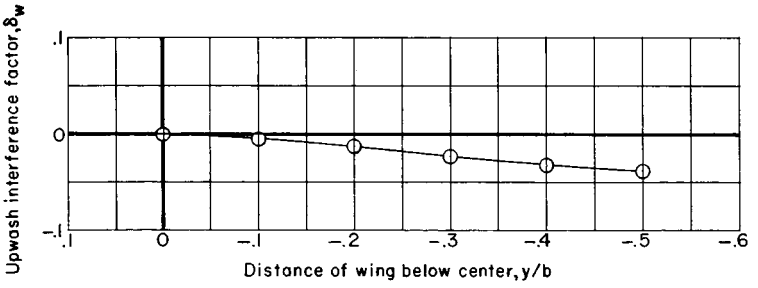

Figure 10.- Variation of upwash interference factor at center as wing centered on vertical center line and spanning 0.58 of test section is moved below center. Height of test section 1.432 times width; top closed; side walls and bottom slotted with four equispaced slots each; open ratio r_0 = 2.2 percent; trailing vortices horizontal.

may be somewhat greater than (but less than twice) that indicated in figure 10. On the other hand, for the center-mounted model the vortex wake must start approximately in the horizontal center plane and in most cases should not be deflected much below the tail. It seems therefore that the downwash interference at the tail caused by deflection of the vortex wake in the test section with slotted sides and bottom should be small. With the completely open (that is, softer) lower boundary, the downwash at the tail due to wake deflection should be somewhat greater, and it is perhaps for this reason that the slotted-bottom configuration seemed experimentally to produce smaller interference at the tail.

In contrast to the interference at the wing, that at the tail requires consideration of the interaction of test-section boundaries on the bound vortex as well as on the trailing vortices; that is, the estimation of interference at the tail is a three-dimensional problem. For the closed-top open-bottom configuration, a qualitative consideration is easy. The top- and bottom-boundary conditions are satisfied by image vortices. The first three images above and below the original bound vortex are indicated in figure 11, where the sense of the vortex is in each case indicated by an arrow. The vortex images 1 combine as do also vortex images 3 to produce zero upwash on the horizontal center plane. A small upwash is produced by images 2, and even this upwash is somewhat reduced by the series of images at distances greater than three test-section heights above and below the original bound vortex. Note that this upwash tends to cancel with the downwash caused

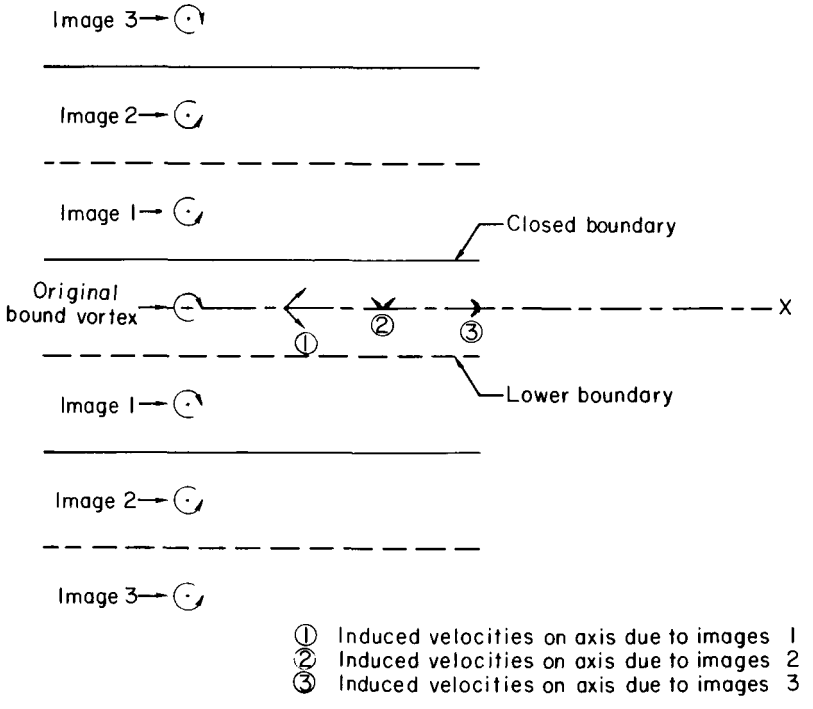

Figure 11.- Illustration of upwash interference of closed top and open bottom boundaries in presence of the bound vortex.

by deflection of the trailing-vortex wake. For a slotted rather than open lower boundary, the resulting upwash at the tail due to interference on the complete vortex system would be slightly increased.

To the extent that it is allowable to treat the bound vortex separately from the remainder of the vortex system, solid side walls produce no interaction, inasmuch as vertical planes normal to the vortex axis contain streamlines of the flow. At slots, however, the constant-pressure boundary condition requires a flow opposing the vorticity, and for the lifting vortex this flow is upward at the tail position. This effect should be small as long as the span of the lifting device is small relative to the test-section width. From this qualitative theoretical consideration, it is seen that for a zero-lift-interference (at the wing) test section with closed top, slotted side walls, and slotted or open bottom, and with the lifting wing mounted at the center,

(a) The interference at the tail due to interaction of the boundaries with a horizontal trailing-vortex system is zero provided the tail is located near the horizontal center line,

(b) Passage of the vortex wake horizontally somewhat below the tail produces downwash interference at the tail, and

(c) Interaction of the test-section boundaries with the bound vortex produces upwash interference at the tail.

These conclusions are, of course, conditioned by the assumption of potential flow at the slots.

In order to obtain further information concerning the contribution of slotted side walls to the upwash interference at the tail, equation (C61) was used to compute upwash interference factors for a lifting element centered between two vertical-plane infinite parallel slotted walls spaced a distance b apart. The development of equation (C61) implies application to a small, lightly loaded wing (horizontal wake) for which the interference on the bound part of a possible vortex-system representation is included. The stream flow (velocity V) is assumed to extend infinitely far above and below the wing. Examination of the right-hand side of this equation shows that at the position of the wing $\left(\frac{x}{b} = \frac{z}{b} = 0\right)$, the interference is given entirely by the second term. On the horizontal center line far downstream $\left(\frac{x}{b} \to \infty, \ \frac{z}{b} = 0\right)$, on the other hand, the first term makes a contribution equal to the second; thus, in agreement with a well-known theorem, the upwash interference at the wing is exactly half that at the far-downstream (Trefftz) plane.

The value of the restriction constant l (see eq. (B2)) required for zero upwash interference at the wing was found to be 0.592b. This value is about the same as that needed for zero interference in the test section with closed top and open bottom and with height 1.432 times its width. Some consideration shows the nature of the slotted-wall effect. The flow through the slots far from the wing permits a general downflow to

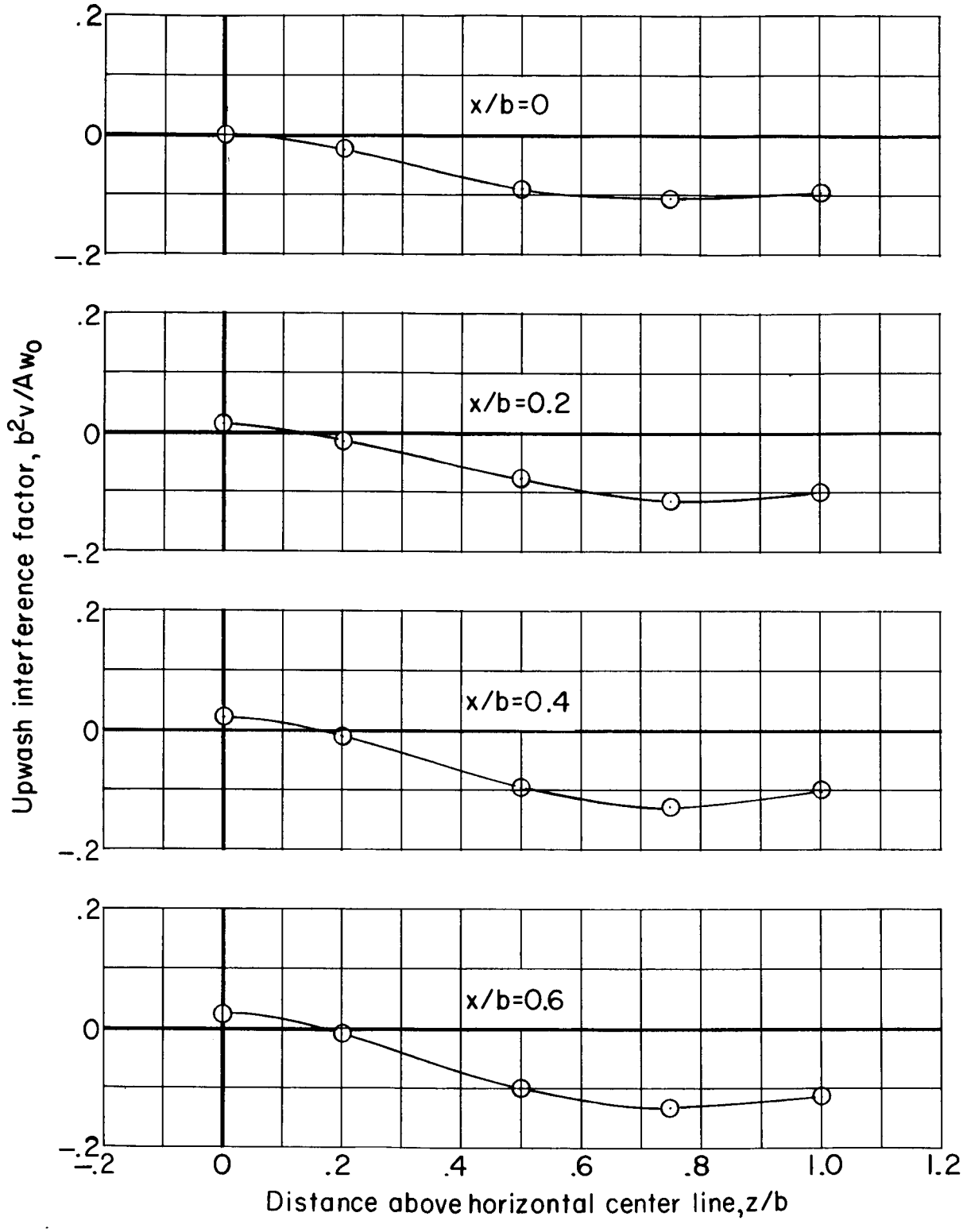

Figure 12.- Variation with distance above horizontal center plane of upwash interference factor for lifting element centered between infinite vertical parallel slotted walls spaced distance b apart. $\ell/b = 0.592$. Wake horizontal.

develop in the whole field above and below the wing, an effect similar to the downflow known to develop in a test section having closed sides and open top and bottom. The open ratio r_0 required for zero upwash interference must be of such a value that at the wing this downflow is exactly counterbalanced by the upflow induced by the vorticity developed in the presence of the lifting wing by the portion of the side walls opposite the wing. Computed upwash interference factors in the vertical center plane above and downstream from the wing are shown in figure 12. These results are in agreement with the qualitative analysis here presented. The interference velocities, which at $\frac{x}{b} = 0$ are zero at the wing, show the expected downwash above the wing. Since equation (C61) is even in z/b, exactly the same variation occurs below the wing. Superposed on this variation above and below the wing is a much smaller streamwise variation (the interference corresponding to the bound part of the vortex system) which, as seen from the first term on the right of equation (C61), is odd and therefore for upstream (negative) values of x/b is the negative of that indicated in figure 12.

The downstream variation of the downwash interference factor on the horizontal center line is shown in figure 13. The previously deduced upwash in the region likely to be occupied by the tail is evident. The interference velocity on the center line reduces to zero for x/b approaching ∞ (for zero interference at the wing) but at $\frac{x}{b} = 0.6$ it is still increasing.

The general downwash interference induced with the parallel infinite walls shows the importance of the top and bottom walls (perhaps also of closed-test-section entrance and exit) and suggests that the uniformity of flow in the region of the wing is favored by a moderate ratio of test-section height to width (for example, less than 2).

Note that the upwash interference factor shown in figures 12 and 13 is a helicopter rotor interference factor based on the square of the width b and therefore must be multiplied by $\frac{1.432}{4}$ before comparison with the upwash interference factor δ_w for the wing in the test section with height-width ratio of 1.432.

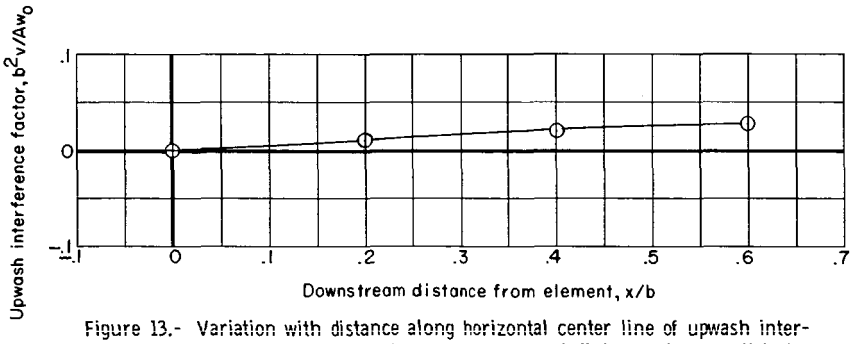

Figure 13.- Variation with distance along horizontal center line of upwash interference factor for lifting element centered between infinite vertical parallel slotted walls spaced distance b apart. $l/b = 0.592$; $z/b = 0$.

For the test section with closed top wall, slotted side walls, and open lower boundary, the interference at the tail can be calculated from the theory of appendix C. The upwash interference factor $\delta_{R,z}$ along the tunnel center line downstream from a lightly loaded lifting element (small wing, $\alpha = 0$, $\chi = 90^{o}$) mounted at the center of such a test section with height-width ratio $\frac{h}{b} = 1.5$ was calculated from equation (C65). The calculated values for $r_0 = 0.0455$, as in figure 6, and for $r_0 = 0.0073$, corresponding to zero upwash interference at the lifting element, are presented in figure 14. For $r_0 = 0.0455$, a downwash interference occurs at the wing and the downwash increases monotonically downstream. For $r_0 = 0.0073$, the upwash interference is zero at the wing; downstream, it is due entirely to the interference on the bound vortex and, as might be expected and as indicated by the qualitative theory previously presented, after first increasing it decreases toward zero at large distances downstream.

The values of $\delta_{R,z}$ on the upper curve of figure 14, which corresponds to $\chi = 90^{o}$, may be compared at $\frac{x}{h} = 0$, 0.1, 0.3, and 0.5 with the values for other skew angles χ at $\alpha = 0$ in figure 6. The interference is seen to vary from upwash to downwash as χ is increased from zero toward 90^{o}, and the variation increases with distance (at least to $\frac{x}{h} = 0.5$) downstream from the lifting element. At $\frac{x}{h} = 0.5$ the downwash reaches values near $\chi = 70^{o}$ significantly greater than that indicated in figure 14. This variation cannot be explained as being caused by displacement of the wake as in figure 10, but is evidently a function of the wake angle itself as well as of the position of the wake relative to the field point of interest and to the lower boundary of the test section.

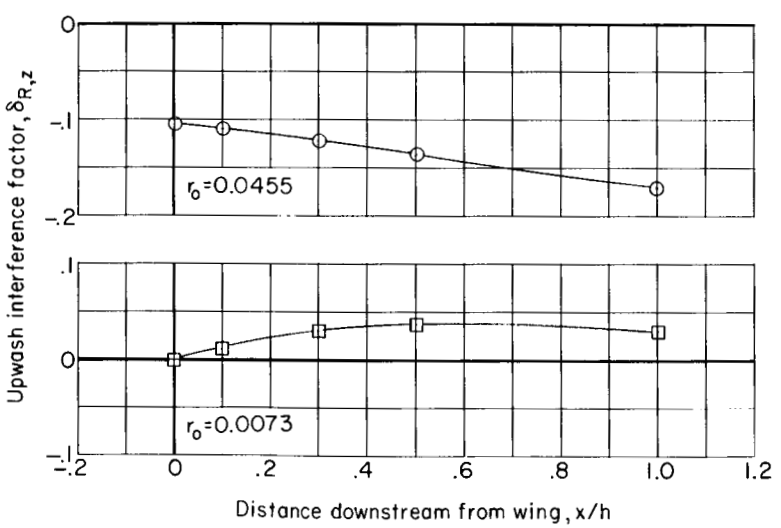

Figure 14.- Upwash interference factor along tunnel center line downstream from small wing mounted at center of test section with closed top wall, slotted side walls, and open lower boundary. h/b = 1.5; wake horizontal.

CONCLUDING REMARKS

By use of a test section having top wall solid, side walls slotted with four equispaced slots each, and bottom boundary open, it is found possible to reduce to zero the theoretical wind-tunnel-boundary upwash interference at a small, lightly loaded (trailing horizontal wake) wing mounted at the center of the test section. For a high-lift-coefficient model, for which the wake is not horizontal, the theoretical upwash interference in this test section does not vary greatly with variation of wake deflection. The slot width required for zero lift interference at a wing is found to be very small, but because of boundary-layer and viscous effects, as well as other uncertainties in practical application of the theory, the theory is regarded as unreliable for determining the slot width, and an experimental determination is therefore suggested. It is a fortunate circumstance that the lift interference at a small wing is relatively insensitive to slot width for widths near and somewhat greater than that required for zero interference. Aside from easing the problem of slot-width selection, this behavior permits compromise in favor of reducing solid blockage interference, which is known to require wider slots than are needed to produce zero lift interference.

For a test section of the type herein suggested, the theoretical interference upwash on the tunnel center line downstream from the lifting element is slightly positive, provided the slot width is such as to produce zero upwash interference at the wing and provided the vortex wake from the wing lies in the horizontal center plane. However, there is reason to believe that even with this ideal arrangement, a downwash interference exists both above and below the horizontal center plane so that if the tail is appreciably off this horizontal plane, it may experience a downwash rather than an upwash. This effect, along with the effect of movement of the vortex wake toward the open lower boundary and the effect of wake angle itself, leads to an appreciable downwash at the tail if the wake is even moderately deflected, for example, 10°. Moreover, if the slot width is greater than that needed for zero lift interference at the wing, the corresponding downwash produced downstream from the wing is greater than that at the wing. In practical application, therefore, the interference at the tail of a winged model mounted at the center of such a test section is very likely to be of the nature of a downwash. On the other hand, for high-lift-coefficient models, the interference on the tunnel center line downstream from the position of the model tends toward an upwash as the vortex wake approaches the downward vertical direction.

Zero interference at a small wing with horizontal vortex wake can be obtained with other test-section configurations, but to prevent large variations with skew angle while maintaining small interference at the model, an open or effectively open (many-slotted or screened) lower boundary seems necessary. However, the use of such a boundary introduces additional uncertainties in boundary conditions and therefore further degrades the

reliability of the interference calculations relative to such calculations for completely closed boundaries. A many-slotted or screened, rather than completely open, lower boundary may be desirable to prevent oscillations of the test-section flow. If the requirement for small interference variation with skew angle can be relaxed, the zero interference on a wing with horizontal wake can be obtained in a test section having all four walls slotted with coarse slots. The flow in the region of the wing might then be more nearly uniform than that for the test section herein suggested, and the effect of moderate downward deflection of the wake might also be less. With high-lift devices a slotted upper wall might behave essentially as an open boundary because of the effectively thick boundary layer produced by inflow through the slots, but there is reason to believe that this behavior would not affect the interference much provided the bottom wall were sufficiently effectively rigid to carry the reaction to the lift. In contrast, with an open lower boundary a too great lift loading on the test-section flow might result in flow separation from even a solid upper wall, and the resulting interference would be a downwash as in a test section with completely open top and bottom walls.

Because the practical boundary conditions at mixed (open and closed) boundaries are not well determined, particularly with high lift and narrow slots, the theory herein presented is regarded as unreliable for predicting numerical values for lift interference in given test-section configurations. It should be useful in showing the nature of the interference and the possibility of reducing it, and it should serve as a guide to design and experimentation. The slot widths required for zero interference should be determined by experiment, although the experimental investigation of wind-tunnel-boundary interference is difficult, largely because the quantities of interest are usually relatively small differences. In a zero-interference (at the wing) test section the distribution of upwash velocities and their variation with skew angle might well be approximated by the theory even though the practical slot widths are different from those theoretically determined. It is believed that further theoretical investigation might lead to test-section configurations having more nearly uniform flow in the vicinity of the model, including the position of the tail, than exists for those so far investigated. With considerable additional labor, the effects of curvature of the wake (as for downward-directed jets) might also be taken into account.

Langley Research Center,
National Aeronautics and Space Administration,
Langley Station, Hampton, Va., February 1, 1968,
721-01-00-20-23.

APPENDIX A

DERIVATION OF EQUATION FOR CALCULATING UPWASH INTERFERENCE VELOCITY ON SMALL LIFTING MODEL IN TEST SECTION WITH CLOSED TOP AND SIDE WALLS AND OPEN LOWER BOUNDARY

The model is located on the vertical center line of a rectangular test section of height h and width b with closed top and side walls and open lower boundary. The model is located at height g above the lower (open) boundary. The upwash interference velocity v is that induced by the test-section boundaries on a vortex doublet corresponding to the lift of the model and trailing horizontally downstream from the model. The induced upwash velocity is first obtained in a plane normal to the vortex doublet line far downstream (the Trefftz plane), where the flow is essentially two-dimensional. The induced upwash velocity at the model is then just half that at this far-downstream plane.

The symbols peculiar to this appendix are as follows:

n,k	any integers
y_1,z_1	Cartesian coordinates of a vortex doublet
ϕ_+	velocity potential of line doublet corresponding to positive lift
ϕ_-	velocity potential of line doublet corresponding to negative lift

The arrangement of vortex doublet images satisfying the boundary conditions is indicated in figure 1. With the origin of y,z coordinates taken at the position of the original lifting doublet, vertical image rows occur at $y = kb$, k being all integers from $-\infty$ to ∞. Horizontal rows of positive (lifting) vortex doublets occur at $z = (2n)(2h)$ and at $z = (2n)(2h) - 2g$, n being all integers from $-\infty$ to ∞. Horizontal rows of negative vortex doublets are located at $z = (2n + 1)(2h)$ and at $z = (2n + 1)(2h) - 2g$, n being all integers from $-\infty$ to ∞.

The velocity potential of a lifting-line vortex doublet of strength μ located at (0,0) is (see ref. 14)

$$\phi_+ = \frac{\mu}{2\pi} \frac{z}{y^2 + z^2} \tag{A1}$$

The potential for the line doublet of opposite sense is

$$\phi_- = \frac{-\mu}{2\pi} \frac{z}{y^2 + z^2} \tag{A2}$$

APPENDIX A

If the vortex doublet is located at y_1, z_1, the potential is

$$\phi_+ = \frac{\mu}{2\pi} \frac{z - z_1}{(y - y_1)^2 + (z - z_1)^2} \tag{A3}$$

or

$$\phi_- = \frac{-\mu}{2\pi} \frac{z - z_1}{(y - y_1)^2 + (z - z_1)^2} \tag{A4}$$

On the Z-axis, $y = 0$ and these potentials give

$$\phi_+ = \frac{\mu}{2\pi} \frac{z - z_1}{(z - z_1)^2 + y_1^2} \qquad (y = 0) \tag{A5}$$

$$\phi_- = \frac{-\mu}{2\pi} \frac{z - z_1}{(z - z_1)^2 + y_1^2} \qquad (y = 0) \tag{A6}$$

For $z \neq z_1$ the sum for any horizontal row is

$$\phi_{(row)+} = \frac{\mu}{2\pi} \sum_{k=-\infty}^{\infty} \frac{z - z_1}{(z - z_1)^2 + k^2 b^2} \qquad (y = 0) \tag{A7}$$

or

$$\phi_{(row)-} = \frac{-\mu}{2\pi} \sum_{k=-\infty}^{\infty} \frac{z - z_1}{(z - z_1)^2 + k^2 b^2} \qquad (y = 0) \tag{A8}$$

As indicated by equation (I) of reference 8, the sum of the infinite series in equation (A7) is

$$\phi_{(row)+} = \frac{\mu}{2b} \coth \frac{\pi(z - z_1)}{b} \qquad (y = 0) \tag{A9}$$

and that of the infinite series in equation (A8) is

$$\phi_{(row)-} = \frac{-\mu}{2b} \coth \frac{\pi(z - z_1)}{b} \qquad (y = 0) \tag{A10}$$

The corresponding upwash velocities at $y = 0$ are

$$v_{(row)+} = \frac{\mu}{2b}\left[-\frac{\pi}{b} \operatorname{csch}^2 \frac{\pi(z - z_1)}{b}\right] = -\frac{\pi\mu}{2b^2} \operatorname{csch}^2 \frac{\pi(z - z_1)}{b} \qquad (y = 0) \tag{A11}$$

APPENDIX A

$$v_{(row)-} = \frac{\pi\mu}{2b^2}\,\mathrm{csch}^2\,\frac{\pi(z - z_1)}{b} \qquad (y = 0) \qquad (A12)$$

In order to find the interference, the potential of the doublet located at 0,0 must be removed from that of the row at $z_1 = 0$. Since the potential is required on the Z-axis in the neighborhood of $z = 0$, the potential may be expressed as

$$\phi_{(row)} = \frac{\mu}{2\pi}\left(\frac{\pi}{b}\coth\frac{\pi z}{b} - \frac{1}{z}\right) = \frac{\mu}{2\pi}\left\{\frac{\pi}{b}\left[\frac{1}{\pi z/b} + \frac{1}{3}\left(\frac{\pi z}{b}\right) - \frac{1}{45}\left(\frac{\pi z}{b}\right)^3 + \cdots\right] - \frac{1}{z}\right\} \approx \frac{\pi\mu}{6b^2}\,z \qquad (A13)$$

$$(y = 0;\ z_1 = 0)$$

Hence the interference upwash at 0,0 due to the horizontal row at $z_1 = 0$ is $\pi\mu/6b^2$. At the position of the model the upwash is just half that at the near downstream Trefftz plane so far considered. The total interference upwash at the position of the model where z approaches 0 is therefore

$$v = \frac{\pi\mu}{12b^2} - \frac{\pi\mu}{4b^2}\,\mathrm{csch}^2\,\frac{2\pi g}{b} - \frac{\pi\mu}{4b^2}\sum_{\substack{n=-\infty \\ n\neq 0}}^{\infty}\left(\mathrm{csch}^2\,\frac{4\pi nh}{b} + \mathrm{csch}^2\,\frac{4\pi nh - 2\pi g}{b}\right)$$

$$+ \frac{\pi\mu}{4b^2}\sum_{n=-\infty}^{\infty}\left[\mathrm{csch}^2\,\frac{2\pi(2n+1)h}{b} + \mathrm{csch}^2\,\frac{2\pi(2n+1)h - 2\pi g}{b}\right]$$

With some rearrangement this equation can be rewritten as

$$v = \frac{\pi\mu}{4b^2}\left\{\frac{1}{3} - \mathrm{csch}^2\,\frac{2\pi g}{b} - \sum_{n=1}^{\infty}\left(2\,\mathrm{csch}^2\,\frac{4\pi nh}{b} + \mathrm{csch}^2\,\frac{4\pi nh - 2\pi g}{b} + \mathrm{csch}^2\,\frac{4\pi nh + 2\pi g}{b}\right)\right.$$

$$\left. + \sum_{n=1}^{\infty}\left[2\,\mathrm{csch}^2\,\frac{2\pi(2n-1)h}{b} + \mathrm{csch}^2\,\frac{2\pi(2n-1)h - 2\pi g}{b} + \mathrm{csch}^2\,\frac{2\pi(2n-1)h + 2\pi g}{b}\right]\right\} \qquad (A14)$$

This form is easily seen to be an alternating convergent series of monotonically decreasing terms. The error in cutting off the summation at any term is therefore less than the value of that term. The convergence is so rapid that only the first few terms need to be considered.

APPENDIX B

DEVELOPMENT OF EQUATION FOR CALCULATING UPWASH INTERFERENCE IN TEST SECTION WITH CLOSED TOP, SLOTTED SIDES, AND OPEN LOWER BOUNDARY

The configuration is the same as that of appendix A except that the side walls are now slotted; therefore, the boundary condition at the slotted walls must be satisfied directly rather than by means of images. The symbols for this appendix are as follows:

$A(\omega)$	arbitrary function of ω determined to satisfy slotted boundary condition
b	width of test section
d	distance between centers of two adjacent slots
g	distance of model from open lower boundary
h	height of test section
l	restriction constant defined in equation (B2)
n	any integer
q	variable of integration, ωb
r_0	ratio of slot width to distance d
V	tunnel stream velocity
v	upwash velocity at the model
y,z	rectangular Cartesian coordinates
y_1,z_1	coordinates of a line vortex doublet
$\Delta\delta_i$	contribution to upwash interference factor at 0,0 due to a line vortex image

APPENDIX B

$\Delta\delta_s$ contribution to upwash interference factor at 0,0 due to interference of slotted side walls on a line vortex doublet

δ_w upwash interference factor

μ strength of vortex doublet

ϕ velocity potential

ϕ_d velocity potential of vortex doublet

ϕ_s velocity potential induced by slotted side walls in presence of vortex doublet

Ω transform of ϕ on $z - z_1$

Ω_s transform of ϕ_s on $z - z_1$

ω variable of transformation on $z - z_1$

For simplicity the slotted-side-wall boundary is replaced by a homogeneous boundary, the boundary condition on the velocity potential ϕ being given by (see ref. 9)

$$\phi \pm l \frac{\partial \phi}{\partial y} = 0 \tag{B1}$$

where the positive sign applies at the boundary $y = \frac{b}{2}$ and the negative sign applies at the boundary $y = -\frac{b}{2}$. Equation (B1) is derived under the small-disturbance assumption for slots in the direction of the tunnel stream V; thus, the velocities at the boundaries normal to the slot direction are small. The restriction constant l is given by equation (3) of reference 9 as

$$l = \frac{d}{\pi} \log_e \csc \frac{\pi r_0}{2} \tag{B2}$$

where d is the distance between the centers of two adjacent slots and r_0 is the ratio of slot width to the distance d, or for a uniformly slotted wall simply the proportion of the wall that is open. The restriction constant has the dimension of a distance and approaches zero for an open tunnel and infinity for a closed tunnel. The homogeneous boundary approximation is satisfactory for determining the interference at distances from the wall that are large relative to the distance between slots. (See, for example, ref. 9.)

APPENDIX B

The boundary condition (B1) is satisfied by adding to the potential ϕ_d of a vortex doublet located at $0,z_1$ in the far-downstream plane (Trefftz plane) normal to the test stream a potential ϕ_s such that $\phi_d + \phi_s$ satisfies equation (B1). Of course, ϕ_s as well as ϕ_d must satisfy the Laplace equation

$$\frac{\partial^2\phi}{\partial y^2} + \frac{\partial^2\phi}{\partial z^2} = 0 \tag{B3}$$

From equations (A3) and (A4) the potential of a positive (lifting) line vortex doublet located at $0,z_1$ is

$$\phi_{d,+} = \frac{\mu}{2\pi} \frac{z - z_1}{y^2 + (z - z_1)^2} \tag{B4}$$

and the potential of a negative line vortex doublet located at $0,z_1$ is

$$\phi_{d,-} = -\frac{\mu}{2\pi} \frac{z - z_1}{y^2 + (z - z_1)^2} \tag{B5}$$

In order to obtain the additional potential ϕ_s due to the influence of the slotted side walls, the exponential Fourier integral transform (see ref. 15) on $z - z_1$ with variable of transformation ω is taken. Transformation of equation (B1) then gives

$$\Omega(y,\omega) \pm \frac{l}{} \frac{\partial\Omega(y,\omega)}{\partial y} = 0 \tag{B6}$$

The Laplace equation (eq. (B3)) transforms to

$$\frac{\partial^2\Omega(y,\omega)}{\partial y^2} = \omega^2\Omega(y,\omega) \tag{B7}$$

A solution of equation (B7) intended to correspond to ϕ_s and having the required symmetry in y is

$$\Omega_s(y,\omega) = A(\omega)\cosh(\omega y) \tag{B8}$$

where $A(\omega)$ is an arbitrary function of ω. The potentials (eqs. (B4) and (B5)) of the line doublets transform to

$$\Omega_{d,\pm}(y,\omega) = \mp \frac{i\mu}{2} \frac{\omega}{|\omega|} e^{-|y||\omega|} \tag{B9}$$

This transformation is easily derived from formula (15), p. 65 of reference 15.

Substitution of $(\Omega_s + \Omega_{d,\pm})$ for Ω in the boundary condition (eq. (B6)) at the right-hand wall $y = \frac{b}{2}$ gives

APPENDIX B

$$A(\omega)\left[\cosh\left(\omega\,\frac{b}{2}\right)+l\omega\,\sinh\left(\omega\,\frac{b}{2}\right)\right]=\pm\frac{i\mu}{2}\left(\frac{\omega}{|\omega|}-l\omega\right)e^{-\frac{b}{2}|\omega|}$$

The same equation holds at the left-hand boundary. Consequently,

$$A(\omega)=\pm\frac{i\mu}{2}\,\frac{\left(\frac{\omega}{|\omega|}-l\omega\right)e^{-\frac{b}{2}|\omega|}}{\cosh\left(\omega\,\frac{b}{2}\right)+l\omega\,\sinh\left(\omega\,\frac{b}{2}\right)}$$

and the transform Ω_s of the interference potential ϕ_s due to the reaction of the slotted side walls on the line doublet potential $\phi_{d,\pm}$ is

$$\Omega_{s,\pm}(y,\omega)=\pm\frac{i\mu}{2}\,\frac{\left(\frac{\omega}{|\omega|}-l\omega\right)e^{-\frac{b}{2}|\omega|}}{\cosh\left(\omega\,\frac{b}{2}\right)+l\omega\,\sinh\left(\omega\,\frac{b}{2}\right)}\cosh(\omega y) \tag{B10}$$

where the positive sign applies for the original lifting doublet or its positive image and the negative sign applies for its negative image.

By inversion,

$$\phi_{s,\pm}=\pm\frac{i\mu}{4\pi}\int_{-\infty}^{\infty}\left[\frac{\left(\frac{\omega}{|\omega|}-l\omega\right)e^{-\frac{b}{2}|\omega|}}{\cosh\left(\omega\,\frac{b}{2}\right)+l\omega\,\sinh\left(\omega\,\frac{b}{2}\right)}\cosh(\omega y)\right]e^{i\omega(z-z_1)}d\omega \tag{B11}$$

The corresponding contribution to the upwash velocity at $y = z = 0$ is

$$\left.\frac{\partial\phi_{s,\pm}}{\partial z}\right]_{\substack{y=0\\z=0}}=\mp\frac{\mu}{4\pi}\int_{-\infty}^{\infty}\frac{\left(\frac{\omega^2}{|\omega|}-l\omega^2\right)e^{-\frac{b}{2}|\omega|}}{\cosh\left(\omega\,\frac{b}{2}\right)+l\omega\,\sinh\left(\omega\,\frac{b}{2}\right)}e^{-i\omega z_1}d\omega$$

$$=\mp\frac{\mu}{2\pi}\int_{0}^{\infty}\frac{\left(\omega-l\omega^2\right)e^{-\omega\frac{b}{2}}}{\cosh\left(\omega\,\frac{b}{2}\right)+l\omega\,\sinh\left(\omega\,\frac{b}{2}\right)}\cos(\omega z_1)d\omega \tag{B12}$$

APPENDIX B

Since, as given by equation (2), the upwash interference factor is $\delta_w = \frac{hb}{2\mu} v$, where v is the upwash velocity at the model (half that in the Trefftz plane), the contribution to the upwash at 0,0 is

$$\Delta\delta_{s,\pm} = \mp \frac{hb}{8\pi} \int_0^\infty \frac{\left(\omega - l\omega^2\right) e^{-\omega\frac{b}{2}}}{\cosh\left(\omega \frac{b}{2}\right) + l\omega \sinh\left(\omega \frac{b}{2}\right)} \cos\left(\omega z_1\right) d\omega$$

$$= \mp \frac{1}{8\pi} \frac{h}{b} \int_0^\infty \frac{\left(\omega b - \frac{l}{b} \omega^2 b^2\right) e^{-\frac{\omega b}{2}}}{\cosh\left(\frac{\omega b}{2}\right) + \frac{l}{b} \omega b \sinh\left(\frac{\omega b}{2}\right)} \cos\left(\omega b \frac{z_1}{h} \frac{h}{b}\right) d(\omega b)$$

and with $\omega b = q$,

$$\Delta\delta_{s,\pm} = \mp \frac{1}{8\pi} \frac{h}{b} \int_0^\infty \frac{\left(q - \frac{l}{b} q^2\right) e^{-\frac{q}{2}}}{\cosh \frac{q}{2} + \frac{l}{b} q \sinh \frac{q}{2}} \cos\left(\frac{h}{b} \frac{z_1}{h} q\right) dq \tag{B13}$$

From equations (B4) and (B5) the upwash velocity at 0,0 due to a doublet image at $0,z_1$ is found to be

$$\frac{\partial \phi_{d,\pm}}{\partial z} = \mp \frac{\mu}{2\pi {z_1}^2}$$

and therefore the contribution to the interference factor at the model is

$$\Delta\delta_{i,\pm} = \mp \frac{1}{8\pi} \frac{b}{h} \frac{1}{\left(\frac{z_1}{h}\right)^2} \tag{B14}$$

As for the configuration with solid top and side walls and open bottom boundary, positive images in the top and bottom boundaries occur at $z_1 = (2n)(2h)$ and at $z_1 = (2n)(2h) - 2g$ for all positive, negative, and zero values of n, the original lifting doublet being at $z_1 = 0$. Negative images occur at $z_1 = (2n + 1)(2h)$ and at $z_1 = (2n + 1)(2h) - 2g$ where n is all integers from $-\infty$ to ∞ and g is the distance of the model from the open lower boundary. It follows therefore from equations (B13) and (B14), since the velocity due to the original lifting doublet is not to be included, that the upwash interference factor at the center of the tunnel is

APPENDIX B

$$\delta_w = \frac{1}{8\pi}\frac{h}{b}\left[-\frac{\left(\frac{b}{h}\right)^2}{4\left(\frac{g}{h}\right)^2} - \int_0^\infty \frac{\left(q - \frac{l}{b}q^2\right)e^{-\frac{q}{2}}\left[1 + \cos\left(2\,\frac{g}{h}\,\frac{h}{b}\,q\right)\right]dq}{\cosh\frac{q}{2} + \frac{l}{b}\,q\,\sinh\frac{q}{2}} - \sum_{\substack{n=-\infty \\ n\neq 0}}^{\infty}\left(\left(\frac{b}{h}\right)^2\left[\frac{1}{16n^2} + \frac{1}{4\left(2n - \frac{g}{h}\right)^2}\right]\right.\right.$$

$$+ \int_0^\infty \frac{\left(q - \frac{l}{b}q^2\right)e^{-\frac{q}{2}}}{\cosh\frac{q}{2} + \frac{l}{b}\,q\,\sinh\frac{q}{2}}\left\{\cos\left(\frac{h}{b}\,4nq\right) + \cos\left[\frac{h}{b}\left(4n - 2\,\frac{g}{h}\right)q\right]\right\}dq\Bigg) + \sum_{n=-\infty}^{\infty}\left(\left(\frac{b}{h}\right)^2\left[\frac{1}{4(2n+1)^2} + \frac{1}{4\left(2n + 1 - \frac{g}{h}\right)^2}\right]\right.$$

$$\left.\left. + \int_0^\infty \frac{\left(q - \frac{l}{b}q^2\right)e^{-\frac{q}{2}}}{\cosh\frac{q}{2} + \frac{l}{b}\,q\,\sinh\frac{q}{2}}\left\{\cos\left[\frac{h}{b}\,2(2n+1)q\right] + \cos\left[\frac{h}{b}\,2\left(2n + 1 - \frac{g}{h}\right)q\right]\right\}dq\right)\right] \qquad \text{(B15)}$$

Convergence should be rapid; thus, only a few positive and negative values of n are needed.

APPENDIX C

DERIVATION OF EQUATIONS FOR CALCULATING BOUNDARY-INTERFERENCE FACTORS FOR A HELICOPTER ROTOR IN A RECTANGULAR TEST SECTION WITH CLOSED TOP, SLOTTED SIDE WALLS, AND OPEN LOWER BOUNDARY

A lifting helicopter rotor is assumed to be mounted at the center of a rectangular wind-tunnel test section with closed top wall, slotted side walls, and open lower boundary. Equations for calculating the streamwise interference factor $\delta_{R,x}$ and the upwash interference factor $\delta_{R,z}$ induced by the test-section boundaries are to be derived. Symbols applicable particularly to this derivation are as follows:

A area of rotor disk

$\overline{A}$ vector area of rotor disk

$B(\omega,g)$ arbitrary function of ω and g

$B_S(\omega,g), B'_S(\omega',g')$ values of $B(\omega,g)$ appropriate to $dG_{n,s}$ and $dG'_{n,s}$, respectively

b width of test section

C cross-sectional area of test section, hb

G exponential Fourier transform of Ω on z

G_n exponential Fourier transform of Ω_n on $z - 2nh + s\cos(\chi - \alpha)$

G'_n exponential Fourier transform of Ω'_n on $z - (2n - 1)h - s'\cos(\chi - \alpha)$

$G_{n,s}, G'_{n,s}$ values to be added to G_n and G'_n to satisfy slotted boundary condition

g variable of transformation on $z - 2nh + s\cos(\chi - \alpha)$

g' variable of transformation on $z - (2n - 1)h - s'\cos(\chi - \alpha)$

h height of test section

$i = \sqrt{-1}$

APPENDIX C

I_1, I_2, I_3, I_4 integrals defined by equations (C48)

$\left[I_{w1}\right]_{\substack{y=0 \\ n=0}}, \left[I_{w2}\right]_{\substack{y=0 \\ n=0}}$ contributions to potential of interference velocities arising from subtraction of vortex cylinder extending below lower open boundary

$\bar{i}, \bar{j}, \bar{k}$ unit vectors in direction of X-, Y-, and Z-axes, respectively

K_0, K_1 modified Bessel functions of second kind

l restriction constant

M_1, M_2 parameters defined by equations (C37) and (C42)

n any integer

P field point

$p = \omega h$ or ωb

$q = gh$ or gb

r distance from element of surface to field point P

$\bar{r}$ vector distance from element of surface to field point P

s distance from rotor disk to vortex ring

T thrust

u,v interference velocities in x- and z-direction, respectively

V tunnel stream velocity

V_R magnitude of resultant of V and w_0 regarded as vectors

w_0 induced velocity at rotor disk

X,Y,Z coordinate axes

x,y,z	coordinates
z_0,z_0'	variables defined by equations (C38) and (C44)
α	angle of attack of rotor-tip-path plane
Γ	circulation, positive for positive lift
$(\Delta\delta_{R,x})_{ns}$	slotted-side-wall contribution to streamwise interference factor at (x,0,0) for a vortex cylinder cell nominally located at (0,0,2nh)
$(\Delta\delta_{R,z})_{ns}$	slotted-side-wall contribution to upwash interference factor at (x,0,0) for a vortex cylinder cell nominally located at (0,0,2nh)
ϵ	small positive number
θ	angle between $\bar{A}$ and $\bar{r}$
ρ	density of test medium
ϕ	velocity potential
ϕ_0	velocity potential of vortex cylinder cell nominally lying at (0,0,0)
ϕ_n	velocity potential of part of vortex cylinder cell image corresponding to part of original vortex wake between rotor and open boundary
$\phi_{0,n}$	velocity potential of vortex cylinder cell nominally located at (0,0,2nh)
ϕ_w	velocity potential of part of rotor wake outside position of open lower boundary
$\phi_{0,w}$	velocity potential of part of rotor wake outside position of open lower boundary plus image in that boundary
$\phi_1,\phi_2,\phi_1',\phi_2'$	contributions to ϕ_0 given by equations (C41), (C43), (C45), and (C46), respectively
χ	skew angle, positive counterclockwise
ω	variable of transformation on $x - s\sin(\chi - \alpha)$

APPENDIX C

Ω exponential Fourier transform of ϕ on x

Ω_n exponential Fourier transform of ϕ_n on $x - s \sin(\chi - \alpha)$

Primes on symbols indicate values applying to image of vortex cylinder reflected across open boundary. Subscript s indicates a slotted-wall contribution.

As in references 2, 10, and 11, the disturbance caused by the helicopter rotor is represented by a straight elliptic cylindrical vortex sheet extending from the rotor. The vortex sheet is made up of a continuous constant-strength density distribution of circular vortex rings lying in planes parallel to the rotor-tip-path plane. (See fig. 5.) In figure 5 right-handed axes X,Y,Z are chosen, but for simplicity the Y-axis is not shown; this omission causes no difficulty, because the rotor disk and the flow field are symmetric about the X,Z plane. The wind-tunnel stream velocity V lies in the direction of the positive X-axis. The rotor disk (tip-path plane) makes an angle α with this direction and is positive in the sense indicated in figure 5. The angle between the normal to the rotor disk and the axis of the cylindrical vortex sheet is designated χ.

The element of potential $d\phi$ at the field point P due to the vortex ring of strength $\frac{d\Gamma}{ds} ds$ from reference 16, page 212, is, in the notation of this paper,

$$d\phi = \frac{\frac{d\Gamma}{ds} ds}{4\pi} \iint \frac{\cos \theta}{r^2} dA \tag{C1}$$

where r is the distance from an element of surface enclosed by the vortex ring to the point P, and s is distance from the rotor disk to the vortex ring. In the calculation of the boundary interference the points P of interest are considered to be far from the vortex rings contributing to the interference so that the relative variation of r over the surface A enclosed by any vortex ring is small. Since also the angle θ between the vector area $\bar{A}$ and the vector distance $\bar{r}$ is almost constant for the integration, equation (C1) is well approximated by

$$d\phi = \frac{A}{4\pi r^2} \cos \theta \frac{d\Gamma}{ds} ds \tag{C2}$$

If $\bar{A}$ and θ have the directions indicated in figure 5, $\bar{r}$ lies along $\bar{A}$ if θ is zero. With Γ positive as indicated in figure 5, the velocity through the vortex ring is opposite to $\bar{r}$ in direction and corresponds to that of a lifting rotor. The partial derivative of $d\phi$ with respect to r gives a negative velocity (for $\theta = 0$) as should exist on the axis of the vortex ring for the lifting rotor. Thus, the sign in equation (C2) is correct.

In order to express r and $\cos \theta$ in terms of x, y, z, and s, note that from figure 5, with $\bar{i},\bar{j},\bar{k}$ unit vectors in the directions of the X-, Y-, and Z-axes, respectively,

APPENDIX C

$$\bar{A} = \bar{i}A \sin \alpha + \bar{k}A \cos \alpha$$

and

$$\bar{r} = \bar{i}\left[x - s \sin(\chi - \alpha)\right] + \bar{j}y + \bar{k}\left[z + s \cos(\chi - \alpha)\right]$$

so that

$$r^2 = \left[x - s \sin(\chi - \alpha)\right]^2 + y^2 + \left[z + s \cos(\chi - \alpha)\right]^2$$

and

$$\cos \theta = \frac{\bar{A} \cdot \bar{r}}{Ar} = \frac{\left[x - s \sin(\chi - \alpha)\right]\sin \alpha}{r} + \frac{\left[z + s \cos(\chi - \alpha)\right]\cos \alpha}{r}$$

It follows that

$$d\phi = \frac{A \frac{d\Gamma}{ds} ds}{4\pi} \frac{\left[x - s \sin(\chi - \alpha)\right]\sin \alpha + \left[z + s \cos(\chi - \alpha)\right]\cos \alpha}{r^3} \tag{C3}$$

In reference 10 it is shown that the density $d\Gamma/ds$ of vortex strength along the cylindrical vortex sheet is numerically equal to the final induced velocity along the axis of the cylinder. It is also shown that this final induced velocity is numerically equal to the final induced velocity normal to the rotor disk. Moreover, the normal induced velocity at the disk is half that in the (final) far-distant wake. Thus, $d\Gamma/ds$ may be replaced with $2w_0$, where w_0 is the normal induced velocity at the rotor disk, positive for positive lift:

$$\frac{d\Gamma}{ds} = 2w_0 \tag{C4}$$

Equation (C3) may therefore be written as

$$d\phi = \frac{Aw_0}{2\pi} \frac{\left[x - s \sin(\chi - \alpha)\right]\sin \alpha + \left[z + s \cos(\chi - \alpha)\right]\cos \alpha}{r^3} ds \tag{C5}$$

Although the skew angle χ and the velocity w_0 induced at the rotor disk are the significant parameters of the helicopter wake, they cannot be specified independently of the wind-tunnel stream velocity V. According to equation (8) of reference 10, the parameters are related, in the notation of this paper, by

$$\frac{V}{w_0} = \frac{2 \tan \frac{\chi}{2}}{\cos(\chi - \alpha)} \tag{C6}$$

(Note that the angle α is here the negative of the angle designated α in ref. 10.) For skew angles other than zero, the induced velocitiy varies over the rotor disk, but w_0 may be regarded either as the induced velocity at the center or as the average of the induced velocities from front to rear over the diameter, since according to reference 10 these values are equal. The average induced velocity w_0 may be used in the Glauert relation to compute the thrust T:

APPENDIX C

$$T = 2\rho A V_R w_0$$

where V_R is the magnitude of the resultant of V and w_0 regarded as vectors.

In free air the vortex cylinder of figure 5 extends far below the lifting rotor; therefore, the velocity potential is found by integrating the expression (C5) over s from 0 to ∞. In the wind tunnel with open lower boundary, the rotor wake is assumed to pass out of the test stream and to have no further effect on the model. The possible consequences of this assumption have already been pointed out. Under this assumption part of the boundary interference is therefore represented by subtracting the potential (or the corresponding induced velocities) due to the part of the vortex cylinder extending below the open boundary as indicated by the dashed lines in figure 15.

The zero-pressure-disturbance condition at the open lower boundary, which corresponds to zero induced velocities in the direction of the tunnel stream at that boundary, is satisfied by a mirror reflection of the vortex cylinder across the boundary without change in sense of the vorticity. The original disturbance and its reflection across the open boundary make up a vortex cylinder cell. The solid-boundary condition is satisfied by a similar reflection, but with reversal of sense of the vorticity. The complete image system satisfying the boundary conditions at the upper and lower boundaries in a test section with solid upper boundary and open lower boundary and with the rotor at the center of the test section consists of a vertical row of vortex cylinder cells spaced at twice the test-section height h along the Z-axis as shown in figure 15. The image of the original disturbance reflected across that boundary is of the same sense as that in the subtracted part of the original vortex cylinder and may therefore be expected to provide some compensation for the loss. However, the upstream displacement of vorticity may result in distortion of the flow downstream from the rotor.

For a vortex ring lying on the image of the original disturbance vortex cylinder reflected across the open boundary, the element of potential (eq. (C5)) must be replaced with

$$d\phi' = \frac{Aw_0}{2\pi}\left\{\frac{-\left[x - s'\sin(\chi - \alpha)\right]\sin\alpha + \left[z + h - s'\cos(\chi - \alpha)\right]\cos\alpha}{r'^3}\right\} ds' \qquad (C7)$$

where

$$r'^2 = \left[x - s'\sin(\chi - \alpha)\right]^2 + y^2 + \left[z + h - s'\cos(\chi - \alpha)\right]^2$$

s' is the distance along the axis of the image in the open boundary starting from the point $(0,0,-h)$, and h is the test-section height.

The potential due to the original disturbance vortex cylinder and its image in the open boundary is obtained as the sum of the integrals of expressions (C5) and (C7), where s runs from 0 to its value at the open boundary and s' runs from 0 to its value at the

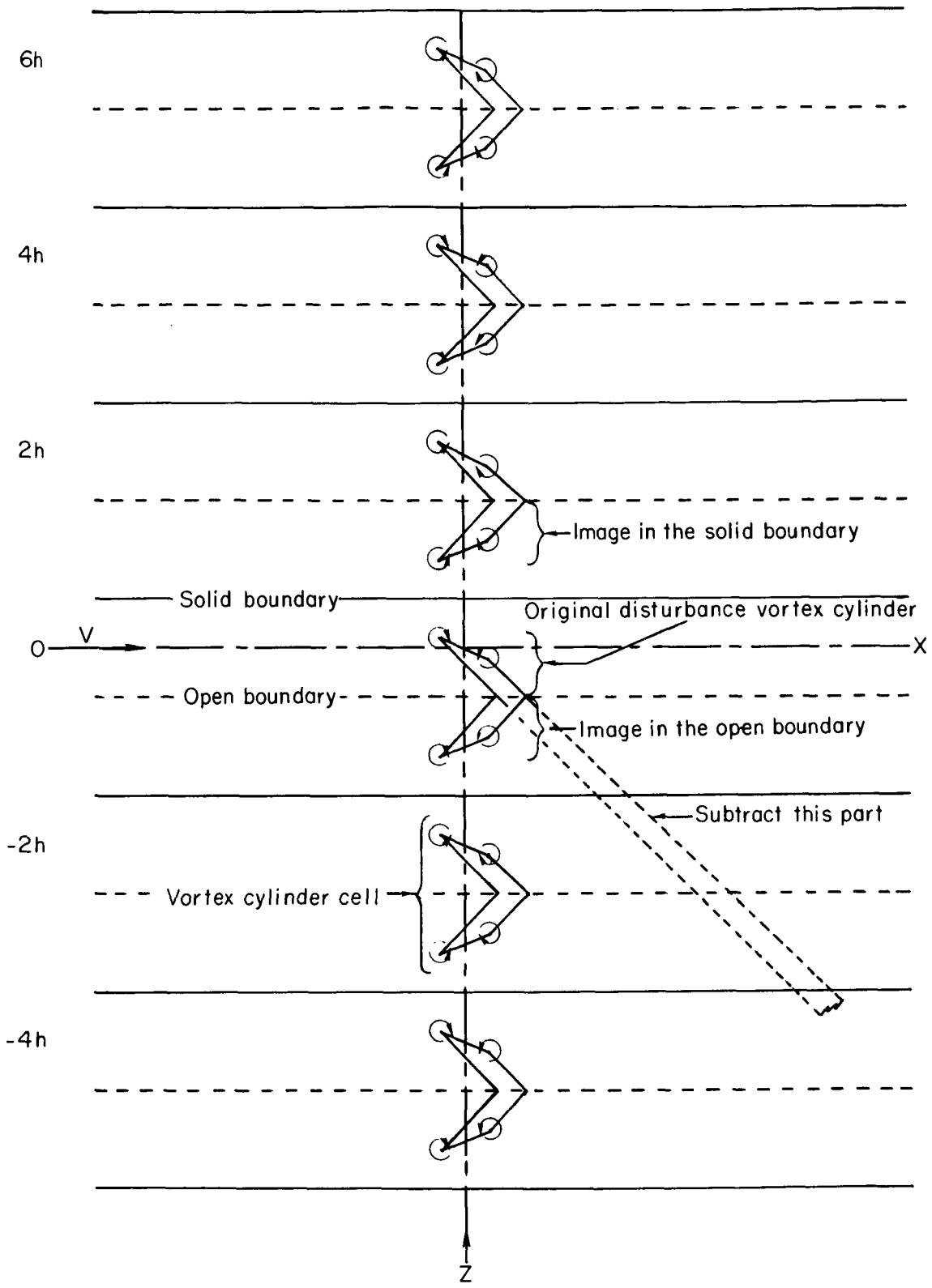

Figure 15.- Elliptic cylindrical vortex sheet image system satisfying boundary conditions for solid upper boundary and open lower boundary.

open boundary. This potential, designated ϕ_0, applies to the vortex cylinder cell nominally located at (0,0,0). The potential $\phi_{0,n}$ of the vortex cylinder cell nominally located at (0,0,2nh) is obtained by obviously similar integrations of

$$d\phi_n = (-1)^n \frac{Aw_0}{2\pi} \left(\frac{\left[x - s\sin(\chi - \alpha)\right]\sin\alpha + \left[z - 2nh + s\cos(\chi - \alpha)\right]\cos\alpha}{\left\{\sqrt{\left[x - s\sin(\chi - \alpha)\right]^2 + y^2 + \left[z - 2nh + s\cos(\chi - \alpha)\right]^2}\right\}^3} \right) ds \qquad (C8)$$

and

$$d\phi'_n = (-1)^n \frac{Aw_0}{2\pi} \left(\frac{-\left[x - s'\sin(\chi - \alpha)\right]\sin\alpha + \left[z - (2n - 1)h - s'\cos(\chi - \alpha)\right]\cos\alpha}{\left\{\sqrt{\left[x - s'\sin(\chi - \alpha)\right]^2 + y^2 + \left[z - (2n - 1)h - s'\cos(\chi - \alpha)\right]^2}\right\}^3} \right) ds' \qquad (C9)$$

where n takes on all positive and negative (as well as zero) integer values in the summation of ϕ_n over n to obtain the interference potential. However, because of the alternating signs only a few terms of the infinite summation on n should be required for practical convergence. To obtain the interference, the potential of the original disturbance vortex cylinder must be subtracted out of the summation. Thus, the potential of the whole semi-infinite vortex cylinder extending from the rotor must be subtracted. This potential is obtained by integrating expression (C5) on s from 0 to ∞.

The boundary condition at the slotted side walls must now be satisfied. It is sufficient to satisfy the side-wall boundary condition separately for every original or image differential element $d\phi_n$ and $d\phi'_n$ of the disturbance potential. The side-wall boundary condition is as in appendix B (eq. (B1)):

$$\phi \pm l \frac{\partial \phi}{\partial y} = 0 \qquad (C10)$$

where the positive sign applies at the boundary $y = \frac{b}{2}$ and the negative sign applies at the boundary $y = -\frac{b}{2}$ and where l is the restriction constant defined in appendix B (eq. (B2)).

To facilitate the solution, exponential Fourier transforms of $d\phi_n$ on $x - s\sin(\chi - \alpha)$ with variable of transformation ω and of $d\phi'_n$ on $x - s'\sin(\chi - \alpha)$ with variable of transformation ω' are taken. Then the following equations, corresponding to expressions (C8) and (C9), are given by formulas 7, page 11, and 27, page 66, of reference 15:

$$d\Omega_n = \frac{(-1)^n A w_0\, ds}{\pi}\left(-i(\sin\alpha)\omega K_0\left\{\omega\sqrt{y^2+\left[z-2nh+s\cos(\chi-\alpha)\right]^2}\right\}\right.$$

$$\left.+\left[z-2nh+s\cos(\chi-\alpha)\right](\cos\alpha)\,\frac{\omega K_1\left\{\omega\sqrt{y^2+\left[z-2nh+s\cos(\chi-\alpha)\right]^2}\right\}}{\sqrt{y^2+\left[z-2nh+s\cos(\chi-\alpha)\right]^2}}\right)$$

$$\left(\sqrt{y^2+\left[z-2nh+s\cos(\chi-\alpha)\right]^2}>0\right) \qquad \text{(C11)}$$

$$d\Omega'_n = \frac{(-1)^n A w_0\, ds'}{\pi}\left(i(\sin\alpha)\omega' K_0\left\{\omega'\sqrt{y^2+\left[z-(2n-1)h-s'\cos(\chi-\alpha)\right]^2}\right\}\right.$$

$$\left.+\left[z-(2n-1)h-s'\cos(\chi-\alpha)\right](\cos\alpha)\,\frac{\omega' K_1\left\{\omega'\sqrt{y^2+\left[z-(2n-1)h-s'\cos(\chi-\alpha)\right]^2}\right\}}{\sqrt{y^2+\left[z-(2n-1)h-s'\cos(\chi-\alpha)\right]^2}}\right)$$

$$\left(\sqrt{y^2+\left[z-(2n-1)h-s'\cos(\chi-\alpha)\right]^2}>0\right) \qquad \text{(C12)}$$

A second exponential Fourier transformation on $z - 2nh + s\cos(\chi - \alpha)$ with variable of transformation g and on $z - (2n - 1)h - s'\cos(\chi - \alpha)$ with variable of transformation g' gives by use of formula 43, page 56, and formula 43, page 112, of reference 15 the transforms corresponding to expressions (C11) and (C12),

$$dG_n = (-1)^n A w_0\, ds\left[\frac{-i(\sin\alpha)\omega e^{-|y|\sqrt{g^2+\omega^2}}}{\sqrt{g^2+\omega^2}} - \frac{i(\cos\alpha)g e^{-|y|\sqrt{\omega^2+g^2}}}{\sqrt{\omega^2+g^2}}\right]$$

$$\left(|y|>0;\ |\omega|>0\right) \qquad \text{(C13)}$$

$$dG'_n = (-1)^n A w_0\, ds'\left[\frac{i(\sin\alpha)\omega' e^{-|y|\sqrt{g'^2+\omega'^2}}}{\sqrt{g'^2+\omega'^2}} - \frac{i(\cos\alpha)g' e^{-|y|\sqrt{\omega'^2+g'^2}}}{\sqrt{\omega'^2+g'^2}}\right]$$

$$\left(|y|>0;\ |\omega'|>0\right) \qquad \text{(C14)}$$

APPENDIX C

The boundary condition (C10) transforms to

$$G \pm l \frac{\partial G}{\partial y} = 0 \tag{C15}$$

and the Laplace equation $\frac{\partial^2 \phi}{\partial x^2} + \frac{\partial^2 \phi}{\partial y^2} + \frac{\partial^2 \phi}{\partial z^2} = 0$ to

$$\frac{\partial^2 G}{\partial y^2} = \left(\omega^2 + g^2\right) G \tag{C16}$$

A solution having the required symmetry in y is

$$G(\omega, y, g) = B(\omega, g) \cosh\left(y\sqrt{\omega^2 + g^2}\right) \tag{C17}$$

and if $dG_{n,s} = B_s(\omega,g)\cosh\left(y\sqrt{\omega^2 + g^2}\right)$ is the influence of the slotted boundaries such that $\left(dG_n + dG_{n,s}\right)$ satisfies the boundary condition (eq. (C15)), it follows that at the boundary $y = \frac{b}{2}$,

$$B_s(\omega,g)\left[\cosh\left(\frac{b}{2}\sqrt{\omega^2 + g^2}\right) + l\sqrt{\omega^2 + g^2}\sinh\left(\frac{b}{2}\sqrt{\omega^2 + g^2}\right)\right]$$

$$= (-1)^n A w_0 \, ds \, ie^{-\frac{b}{2}\sqrt{\omega^2+g^2}} (\omega \sin\alpha + g\cos\alpha)\left(\frac{1}{\sqrt{\omega^2 + g^2}} - l\right)$$

Similarly, if $dG'_{n,s} = B'_s \cosh\left(y\sqrt{\omega'^2 + g'^2}\right)$, then

$$B'_s(\omega',g')\left[\cosh\left(\frac{b}{2}\sqrt{\omega'^2 + g'^2}\right) + l\sqrt{\omega'^2 + g'^2}\sinh\left(\frac{b}{2}\sqrt{\omega'^2 + g'^2}\right)\right]$$

$$= (-1)^n A w_0 \, ds' ie^{-\frac{b}{2}\sqrt{\omega'^2+g'^2}} (g'\cos\alpha - \omega'\sin\alpha)\left(\frac{1}{\sqrt{\omega'^2 + g'^2}} - l\right)$$

Satisfaction of the boundary condition at the boundary $y = -\frac{b}{2}$ yields exactly the same equations. It therefore follows that

$$B_s(\omega,g) = \frac{(-1)^n A w_0 \, ds \, ie^{-\frac{b}{2}\sqrt{\omega^2+g^2}} (\omega \sin\alpha + g\cos\alpha)\left(\frac{1}{\sqrt{\omega^2 + g^2}} - l\right)}{\cosh\left(\frac{b}{2}\sqrt{\omega^2 + g^2}\right) + l\sqrt{\omega^2 + g^2}\sinh\left(\frac{b}{2}\sqrt{\omega^2 + g^2}\right)} \qquad \left(|\omega| > 0\right) \tag{C18}$$

and

$$B'_S(\omega',g') = \frac{(-1)^n A w_0\, ds'\, ie^{-\frac{b}{2}\sqrt{\omega'^2+g'^2}}\,(g'\cos\alpha - \omega'\sin\alpha)\left(\frac{1}{\sqrt{\omega'^2+g'^2}} - l\right)}{\cosh\left(\frac{b}{2}\sqrt{\omega'^2+g'^2}\right) + l\sqrt{\omega'^2+g'^2}\sinh\left(\frac{b}{2}\sqrt{\omega'^2+g'^2}\right)} \qquad \left(|\omega'| > 0\right) \qquad \text{(C19)}$$

The transforms of the slotted-boundary interference potentials corresponding to the influence of the slotted boundaries on the differential disturbance potentials $d\phi_n$ and $d\phi'_n$ are now

$$dG_{n,s} = B_S(\omega,g)\cosh\left(y\sqrt{\omega^2+g^2}\right)$$

and

$$dG'_{n,s} = B'_S(\omega',g')\cosh\left(y\sqrt{\omega'^2+g'^2}\right)$$

where B_S and B'_S are given by equations (C18) and (C19), respectively. The corresponding differential interference potentials are

$$d\phi_{n,s} = \frac{(-1)^n A w_0\, ds}{4\pi^2} \lim_{\epsilon\to 0} i\left[\int_{-\infty}^{-\epsilon} + \int_{\epsilon}^{\infty}\right] d\omega \int_{-\infty}^{\infty} e^{i\left\{\omega\left[x - s\sin(\chi-\alpha)\right] + g\left[z - 2nh + s\cos(\chi-\alpha)\right]\right\}} e^{-\frac{b}{2}\sqrt{\omega^2+g^2}}$$

$$\times \frac{(\omega\sin\alpha + g\cos\alpha)\left(\frac{1}{\sqrt{\omega^2+g^2}} - l\right)}{\cosh\left(\frac{b}{2}\sqrt{\omega^2+g^2}\right) + l\sqrt{\omega^2+g^2}\sinh\left(\frac{b}{2}\sqrt{\omega^2+g^2}\right)} \cosh\left(y\sqrt{\omega^2+g^2}\right) dg \qquad (\epsilon > 0) \qquad \text{(C20)}$$

and

$$d\phi'_{n,s} = \frac{(-1)^n A w_0\, ds'}{4\pi^2} \lim_{\epsilon\to 0} i\left[\int_{-\infty}^{-\epsilon} + \int_{\epsilon}^{\infty}\right] d\omega' \int_{-\infty}^{\infty} e^{i\left\{\omega'\left[x - s'\sin(\chi-\alpha)\right] + g'\left[z - (2n-1)h - s'\cos(\chi-\alpha)\right]\right\}}$$

$$\times \frac{e^{-\frac{b}{2}\sqrt{\omega'^2+g'^2}}\,(g'\cos\alpha - \omega'\sin\alpha)\left(\frac{1}{\sqrt{\omega'^2+g'^2}} - l\right)\cosh\left(y\sqrt{\omega'^2+g'^2}\right)}{\cosh\left(\frac{b}{2}\sqrt{\omega'^2+g'^2}\right) + l\sqrt{\omega'^2+g'^2}\sinh\left(\frac{b}{2}\sqrt{\omega'^2+g'^2}\right)} dg' \qquad (\epsilon > 0) \qquad \text{(C21)}$$

APPENDIX C

In equations (C20) and (C21), $\left[\int_{-\infty}^{-\epsilon} + \int_{\epsilon}^{\infty}\right] d\omega$ means $\int_{-\infty}^{-\epsilon} d\omega + \int_{\epsilon}^{\infty} d\omega$. The limits evidently exist, at least for any finite value of l.

The velocities in the x-direction on the vertical center plane $y = 0$ are now

$$\frac{\partial\left(d\phi_{n,s}\right)}{\partial x} = \frac{(-1)^n A w_0\, ds}{4\pi^2} \int_{-\infty}^{\infty}\int_{-\infty}^{\infty} e^{i\left\{\omega\left[x - s\sin(\chi-\alpha)\right] + g\left[z - 2nh + s\cos(\chi-\alpha)\right]\right\}} e^{-\frac{b}{2}\sqrt{\omega^2+g^2}}$$

$$\times \frac{(\omega\sin\alpha + g\cos\alpha)\left(\omega l - \dfrac{\omega}{\sqrt{\omega^2+g^2}}\right)}{\cosh\left(\dfrac{b}{2}\sqrt{\omega^2+g^2}\right) + l\sqrt{\omega^2+g^2}\sinh\left(\dfrac{b}{2}\sqrt{\omega^2+g^2}\right)} d\omega\, dg \qquad \text{(C22)}$$

$$\frac{\partial\left(d\phi'_{n,s}\right)}{\partial x} = \frac{(-1)^n A w_0\, ds'}{4\pi^2} \int_{-\infty}^{\infty}\int_{-\infty}^{\infty} e^{i\left\{\omega'\left[x - s'\sin(\chi-\alpha)\right] + g'\left[z - (2n-1)h - s'\cos(\chi-\alpha)\right]\right\}}$$

$$\times \frac{e^{-\frac{b}{2}\sqrt{\omega'^2+g'^2}}(g'\cos\alpha - \omega'\sin\alpha)\left(\omega' l - \dfrac{\omega'}{\sqrt{\omega'^2+g'^2}}\right)}{\cosh\left(\dfrac{b}{2}\sqrt{\omega'^2+g'^2}\right) + l\sqrt{\omega'^2+g'^2}\sinh\left(\dfrac{b}{2}\sqrt{\omega'^2+g'^2}\right)} d\omega'\, dg' \qquad \text{(C23)}$$

The expressions for the velocities in the z-direction on the vertical plane are the same as equations (C22) and (C23) except that the quantities $\omega l - \dfrac{\omega}{\sqrt{\omega^2+g^2}}$ and $\omega' l - \dfrac{\omega'}{\sqrt{\omega'^2+g'^2}}$ are replaced by $gl - \dfrac{g}{\sqrt{\omega^2+g^2}}$ and $g' l - \dfrac{g'}{\sqrt{\omega'^2+g'^2}}$, respectively. To obtain the interference velocities due to the influence of the slotted side walls on a vortex cylinder cell, these expressions must be integrated over s and s', where s and s' run from 0 to $\dfrac{h}{2}\sec(\chi - \alpha)$. The integrations of expressions (C22) and (C23) on s give

APPENDIX C

$$\frac{\left(\partial\phi_{0,n}\right)_s}{\partial x} = \frac{\partial\left(\phi_n + \phi'_n\right)_s}{\partial x} = \frac{(-1)^n A w_0}{4\pi^2 i}\left(\int_{-\infty}^{\infty}\int_{-\infty}^{\infty} \frac{e^{i\left[\omega x + g(z-2nh)\right]} - e^{i\left\{\omega\left[x - \frac{h}{2}\tan(\chi-\alpha)\right] + g\left(z-2nh+\frac{h}{2}\right)\right\}}}{\omega\sin(\chi-\alpha) - g\cos(\chi-\alpha)}\right.$$

$$\times \frac{e^{-\frac{b}{2}\sqrt{\omega^2+g^2}}(\omega\sin\alpha + g\cos\alpha)\left(\omega l - \frac{\omega}{\sqrt{\omega^2+g^2}}\right)}{\cosh\left(\frac{b}{2}\sqrt{\omega^2+g^2}\right) + l\sqrt{\omega^2+g^2}\sinh\left(\frac{b}{2}\sqrt{\omega^2+g^2}\right)} d\omega\, dg$$

$$+ \int_{-\infty}^{\infty}\int_{-\infty}^{\infty} \frac{e^{i\left(\omega' x + g'\left[z-(2n-1)h\right]\right)} - e^{i\left\{\omega'\left[x-\frac{h}{2}\tan(\chi-\alpha)\right] + g'\left[z-(2n-1)h-\frac{h}{2}\right]\right\}}}{\omega'\sin(\chi-\alpha) + g'\cos(\chi-\alpha)}$$

$$\left.\times \frac{e^{-\frac{b}{2}\sqrt{\omega'^2+g'^2}}(g'\cos\alpha - \omega'\sin\alpha)\left(\omega' l - \frac{\omega'}{\sqrt{\omega'^2+g'^2}}\right)}{\cosh\left(\frac{b}{2}\sqrt{\omega'^2+g'^2}\right) + l\sqrt{\omega'^2+g'^2}\sinh\left(\frac{b}{2}\sqrt{\omega'^2+g'^2}\right)} d\omega'\, dg'\right) \qquad \text{(C24)}$$

An obviously similar equation holds for the interference velocity in the z-direction.

Equation (C24) and the similar equation for the velocity in the z-direction must be expanded into form suitable for computation as follows:

$$\frac{\partial\left(\phi_n + \phi'_n\right)_s}{\partial x} = \frac{(-1)^n A w_0}{\pi^2}\int_0^{\infty}\int_0^{\infty} \frac{e^{-\frac{b}{2}\sqrt{\omega^2+g^2}}\left(\omega l - \frac{\omega}{\sqrt{\omega^2+g^2}}\right)}{\cosh\left(\frac{b}{2}\sqrt{\omega^2+g^2}\right) + l\sqrt{\omega^2+g^2}\sinh\left(\frac{b}{2}\sqrt{\omega^2+g^2}\right)}$$

$$\left[\frac{\left[\omega^2\sin(\chi-\alpha)\sin\alpha + g^2\cos(\chi-\alpha)\cos\alpha\right]\left(\sin(\omega x)\cos\left[g(z-2nh)\right] - \sin\left\{\omega\left[x-\frac{h}{2}\tan(\chi-\alpha)\right]\right\}\cos\left[g\left(z-2nh+\frac{h}{2}\right)\right]\right) + \omega g\left[\sin(\chi-\alpha)\cos\alpha + \cos(\chi-\alpha)\sin\alpha\right]\left(\cos(\omega x)\sin\left[g(z-2nh)\right] - \cos\left\{\omega\left[x-\frac{h}{2}\tan(\chi-\alpha)\right]\right\}\sin\left[g\left(z-2nh+\frac{h}{2}\right)\right]\right)}{\omega^2\sin^2(\chi-\alpha) - g^2\cos^2(\chi-\alpha)}\right.$$

$$\left.+\frac{-\left[\omega^2\sin(\chi-\alpha)\sin\alpha + g^2\cos(\chi-\alpha)\cos\alpha\right]\left(\sin(\omega x)\cos\left\{g\left[z-(2n-1)h\right]\right\} - \sin\left\{\omega\left[x-\frac{h}{2}\tan(\chi-\alpha)\right]\right\}\cos\left\{g\left[z-(2n-1)h-\frac{h}{2}\right]\right\}\right) + \omega g\left[\sin(\chi-\alpha)\cos\alpha + \cos(\chi-\alpha)\sin\alpha\right]\left(\cos(\omega x)\sin\left\{g\left[z-(2n-1)h\right]\right\} - \cos\left\{\omega\left[x-\frac{h}{2}\tan(\chi-\alpha)\right]\right\}\sin\left\{g\left[z-(2n-1)h-\frac{h}{2}\right]\right\}\right)}{\omega^2\sin^2(\chi-\alpha) - g^2\cos^2(\chi-\alpha)}\right] d\omega\, dg \qquad \text{(C25)}$$

APPENDIX C

$$\frac{\partial(\phi_n + \phi_n')_s}{\partial z} = \frac{(-1)^n A w_0}{\pi^2} \int_0^{\infty} \int_0^{\infty} \frac{e^{-\frac{b}{2}\sqrt{\omega^2+g^2}}\left(gl - \frac{g}{\sqrt{\omega^2+g^2}}\right)}{\cosh\left(\frac{b}{2}\sqrt{\omega^2+g^2}\right) + l\sqrt{\omega^2+g^2}\sinh\left(\frac{b}{2}\sqrt{\omega^2+g^2}\right)} \left[\frac{\left[\omega^2\sin(\chi-\alpha)\sin\alpha + g^2\cos(\chi-\alpha)\cos\alpha\right]\left(\cos(\omega x)\sin\left[g(z-2nh)\right] - \cos\left\{\omega\left[x - \frac{h}{2}\tan(\chi-\alpha)\right]\right\}\sin\left[g\left(z - 2nh + \frac{h}{2}\right)\right]\right) + \omega g\left[\sin(\chi-\alpha)\cos\alpha + \cos(\chi-\alpha)\sin\alpha\right]\left(\sin(\omega x)\cos\left[g(z-2nh)\right] - \sin\left\{\omega\left[x - \frac{h}{2}\tan(\chi-\alpha)\right]\right\}\cos\left[g\left(z - 2nh + \frac{h}{2}\right)\right]\right)}{\omega^2\sin^2(\chi-\alpha) - g^2\cos^2(\chi-\alpha)} \right.$$

$$\left. + \frac{-\left[\omega^2\sin(\chi-\alpha)\sin\alpha + g^2\cos(\chi-\alpha)\cos\alpha\right]\left(\cos(\omega x)\sin\left\{g\left[z-(2n-1)h\right]\right\} - \cos\left\{\omega\left[x - \frac{h}{2}\tan(\chi-\alpha)\right]\right\}\sin\left\{g\left[z-(2n-1)h - \frac{h}{2}\right]\right\}\right) + \omega g\left[\sin(\chi-\alpha)\cos\alpha + \cos(\chi-\alpha)\sin\alpha\right]\left(\sin(\omega x)\cos\left\{g\left[z-(2n-1)h\right]\right\} - \sin\left\{\omega\left[x - \frac{h}{2}\tan(\chi-\alpha)\right]\right\}\cos\left\{g\left[z-(2n-1)h - \frac{h}{2}\right]\right\}\right)}{\omega^2\sin^2(\chi-\alpha) - g^2\cos^2(\chi-\alpha)} \right] d\omega\, dg \qquad \text{(C26)}$$

By equations (3) and (4)

$$\delta_{R,x} = \frac{u}{w_0}\frac{C}{A} \qquad \text{(C27)}$$

and

$$\delta_{R,z} = \frac{v}{w_0}\frac{C}{A} \qquad \text{(C28)}$$

where u and v are interference velocities in the x- and z-directions, respectively, and $C = hb$ is the cross-sectional area of the test section. Then with $p = \omega h$ and $q = gh$, the contributions $(\Delta\delta_{R,x})_{ns}$ and $(\Delta\delta_{R,z})_{ns}$ to $\delta_{R,x}$ and $\delta_{R,z}$, respectively, of the slotted-side-wall interference at $y = 0$, $z = 0$ on a vortex-cylinder cell are given by

$$(\Delta\delta_{R,x})_{ns} = \frac{(-1)^n}{\pi^2}\frac{b}{h} \int_0^{\infty} \int_0^{\infty} \frac{e^{-\frac{1}{2}\frac{b}{h}\sqrt{p^2+q^2}}\left(p\frac{l}{h} - \frac{p}{\sqrt{p^2+q^2}}\right)}{\cosh\left(\frac{1}{2}\frac{b}{h}\sqrt{p^2+q^2}\right) + \frac{l}{h}\sqrt{p^2+q^2}\sinh\left(\frac{1}{2}\frac{b}{h}\sqrt{p^2+q^2}\right)} \left[\frac{\left[p^2\sin(\chi-\alpha)\sin\alpha + q^2\cos(\chi-\alpha)\cos\alpha\right]\left(\sin\left(p\frac{x}{h}\right)\cos(2nq) - \sin\left\{p\left[\frac{x}{h} - \frac{1}{2}\tan(\chi-\alpha)\right]\right\}\cos\left[q\left(2n-\frac{1}{2}\right)\right]\right) - pq\left[\sin(\chi-\alpha)\cos\alpha + \cos(\chi-\alpha)\sin\alpha\right]\left(\cos\left(p\frac{x}{h}\right)\sin(2nq) - \cos\left\{p\left[\frac{x}{h} - \frac{1}{2}\tan(\chi-\alpha)\right]\right\}\sin\left[q\left(2n-\frac{1}{2}\right)\right]\right)}{p^2\sin^2(\chi-\alpha) - q^2\cos^2(\chi-\alpha)} \right.$$

$$\left. - \frac{\left[p^2\sin(\chi-\alpha)\sin\alpha + q^2\cos(\chi-\alpha)\cos\alpha\right]\left(\sin\left(p\frac{x}{h}\right)\cos\left[q(2n-1)\right] - \sin\left\{p\left[\frac{x}{h} - \frac{1}{2}\tan(\chi-\alpha)\right]\right\}\cos\left[q\left(2n-\frac{1}{2}\right)\right]\right) + pq\left[\sin(\chi-\alpha)\cos\alpha + \cos(\chi-\alpha)\sin\alpha\right]\left(\cos\left(p\frac{x}{h}\right)\sin\left[q(2n-1)\right] - \cos\left\{p\left[\frac{x}{h} - \frac{1}{2}\tan(\chi-\alpha)\right]\right\}\sin\left[q\left(2n-\frac{1}{2}\right)\right]\right)}{p^2\sin^2(\chi-\alpha) - q^2\cos^2(\chi-\alpha)} \right] dp\, dq \qquad \text{(C29)}$$

APPENDIX C

$$(\Delta\delta_{R,z})_{ns} = \frac{(-1)^n}{\pi^2}\frac{b}{h}\int_0^{\infty}\int_0^{\infty} \frac{e^{-\frac{1}{2}\frac{b}{h}\sqrt{p^2+q^2}}\left(q\frac{l}{h} - \frac{q}{\sqrt{p^2+q^2}}\right)}{\cosh\left(\frac{1}{2}\frac{b}{h}\sqrt{p^2+q^2}\right) + \frac{l}{h}\sqrt{p^2+q^2}\sinh\left(\frac{1}{2}\frac{b}{h}\sqrt{p^2+q^2}\right)} \left[\frac{\left[p^2\sin(\chi-\alpha)\sin\alpha + q^2\cos(\chi-\alpha)\cos\alpha\right]\left(\cos\left\{p\left[\frac{x}{h} - \frac{1}{2}\tan(\chi-\alpha)\right]\right\}\sin\left[q\left(2n-\frac{1}{2}\right)\right]\right.\right.$$

$$\left. - \cos\left(p\frac{x}{h}\right)\sin(2nq)\right) + pq\left[\sin(\chi-\alpha)\cos\alpha + \cos(\chi-\alpha)\sin\alpha\right]\left(\sin\left(p\frac{x}{h}\right)\cos(2nq)\right.$$

$$\left.\left. - \sin\left\{p\left[\frac{x}{h} - \frac{1}{2}\tan(\chi-\alpha)\right]\right\}\cos\left[q\left(2n-\frac{1}{2}\right)\right]\right)}{p^2\sin^2(\chi-\alpha) - q^2\cos^2(\chi-\alpha)}$$

$$+ \frac{\left[p^2\sin(\chi-\alpha)\sin\alpha + q^2\cos(\chi-\alpha)\cos\alpha\right]\left(\cos\left(p\frac{x}{h}\right)\sin\left[q(2n-1)\right] - \cos\left\{p\left[\frac{x}{h} - \frac{1}{2}\tan(\chi-\alpha)\right]\right\}\sin\left[q\left(2n-\frac{1}{2}\right)\right]\right) + pq\left[\sin(\chi-\alpha)\cos\alpha\right.}{\left. + \cos(\chi-\alpha)\sin\alpha\right]\left(\sin\left(p\frac{x}{h}\right)\cos\left[q(2n-1)\right] - \sin\left\{p\left[\frac{x}{h} - \frac{1}{2}\tan(\chi-\alpha)\right]\right\}\cos\left[q\left(2n-\frac{1}{2}\right)\right]\right)}{p^2\sin^2(\chi-\alpha) - q^2\cos^2(\chi-\alpha)}\Bigg] dp\,dq \qquad \text{(C30)}$$

For p and q both zero, the integrands in equations (C29) and (C30) are zero. For q approaching $\pm p\tan(\chi - \alpha)$, the limits exist, and since the functions are continuous, no difficulty should arise in integrating across the singularity provided proper attention is given to accuracy in the neighborhood of the singular point.

For the condition $p\sin(\chi - \alpha)$ approaching $\pm q\cos(\chi - \alpha)$, that is, $\frac{q}{p} = \pm\tan(\chi - \alpha)$, the quantities in braces in equations (C29) and (C30) become indeterminate and must be replaced as follows:

For $\tan(\chi - \alpha)$ positive and q/p approaching $\tan(\chi - \alpha)$, the quantities in braces $\{\}$ in equations (C29) and (C30), respectively, are replaced with

$$\left[\frac{q\cos\alpha + p\sin\alpha}{4\cos(\chi-\alpha)}\right]\left\{\cos\left(p\frac{x}{h} - 2nq\right) - \cos\left[p\frac{x}{h} + (2n-1)q\right]\right\}$$

$$+ \sin\left(p\frac{x}{h}\right)\left[\frac{q\cos\alpha - p\sin\alpha}{2q\cos(\chi-\alpha)}\right]\left\{\cos\left[(2n-1)q\right] - \cos(2nq)\right\} \qquad \text{(C31)}$$

and

$$\left[\frac{q\cos\alpha + p\sin\alpha}{4\cos(\chi-\alpha)}\right]\left\{\cos\left(p\frac{x}{h} - 2nq\right) + \cos\left[p\frac{x}{h} + (2n-1)q\right]\right\}$$

$$+ \cos\left(p\frac{x}{h}\right)\left[\frac{q\cos\alpha - p\sin\alpha}{2q\cos(\chi-\alpha)}\right]\left\{\sin(2nq) - \sin\left[(2n-1)q\right]\right\} \qquad \text{(C32)}$$

APPENDIX C

For $\tan(\chi - \alpha)$ negative and q/p approaching $-\tan(\chi - \alpha)$ the quantities in braces $\{\}$ in equations (C29) and (C30), respectively, are replaced with

$$\left[\frac{q\cos\alpha - p\sin\alpha}{4\cos(\chi - \alpha)}\right]\left\{\cos\left[p\frac{x}{h} - (2n - 1)q\right] - \cos\left(p\frac{x}{h} + 2nq\right)\right\}$$

$$+ \sin\left(p\frac{x}{h}\right)\left[\frac{q\cos\alpha + p\sin\alpha}{2q\cos(\chi - \alpha)}\right]\left\{\cos\left[(2n - 1)q\right] - \cos(2nq)\right\} \tag{C33}$$

and

$$\left[\frac{q\cos\alpha - p\sin\alpha}{4\cos(\chi - \alpha)}\right]\left\{\cos\left[p\frac{x}{h} - (2n - 1)q\right] + \cos\left(p\frac{x}{h} + 2nq\right)\right\}$$

$$+ \cos\left(p\frac{x}{h}\right)\left[\frac{q\cos\alpha + p\sin\alpha}{2q\cos(\chi - \alpha)}\right]\left\{\sin(2nq) - \sin\left[(2n - 1)q\right]\right\} \tag{C34}$$

For $\tan(\chi - \alpha) = 0$ and $q = 0$ the quantities in braces $\{\}$ in equations (C29) and (C30) are to be taken as zero for any value of p. The total contributions of the slotted side walls to the interference factors are obtained by summing expressions (C29) and (C30) over all values of n:

$$\left(\delta_{R,x}\right)_s = \sum_n \left(\Delta\delta_{R,x}\right)_{ns} \tag{C35}$$

$$\left(\delta_{R,z}\right)_s = \sum_n \left(\Delta\delta_{R,z}\right)_{ns} \tag{C36}$$

To these contributions of the slotted side walls must now be added those of the images in the closed top and in the open lower boundary. For this purpose, expressions (C5) and (C7) must be integrated over s and s', respectively.

For the integration of expression (C5) over the original disturbance vortex sheet extending from the rotor disk to the free boundary (see fig. 15) let

$$M_1 = \frac{Aw_0}{2\pi}\frac{\sin\alpha}{\cos(\chi - \alpha)} \tag{C37}$$

$$z_0 = s\cos(\chi - \alpha) \tag{C38}$$

Then

$$s = \frac{z_0}{\cos(\chi - \alpha)} \tag{C39}$$

$$s \sin(\chi - \alpha) = z_0 \tan(\chi - \alpha) \tag{C40}$$

and the potential corresponding to the first term in equation (C5) is

$$\phi_1 = M_1 \int_0^{h/2} \frac{\left[x - z_0 \tan(\chi - \alpha)\right] dz_0}{\left\{\left[x - z_0 \tan(\chi - \alpha)\right]^2 + y^2 + \left(z + z_0\right)^2\right\}^{3/2}} \tag{C41}$$

where h is the test-section height.

For the integration of the second term in expression (C5), let

$$M_2 = \frac{A w_0 \cos \alpha}{2\pi \cos(\chi - \alpha)} \tag{C42}$$

The integral is then

$$\phi_2 = M_2 \int_0^{h/2} \frac{\left(z + z_0\right) dz_0}{\left\{\left[x - z_0 \tan(\chi - \alpha)\right]^2 + y^2 + \left(z + z_0\right)^2\right\}^{3/2}} \tag{C43}$$

With

$$z_0' = s' \cos(\chi - \alpha) \tag{C44}$$

similar expressions are obtained for the terms of the potential of the image in the open boundary. (See fig. 15.) By integration of expression (C7)

$$\phi_1' = -M_1 \int_0^{h/2} \frac{\left[x - z_0' \tan(\chi - \alpha)\right] dz_0'}{\left\{\left[x - z_0' \tan(\chi - \alpha)\right]^2 + y^2 + \left(z + h - z_0'\right)^2\right\}^{3/2}} \tag{C45}$$

and

$$\phi_2' = M_2 \int_0^{h/2} \frac{\left(z + h - z_0'\right) dz_0'}{\left\{\left[x - z_0' \tan(\chi - \alpha)\right]^2 + y^2 + \left(z + h - z_0'\right)^2\right\}^{3/2}} \tag{C46}$$

The velocity potential of the vortex cylinder cell nominally located at (0,0,0) is thus

$$\phi_0 = \phi_1 + \phi_1' + \phi_2 + \phi_2' \tag{C47}$$

The potential $(-1)^n \phi_n$ of a vortex cylinder cell with vorticity of the same sense nominally located at (0,0,2nh) is obtained from equation (C47) by replacing z in the expressions for ϕ_1, ϕ_1', ϕ_2, and ϕ_2' with z - 2nh. The integrations to obtain ϕ_0 and the corresponding streamwise and vertical velocities follow.

APPENDIX C

$$\phi_0 = I_1 + I_2 + I_3 + I_4$$

where

$$\left.\begin{aligned}
I_1 &= \int_0^{h/2} \frac{(M_1 x + M_2 z)\,dz_0}{\left\{x^2 + y^2 + z^2 + 2\left[z - x\tan(\chi - \alpha)\right]z_0 + \left[1 + \tan^2(\chi - \alpha)\right]z_0^2\right\}^{3/2}} \\
I_2 &= \int_0^{h/2} \frac{\left[M_2 - M_1\tan(\chi - \alpha)\right]z_0\,dz_0}{\left\{x^2 + y^2 + z^2 + 2\left[z - x\tan(\chi - \alpha)\right]z_0 + \left[1 + \tan^2(\chi - \alpha)\right]z_0^2\right\}^{3/2}} \\
I_3 &= \int_0^{h/2} \frac{(M_2 z + M_2 h - M_1 x)\,dz_0'}{\left\{x^2 + y^2 + (z + h)^2 - 2\left[z + h + x\tan(\chi - \alpha)\right]z_0' + \left[1 + \tan^2(\chi - \alpha)\right]z_0'^2\right\}^{3/2}} \\
I_4 &= \int_0^{h/2} \frac{\left[M_1\tan(\chi - \alpha) - M_2\right]z_0'\,dz_0'}{\left\{x^2 + y^2 + (z + h)^2 - 2\left[z + h + x\tan(\chi - \alpha)\right]z_0' + \left[1 + \tan^2(\chi - \alpha)\right]z_0'^2\right\}^{3/2}}
\end{aligned}\right\} \quad \text{(C48)}$$

Then for x, y, and z not all zero in I_1 and I_2,

$$I_1 = \frac{2\left\{2\left[1 + \tan^2(\chi - \alpha)\right]z_0 + 2\left[z - x\tan(\chi - \alpha)\right]\right\}(M_1 x + M_2 z)}{\left\{4\left(x^2 + y^2 + z^2\right)\left[1 + \tan^2(\chi - \alpha)\right] - 4\left[z - x\tan(\chi - \alpha)\right]^2\right\}\left\{x^2 + y^2 + z^2 + 2\left[z - x\tan(\chi - \alpha)\right]z_0 + \left[1 + \tan^2(\chi - \alpha)\right]z_0^2\right\}^{1/2}}\Bigg]_0^{h/2}$$

$$= \frac{(M_1 x + M_2 z)\left\{\left[1 + \tan^2(\chi - \alpha)\right]\frac{h}{2} + \left[z - x\tan(\chi - \alpha)\right]\right\}}{\left\{\left(x^2 + y^2 + z^2\right)\left[1 + \tan^2(\chi - \alpha)\right] - \left[z - x\tan(\chi - \alpha)\right]^2\right\}\left\{x^2 + y^2 + z^2 + 2\left[z - x\tan(\chi - \alpha)\right]\frac{h}{2} + \left[1 + \tan^2(\chi - \alpha)\right]\frac{h^2}{4}\right\}^{1/2}}$$

$$- \frac{(M_1 x + M_2 z)\left[z - x\tan(\chi - \alpha)\right]}{\left\{\left(x^2 + y^2 + z^2\right)\left[1 + \tan^2(\chi - \alpha)\right] - \left[z - x\tan(\chi - \alpha)\right]^2\right\}\left(x^2 + y^2 + z^2\right)^{1/2}}$$

APPENDIX C

$$I_2 = -\frac{2\left[M_2 - M_1\tan(\chi-\alpha)\right]\left\{2\left[z - x\tan(\chi-\alpha)\right]z_0 + 2\left(x^2+y^2+z^2\right)\right\}}{\left\{4\left(x^2+y^2+z^2\right)\left[1+\tan^2(\chi-\alpha)\right] - 4\left[z - x\tan(\chi-\alpha)\right]^2\right\}\left\{x^2+y^2+z^2+2\left[z - x\tan(\chi-\alpha)\right]z_0 + \left[1+\tan^2(\chi-\alpha)\right]z_0^2\right\}^{1/2}}\Bigg]_0^{h/2}$$

$$= -\frac{\left[M_2 - M_1\tan(\chi-\alpha)\right]\left\{\left[z - x\tan(\chi-\alpha)\right]\frac{h}{2} + \left(x^2+y^2+z^2\right)\right\}}{\left\{\left(x^2+y^2+z^2\right)\left[1+\tan^2(\chi-\alpha)\right] - \left[z - x\tan(\chi-\alpha)\right]^2\right\}\left\{x^2+y^2+z^2+2\left[z - x\tan(\chi-\alpha)\right]\frac{h}{2} + \left[1+\tan^2(\chi-\alpha)\right]\frac{h^2}{4}\right\}^{1/2}}$$

$$+\frac{\left[M_2 - M_1\tan(\chi-\alpha)\right]\left(x^2+y^2+z^2\right)}{\left\{\left(x^2+y^2+z^2\right)\left[1+\tan^2(\chi-\alpha)\right] - \left[z - x\tan(\chi-\alpha)\right]^2\right\}\left(x^2+y^2+z^2\right)^{1/2}}$$

$$I_3 = \frac{2\left(M_2z + M_2h - M_1x\right)\left\{2\left[1+\tan^2(\chi-\alpha)\right]z_0' - 2\left[z+h+x\tan(\chi-\alpha)\right]\right\}}{\left\{4\left[x^2+y^2+(z+h)^2\right]\left[1+\tan^2(\chi-\alpha)\right] - 4\left[z+h+x\tan(\chi-\alpha)\right]^2\right\}\left\{x^2+y^2+(z+h)^2 - 2\left[z+h+x\tan(\chi-\alpha)\right]z_0' + \left[1+\tan^2(\chi-\alpha)\right]z_0'^2\right\}^{1/2}}\Bigg]_0^{h/2}$$

$$= \frac{\left(M_2z + M_2h - M_1x\right)\left\{\left[1+\tan^2(\chi-\alpha)\right]\frac{h}{2} - \left[z+h+x\tan(\chi-\alpha)\right]\right\}}{\left\{\left[x^2+y^2+(z+h)^2\right]\left[1+\tan^2(\chi-\alpha)\right] - \left[z+h+x\tan(\chi-\alpha)\right]^2\right\}\left\{x^2+y^2+(z+h)^2 - 2\left[z+h+x\tan(\chi+\alpha)\right]\frac{h}{2} + \left[1+\tan^2(\chi-\alpha)\right]\frac{h^2}{4}\right\}^{1/2}}$$

$$+\frac{\left(M_2z + M_2h - M_1x\right)\left[z+h+x\tan(\chi-\alpha)\right]}{\left\{\left[x^2+y^2+(z+h)^2\right]\left[1+\tan^2(\chi-\alpha)\right] - \left[z+h+x\tan(\chi-\alpha)\right]^2\right\}\left[x^2+y^2+(z+h)^2\right]^{1/2}}$$

$$I_4 = -\frac{2\left[M_1\tan(\chi-\alpha) - M_2\right]\left\{-2\left[z+h+x\tan(\chi-\alpha)\right]z_0' + 2\left[x^2+y^2+(z+h)^2\right]\right\}}{\left\{4\left[x^2+y^2+(z+h)^2\right]\left[1+\tan^2(\chi-\alpha)\right] - 4\left[z+h+x\tan(\chi-\alpha)\right]^2\right\}\left\{x^2+y^2+(z+h)^2 - 2\left[z+h+x\tan(\chi-\alpha)\right]z_0' + \left[1+\tan^2(\chi-\alpha)\right]z_0'^2\right\}^{1/2}}\Bigg]_0^{h/2}$$

$$= \frac{\left[M_1\tan(\chi-\alpha) - M_2\right]\left\{\left[z+h+x\tan(\chi-\alpha)\right]\frac{h}{2} - \left[x^2+y^2+(z+h)^2\right]\right\}}{\left\{\left[x^2+y^2+(z+h)^2\right]\left[1+\tan^2(\chi-\alpha)\right] - \left[z+h+x\tan(\chi-\alpha)\right]^2\right\}\left\{x^2+y^2+(z+h)^2 - 2\left[z+h+x\tan(\chi-\alpha)\right]\frac{h}{2} + \left[1+\tan^2(\chi-\alpha)\right]\frac{h^2}{4}\right\}^{1/2}}$$

$$+\frac{\left[M_1\tan(\chi-\alpha) - M_2\right]\left[x^2+y^2+(z+h)^2\right]}{\left\{\left[x^2+y^2+(z+h)^2\right]\left[1+\tan^2(\chi-\alpha)\right] - \left[z+h+x\tan(\chi-\alpha)\right]^2\right\}\left[x^2+y^2+(z+h)^2\right]^{1/2}}$$

Then

$$\phi_0 = I_1 + I_2 + I_3 + I_4$$

$$= \frac{(M_1x + M_2z)\left\{\left[1 + \tan^2(\chi - \alpha)\right]\frac{h}{2} + \left[z - x\tan(\chi - \alpha)\right]\right\} - \left[M_2 - M_1\tan(\chi - \alpha)\right]\left\{\left[z - x\tan(\chi - \alpha)\right]\frac{h}{2} + \left(x^2 + y^2 + z^2\right)\right\}}{\left[\left(x^2 + y^2\right) + 2xz\tan(\chi - \alpha) + \left(y^2 + z^2\right)\tan^2(\chi - \alpha)\right]\left\{\left[x - \frac{h}{2}\tan(\chi - \alpha)\right]^2 + y^2 + \left(z + \frac{h}{2}\right)^2\right\}^{1/2}}$$

$$+ \frac{\left[M_2 - M_1\tan(\chi - \alpha)\right]\left(x^2 + y^2 + z^2\right) - \left(M_1x + M_2z\right)\left[z - x\tan(\chi - \alpha)\right]}{\left[\left(x^2 + y^2\right) + 2xz\tan(\chi - \alpha) + \left(y^2 + z^2\right)\tan^2(\chi - \alpha)\right]\left(x^2 + y^2 + z^2\right)^{1/2}}$$

$$+ \frac{\left[M_2(z + h) - M_1x\right]\left\{\left[1 + \tan^2(\chi - \alpha)\right]\frac{h}{2} - \left[z + h + x\tan(\chi - \alpha)\right]\right\} - \left[M_2 - M_1\tan(\chi - \alpha)\right]\left\{\left[z + h + x\tan(\chi - \alpha)\right]\frac{h}{2} - \left[x^2 + y^2 + (z + h)^2\right]\right\}}{\left\{\left(x^2 + y^2\right) - 2x(z + h)\tan(\chi - \alpha) + \left[y^2 + (z + h)^2\right]\tan^2(\chi - \alpha)\right\}\left\{\left[x - \frac{h}{2}\tan(\chi - \alpha)\right]^2 + y^2 + \left(z + \frac{h}{2}\right)^2\right\}^{1/2}}$$

$$+ \frac{\left[M_1\tan(\chi - \alpha) - M_2\right]\left[x^2 + y^2 + (z + h)^2\right] - \left[M_1x - M_2(z + h)\right]\left[z + h + x\tan(\chi - \alpha)\right]}{\left\{\left(x^2 + y^2\right) - 2x(z + h)\tan(\chi - \alpha) + \left[y^2 + (z + h)^2\right]\tan^2(\chi - \alpha)\right\}\left[x^2 + y^2 + (z + h)^2\right]^{1/2}}$$

and the corresponding vertical velocity is

$$\frac{\partial\phi_0}{\partial z} = \frac{M_1\left[x + \left(2z + \frac{h}{2}\right)\tan(\chi - \alpha)\right] - M_2\left[x - \frac{h}{2}\tan(\chi - \alpha)\right]\tan(\chi - \alpha)}{\left[\left(x^2 + y^2\right) + 2xz\tan(\chi - \alpha) + \left(y^2 + z^2\right)\tan^2(\chi - \alpha)\right]\left\{\left[x - \frac{h}{2}\tan(\chi - \alpha)\right]^2 + y^2 + \left(z + \frac{h}{2}\right)^2\right\}^{1/2}}$$

$$- \frac{\left[\begin{array}{l}\left\{M_1\left[\left(z + \frac{h}{2}\right)x + \frac{h}{2}z\tan(\chi - \alpha) + \left(y^2 + z^2\right)\tan(\chi - \alpha)\right] + M_2\left[\left(\frac{h}{2} - z\right)x\tan(\chi - \alpha) + \frac{h}{2}z\tan^2(\chi - \alpha) - x^2 - y^2\right]\right\} \\ \times\left(\left[2x\tan(\chi - \alpha) + 2z\tan^2(\chi - \alpha)\right]\left\{\left[x - \frac{h}{2}\tan(\chi - \alpha)\right]^2 + y^2 + \left(z + \frac{h}{2}\right)^2\right\} + \left[x^2 + y^2 + 2xz\tan(\chi - \alpha) + \left(y^2 + z^2\right)\tan^2(\chi - \alpha)\right]\left(z + \frac{h}{2}\right)\right)\end{array}\right]}{\left[\left(x^2 + y^2\right) + 2xz\tan(\chi - \alpha) + \left(y^2 + z^2\right)\tan^2(\chi - \alpha)\right]^2\left\{\left[x - \frac{h}{2}\tan(\chi - \alpha)\right]^2 + y^2 + \left(z + \frac{h}{2}\right)^2\right\}^{3/2}}$$

$$+ \frac{M_2x\tan(\chi - \alpha) - M_1\left[x + 2z\tan(\chi - \alpha)\right]}{\left[\left(x^2 + y^2\right) + 2xz\tan(\chi - \alpha) + \left(y^2 + z^2\right)\tan^2(\chi - \alpha)\right]\left(x^2 + y^2 + z^2\right)^{1/2}}$$

$$- \frac{\left[\begin{array}{l}\left\{M_1\left[-xz - \left(y^2 + z^2\right)\tan(\chi - \alpha)\right] + M_2\left[x^2 + y^2 + xz\tan(\chi - \alpha)\right]\right\}\left\{\left[2x\tan(\chi - \alpha) + 2z\tan^2(\chi - \alpha)\right]\left[x^2 + y^2 + z^2\right]\right. \\ \left. + z\left[\left(x^2 + y^2\right) + 2xz\tan(\chi - \alpha) + \left(y^2 + z^2\right)\tan^2(\chi - \alpha)\right]\right\}\end{array}\right]}{\left[\left(x^2 + y^2\right) + 2xz\tan(\chi - \alpha) + \left(y^2 + z^2\right)\tan^2(\chi - \alpha)\right]^2\left(x^2 + y^2 + z^2\right)^{3/2}}$$

(Equation continued on next page)

$$+\frac{M_1\left[x-\left(2z+\frac{3}{2}h\right)\tan(\chi-\alpha)\right]+M_2\left[\frac{h}{2}\tan(\chi-\alpha)-x\right]\tan(\chi-\alpha)}{\left\{x^2+y^2-2x(z+h)\tan(\chi-\alpha)+\left[y^2+(z+h)^2\right]\tan^2(\chi-\alpha)\right\}\left\{\left[x-\frac{h}{2}\tan(\chi-\alpha)\right]^2+y^2+\left(z+\frac{h}{2}\right)^2\right\}^{1/2}}$$

$$-\frac{\left[\begin{array}{l}\left\{M_1\left[\left(z+\frac{h}{2}\right)x-(z+h)\left(z+\frac{h}{2}\right)\tan(\chi-\alpha)-y^2\tan(\chi-\alpha)\right]+M_2\left[(z+h)\frac{h}{2}\tan^2(\chi-\alpha)-\left(z+3\frac{h}{2}\right)x\tan(\chi-\alpha)+x^2+y^2\right]\right\}\\ \times\left\{\left[-2x\tan(\chi-\alpha)+2(z+h)\tan^2(\chi-\alpha)\right]\left\{\left[x-\frac{h}{2}\tan(\chi-\alpha)\right]^2+y^2+\left(z+\frac{h}{2}\right)^2\right\}\right.\\ \left.+\left\{\left(x^2+y^2\right)-2x(z+h)\tan(\chi-\alpha)+\left[y^2+(z+h)^2\right]\tan^2(\chi-\alpha)\right\}\left(z+\frac{h}{2}\right)\right\}\end{array}\right]}{\left\{\left(x^2+y^2\right)-2x(z+h)\tan(\chi-\alpha)+\left[y^2+(z+h)^2\right]\tan^2(\chi-\alpha)\right\}^2\left\{\left[x-\frac{h}{2}\tan(\chi-\alpha)\right]^2+y^2+\left(z+\frac{h}{2}\right)^2\right\}^{3/2}}$$

$$+\frac{M_2x\tan(\chi-\alpha)-M_1\left[x-2(z+h)\tan(\chi-\alpha)\right]}{\left\{\left(x^2+y^2\right)-2x(z+h)\tan(\chi-\alpha)+\left[y^2+(z+h)^2\right]\tan^2(\chi-\alpha)\right\}\left[x^2+y^2+(z+h)^2\right]^{1/2}}$$

$$-\frac{\left[\begin{array}{l}\left(M_1\left\{\left[y^2+(z+h)^2\right]\tan(\chi-\alpha)-(z+h)x\right\}+M_2\left[(z+h)x\tan(\chi-\alpha)-x^2-y^2\right]\right)\left(\left[-2x\tan(\chi-\alpha)+2(z+h)\tan^2(\chi-\alpha)\right]\right.\\ \left.\times\left[x^2+y^2+(z+h)^2\right]+(z+h)\left\{\left(x^2+y^2\right)-2x(z+h)\tan(\chi-\alpha)+\left[y^2+(z+h)^2\right]\tan^2(\chi-\alpha)\right\}\right)\end{array}\right]}{\left\{\left(x^2+y^2\right)-2x(z+h)\tan(\chi-\alpha)+\left[y^2+(z+h)^2\right]\tan^2(\chi-\alpha)\right\}^2\left[x^2+y^2+(z+h)^2\right]^{3/2}}$$

The induced velocity in the direction of the tunnel stream is

$$\left[\frac{\partial\phi_0}{\partial x}\right]_{x=0}=\frac{M_1\left(z+\frac{h}{2}\right)-M_2\left(z-\frac{h}{2}\right)\tan(\chi-\alpha)}{\left[y^2+\left(y^2+z^2\right)\tan^2(\chi-\alpha)\right]\left[\frac{h^2}{4}\tan^2(\chi-\alpha)+y^2+\left(z+\frac{h}{2}\right)^2\right]^{1/2}}$$

$$-\frac{\left[\begin{array}{l}\left\{M_1\left(\frac{h}{2}z+y^2+z^2\right)\tan(\chi-\alpha)+M_2\left[\frac{h}{2}z\tan^2(\chi-\alpha)-y^2\right]\right\}\\ \times\left\{2z\left[\frac{h^2}{4}\tan^2(\chi-\alpha)+y^2+\left(z+\frac{h}{2}\right)^2\right]\tan(\chi-\alpha)-\frac{h}{2}\left[y^2+\left(y^2+z^2\right)\tan^2(\chi-\alpha)\right]\tan(\chi-\alpha)\right\}\end{array}\right]}{\left[y^2+\left(y^2+z^2\right)\tan^2(\chi-\alpha)\right]^2\left[\frac{h^2}{4}\tan^2(\chi-\alpha)+y^2+\left(z+\frac{h}{2}\right)^2\right]^{3/2}}$$

(Equation continued on next page)

APPENDIX C

$$+\frac{M_2 z\tan(\chi-\alpha)-M_1 z}{\left[y^2+\left(y^2+z^2\right)\tan^2(\chi-\alpha)\right]\left(y^2+z^2\right)^{1/2}}-\frac{2z\left\{M_2y^2-M_1\left[\left(y^2+z^2\right)\tan(\chi-\alpha)\right]\right\}\tan(\chi-\alpha)}{\left[y^2+\left(y^2+z^2\right)\tan^2(\chi-\alpha)\right]^2\left(y^2+z^2\right)^{1/2}}$$

$$+\frac{M_1\left(z+\frac{h}{2}\right)-M_2\left(z+\frac{3h}{2}\right)\tan(\chi-\alpha)}{\left\{y^2+\left[y^2+(z+h)^2\right]\tan^2(\chi-\alpha)\right\}\left[\frac{h^2}{4}\tan^2(\chi-\alpha)+y^2+\left(z+\frac{h}{2}\right)^2\right]^{1/2}}$$

$$-\frac{\left[\left\{M_1\left[\frac{h}{2}(z+h)-y^2-(z+h)^2\right]\tan(\chi-\alpha)+M_2\left[\frac{h}{2}(z+h)\tan^2(\chi-\alpha)+y^2\right]\right\}\times\left(-2(z+h)\left[\frac{h^2}{4}\tan^2(\chi-\alpha)+y^2+\left(z+\frac{h}{2}\right)^2\right]-\frac{h}{2}\left\{y^2+\left[y^2+(z+h)^2\right]\tan^2(\chi-\alpha)\right\}\right)\tan(\chi-\alpha)\right]}{\left\{y^2+\left[y^2+(z+h)^2\right]\tan^2(\chi-\alpha)\right\}^2\left[\frac{h^2}{4}\tan^2(\chi-\alpha)+y^2+\left(z+\frac{h}{2}\right)^2\right]^{3/2}}$$

$$+\frac{M_2(z+h)\tan(\chi-\alpha)-M_1(z+h)}{\left\{y^2+\left[y^2+(z+h)^2\right]\tan^2(\chi-\alpha)\right\}\left[y^2+(z+h)^2\right]^{1/2}}-\frac{\left\{M_1\left[y^2+(z+h)^2\right]\tan(\chi-\alpha)-M_2y^2\right\}\left[-2(z+h)\tan(\chi-\alpha)\right]}{\left\{y^2+\left[y^2+(z+h)^2\right]\tan^2(\chi-\alpha)\right\}^2\left[y^2+(z+h)^2\right]^{1/2}}$$

In form for computation on substituting for M_1 and M_2 from equations (C37) and (C42)

$$\frac{1}{w_0}\frac{hb}{A}\left(\frac{\partial\phi_0}{\partial x}\right)_{x=0}=\frac{b}{h}\frac{1}{2\pi\cos(\chi-\alpha)}\left(\frac{\left(\frac{z}{h}+\frac{1}{2}\right)\sin\alpha-\left(\frac{z}{h}-\frac{1}{2}\right)\tan(\chi-\alpha)\cos\alpha}{\left\{\left(\frac{y}{h}\right)^2+\left[\left(\frac{y}{h}\right)^2+\left(\frac{z}{h}\right)^2\right]\tan^2(\chi-\alpha)\right\}\left\{\frac{1}{4}\tan^2(\chi-\alpha)+\left(\frac{y}{h}\right)^2+\left[\left(\frac{z}{h}\right)-\frac{1}{2}\right]^2\right\}^{1/2}}\right.$$

$$\left.-\frac{\left[\left\{\left[\frac{1}{2}\frac{z}{h}+\left(\frac{y}{h}\right)^2+\left(\frac{z}{h}\right)^2\right]\tan(\chi-\alpha)\sin\alpha+\left[\frac{1}{2}\frac{z}{h}\tan^2(\chi-\alpha)-\left(\frac{y}{h}\right)^2\right]\cos\alpha\right\}\times\left(2\frac{z}{h}\left[\frac{1}{4}\tan^2(\chi-\alpha)+\left(\frac{y}{h}\right)^2+\left(\frac{z}{h}+\frac{1}{2}\right)^2\right]\tan(\chi-\alpha)-\frac{1}{2}\left\{\left(\frac{y}{h}\right)^2+\left[\left(\frac{y}{h}\right)^2+\left(\frac{z}{h}\right)^2\right]\tan^2(\chi-\alpha)\right\}\tan(\chi-\alpha)\right)\right]}{\left\{\left(\frac{y}{h}\right)^2+\left[\left(\frac{y}{h}\right)^2+\left(\frac{z}{h}\right)^2\right]\tan^2(\chi-\alpha)\right\}^2\left[\frac{1}{4}\tan^2(\chi-\alpha)+\left(\frac{y}{h}\right)^2+\left(\frac{z}{h}+\frac{1}{2}\right)^2\right]^{3/2}}\right)$$

$$+\frac{\frac{z}{h}\left[\tan(\chi-\alpha)\cos\alpha-\sin\alpha\right]}{\left\{\left(\frac{y}{h}\right)^2+\left[\left(\frac{y}{h}\right)^2+\left(\frac{z}{h}\right)^2\right]\tan^2(\chi-\alpha)\right\}\left[\left(\frac{y}{h}\right)^2+\left(\frac{z}{h}\right)^2\right]^{1/2}}-\frac{2\frac{z}{h}\left\{\left(\frac{y}{h}\right)^2\cos\alpha-\left[\left(\frac{y}{h}\right)^2+\left(\frac{z}{h}\right)^2\right]\tan(\chi-\alpha)\sin\alpha\right\}\tan(\chi-\alpha)}{\left\{\left(\frac{y}{h}\right)^2+\left[\left(\frac{y}{h}\right)^2+\left(\frac{z}{h}\right)^2\right]\tan^2(\chi-\alpha)\right\}^2\left[\left(\frac{y}{h}\right)^2+\left(\frac{z}{h}\right)^2\right]^{1/2}}$$

(Equation continued on next page)

$$+\frac{\left[\left(\frac{z}{h}\right)+\frac{1}{2}\right]\sin\alpha-\left(\frac{z}{h}+\frac{3}{2}\right)\tan(\chi-\alpha)\cos\alpha}{\left\{\left(\frac{y}{h}\right)^2+\left[\left(\frac{y}{h}\right)^2+\left(\frac{z}{h}+1\right)^2\right]\tan^2(\chi-\alpha)\right\}\left[\frac{1}{4}\tan^2(\chi-\alpha)+\left(\frac{y}{h}\right)^2+\left(\frac{z}{h}+\frac{1}{2}\right)^2\right]^{1/2}}$$

$$-\frac{\left[\left\{\left[\frac{1}{2}\left(\frac{z}{h}+1\right)-\left(\frac{y}{h}\right)^2-\left(\frac{z}{h}+1\right)^2\right]\tan(\chi-\alpha)\sin\alpha+\left[\frac{1}{2}\left(\frac{z}{h}+1\right)\tan^2(\chi-\alpha)+\left(\frac{y}{h}\right)^2\right]\cos\alpha\right\}\right.}{\left\{\left(\frac{y}{h}\right)^2+\left[\left(\frac{y}{h}\right)^2+\left(\frac{z}{h}+1\right)^2\right]\tan^2(\chi-\alpha)\right\}^2\left[\frac{1}{4}\tan^2(\chi-\alpha)+\left(\frac{y}{h}\right)^2+\left(\frac{z}{h}+\frac{1}{2}\right)^2\right]^{3/2}}$$

$$\left.\times\left(-2\left(\frac{z}{h}+1\right)\left[\frac{1}{4}\tan^2(\chi-\alpha)+\left(\frac{y}{h}\right)^2+\left(\frac{z}{h}+\frac{1}{2}\right)^2\right]-\frac{1}{2}\left\{\left(\frac{y}{h}\right)^2+\left[\left(\frac{y}{h}\right)^2+\left(\frac{z}{h}+1\right)^2\right]\tan^2(\chi-\alpha)\right\}\right)\tan(\chi-\alpha)\right]$$

$$+\frac{\left(\frac{z}{h}+1\right)\tan(\chi-\alpha)\cos\alpha-\left(\frac{z}{h}+1\right)\sin\alpha}{\left\{\left(\frac{y}{h}\right)^2+\left[\left(\frac{y}{h}\right)^2+\left(\frac{z}{h}+1\right)^2\right]\tan^2(\chi-\alpha)\right\}\left[\left(\frac{y}{h}\right)^2+\left(\frac{z}{h}+1\right)^2\right]^{1/2}}-\frac{\left\{\left[\left(\frac{y}{h}\right)^2+\left(\frac{z}{h}+1\right)^2\right]\tan(\chi-\alpha)\sin\alpha-\left(\frac{y}{h}\right)^2\cos\alpha\right\}\left[-2\left(\frac{z}{h}+1\right)\tan(\chi-\alpha)\right]}{\left\{\left(\frac{y}{h}\right)^2+\left[\left(\frac{y}{h}\right)^2+\left(\frac{z}{h}+1\right)^2\right]\tan^2(\chi-\alpha)\right\}^2\left[\left(\frac{y}{h}\right)^2+\left(\frac{z}{h}+1\right)^2\right]^{1/2}}\Bigg) \quad \text{(C49)}$$

For the condition $y/h = 0$ with $\tan(\chi - \alpha) = 0$ the right-hand side of equation (C49) must be replaced with

$$\frac{b}{h}\frac{1}{2\pi\cos(\chi-\alpha)}\frac{\sin\alpha}{2}\left\{\frac{z/h}{\left[\left(\frac{z}{h}\right)^2\right]^{3/2}}-\frac{2\left(\frac{z}{h}+\frac{1}{2}\right)}{\left[\left(\frac{z}{h}+\frac{1}{2}\right)^2\right]^{3/2}}+\frac{\left(\frac{z}{h}+1\right)}{\left[\left(\frac{z}{h}+1\right)^2\right]^{3/2}}\right\} \quad \text{(C50)}$$

Similarly, provided not all x, y, and z values are zero,

$$\frac{1}{w_0}\frac{hb}{A}\frac{\partial\phi_0}{\partial z}\left(\frac{x}{h},\frac{y}{h},\frac{z}{h}\right)=\frac{b}{h}\frac{1}{2\pi\cos(\chi-\alpha)}\left[\frac{\left[\frac{x}{h}+\left(2\frac{z}{h}+\frac{1}{2}\right)\tan(\chi-\alpha)\right]\sin\alpha-\left[\frac{x}{h}-\frac{1}{2}\tan(\chi-\alpha)\right]\tan(\chi-\alpha)\cos\alpha}{\left\{\left(\frac{x}{h}\right)^2+\left(\frac{y}{h}\right)^2+2\frac{x}{h}\frac{z}{h}\tan(\chi-\alpha)+\left[\left(\frac{y}{h}\right)^2+\left(\frac{z}{h}\right)^2\right]\tan^2(\chi-\alpha)\right\}\left\{\left[\frac{x}{h}-\frac{1}{2}\tan(\chi-\alpha)\right]^2+\left(\frac{y}{h}\right)^2+\left(\frac{z}{h}+\frac{1}{2}\right)^2\right\}^{1/2}}\right.$$

(Equation continued on next page)

APPENDIX C

$$
\begin{aligned}
&\left[\left(\left\{\left(\frac{z}{h}+\frac{1}{2}\right)\frac{x}{h}+\frac{1}{2}\frac{z}{h}\tan(\chi-\alpha)+\left[\left(\frac{y}{h}\right)^2+\left(\frac{z}{h}\right)^2\right]\tan(\chi-\alpha)\right\}\sin\alpha+\left[\left(\frac{1}{2}-\frac{z}{h}\right)\frac{x}{h}\tan(\chi-\alpha)+\frac{1}{2}\frac{z}{h}\tan^2(\chi-\alpha)-\left(\frac{x}{h}\right)^2-\left(\frac{y}{h}\right)^2\right]\cos\alpha\right)\right.\\
&\times\left(\left[2\frac{x}{h}\tan(\chi-\alpha)+2\frac{z}{h}\tan^2(\chi-\alpha)\right]\left\{\left[\frac{x}{h}-\frac{1}{2}\tan(\chi-\alpha)\right]^2+\left(\frac{y}{h}\right)^2+\left(\frac{z}{h}+\frac{1}{2}\right)^2\right\}+\left\{\left(\frac{x}{h}\right)^2+\left(\frac{y}{h}\right)^2+2\frac{x}{h}\frac{z}{h}\tan(\chi-\alpha)\right.\right.\\
&\left.\left.\left.+\left[\left(\frac{y}{h}\right)^2+\left(\frac{z}{h}\right)^2\right]\tan^2(\chi-\alpha)\right\}\left(\frac{z}{h}+\frac{1}{2}\right)\right)\right]\\
&\Big/\left\{\left(\frac{x}{h}\right)^2+\left(\frac{y}{h}\right)^2+2\frac{x}{h}\frac{z}{h}\tan(\chi-\alpha)+\left[\left(\frac{y}{h}\right)^2+\left(\frac{z}{h}\right)^2\right]\tan^2(\chi-\alpha)\right\}^2\left\{\left[\frac{x}{h}-\frac{1}{2}\tan(\chi-\alpha)\right]^2+\left(\frac{y}{h}\right)^2+\left(\frac{z}{h}+\frac{1}{2}\right)^2\right\}^{3/2}\\
&+\frac{\frac{x}{h}\tan(\chi-\alpha)\cos\alpha-\left[\frac{x}{h}+2\frac{z}{h}\tan(\chi-\alpha)\right]\sin\alpha}{\left\{\left(\frac{x}{h}\right)^2+\left(\frac{y}{h}\right)^2+2\frac{x}{h}\frac{z}{h}\tan(\chi-\alpha)+\left[\left(\frac{y}{h}\right)^2+\left(\frac{z}{h}\right)^2\right]\tan^2(\chi-\alpha)\right\}\left[\left(\frac{x}{h}\right)^2+\left(\frac{y}{h}\right)^2+\left(\frac{z}{h}\right)^2\right]^{1/2}}\\
&+\left[\left(\left\{\frac{x}{h}\frac{z}{h}+\left[\left(\frac{y}{h}\right)^2+\left(\frac{z}{h}\right)^2\right]\tan(\chi-\alpha)\right\}\sin\alpha-\left[\left(\frac{x}{h}\right)^2+\left(\frac{y}{h}\right)^2+\frac{x}{h}\frac{z}{h}\tan(\chi-\alpha)\right]\cos\alpha\right)\left(\left[2\frac{x}{h}\tan(\chi-\alpha)+2\frac{z}{h}\tan^2(\chi-\alpha)\right]\right.\right.\\
&\left.\left.\times\left[\left(\frac{x}{h}\right)^2+\left(\frac{y}{h}\right)^2+\left(\frac{z}{h}\right)^2\right]+\frac{z}{h}\left\{\left(\frac{x}{h}\right)^2+\left(\frac{y}{h}\right)^2+2\frac{x}{h}\frac{z}{h}\tan(\chi-\alpha)+\left[\left(\frac{y}{h}\right)^2+\left(\frac{z}{h}\right)^2\right]\tan^2(\chi-\alpha)\right\}\right)\right]\\
&\Big/\left\{\left(\frac{x}{h}\right)^2+\left(\frac{y}{h}\right)^2+2\frac{x}{h}\frac{z}{h}\tan(\chi-\alpha)+\left[\left(\frac{y}{h}\right)^2+\left(\frac{z}{h}\right)^2\right]\tan^2(\chi-\alpha)\right\}^2\left[\left(\frac{x}{h}\right)^2+\left(\frac{y}{h}\right)^2+\left(\frac{z}{h}\right)^2\right]^{3/2}\\
&+\frac{\left[\frac{x}{h}-\left(2\frac{z}{h}+\frac{3}{2}\right)\tan(\chi-\alpha)\right]\sin\alpha+\left[\frac{1}{2}\tan(\chi-\alpha)-\frac{x}{h}\right]\tan(\chi-\alpha)\cos\alpha}{\left\{\left(\frac{x}{h}\right)^2+\left(\frac{y}{h}\right)^2-2\frac{x}{h}\left(\frac{z}{h}+1\right)\tan(\chi-\alpha)+\left[\left(\frac{y}{h}\right)^2+\left(\frac{z}{h}+1\right)^2\right]\tan^2(\chi-\alpha)\right\}\left\{\left[\frac{x}{h}-\frac{1}{2}\tan(\chi-\alpha)\right]^2+\left(\frac{y}{h}\right)^2+\left(\frac{z}{h}+\frac{1}{2}\right)^2\right\}^{1/2}}\\
&\left[\left\{\left[\left(\frac{z}{h}+\frac{1}{2}\right)\frac{x}{h}-\left(\frac{z}{h}+1\right)\left(\frac{z}{h}+\frac{1}{2}\right)\tan(\chi-\alpha)-\left(\frac{y}{h}\right)^2\tan(\chi-\alpha)\right]\sin\alpha+\left[\frac{1}{2}\left(\frac{z}{h}+1\right)\tan^2(\chi-\alpha)-\left(\frac{z}{h}+\frac{3}{2}\right)\right.\right.\right.\\
&\left.\left.\left.\times\frac{x}{h}\tan(\chi-\alpha)+\left(\frac{x}{h}\right)^2+\left(\frac{y}{h}\right)^2\right]\cos\alpha\right\}\left(\left[2\left(\frac{z}{h}+1\right)\tan^2(\chi-\alpha)-2\frac{x}{h}\tan(\chi-\alpha)\right]\left\{\left[\frac{x}{h}-\frac{1}{2}\tan(\chi-\alpha)\right]^2+\left(\frac{y}{h}\right)^2+\left(\frac{z}{h}+\frac{1}{2}\right)^2\right\}\right.\\
&\left.\left.+\left\{\left(\frac{x}{h}\right)^2+\left(\frac{y}{h}\right)^2-2\frac{x}{h}\left(\frac{z}{h}+1\right)\tan(\chi-\alpha)+\left[\left(\frac{y}{h}\right)^2+\left(\frac{z}{h}+1\right)^2\right]\tan^2(\chi-\alpha)\right\}\left(\frac{z}{h}+\frac{1}{2}\right)\right)\right]\\
&\Big/\left\{\left(\frac{x}{h}\right)^2+\left(\frac{y}{h}\right)^2-2\frac{x}{h}\left(\frac{z}{h}+1\right)\tan(\chi-\alpha)+\left[\left(\frac{y}{h}\right)^2+\left(\frac{z}{h}+1\right)^2\right]\tan^2(\chi-\alpha)\right\}^2\left\{\left[\frac{x}{h}-\frac{1}{2}\tan(\chi-\alpha)\right]^2+\left(\frac{y}{h}\right)^2+\left(\frac{z}{h}+\frac{1}{2}\right)^2\right\}^{3/2}
\end{aligned}
$$

(Equation continued on next page)

APPENDIX C

$$+\frac{\frac{x}{h}\tan(\chi-\alpha)\cos\alpha-\left[\frac{x}{h}-2\left(\frac{z}{h}+1\right)\tan(\chi-\alpha)\right]\sin\alpha}{\left\{\left(\frac{x}{h}\right)^2+\left(\frac{y}{h}\right)^2-2\frac{x}{h}\left(\frac{z}{h}+1\right)\tan(\chi-\alpha)+\left[\left(\frac{y}{h}\right)^2+\left(\frac{z}{h}+1\right)^2\right]\tan^2(\chi-\alpha)\right\}\left[\left(\frac{x}{h}\right)^2+\left(\frac{y}{h}\right)^2+\left(\frac{z}{h}+1\right)^2\right]^{1/2}}$$

$$-\left[\frac{\left\{\left\{\left[\left(\frac{y}{h}\right)^2+\left(\frac{z}{h}+1\right)^2\right]\tan(\chi-\alpha)-\left(\frac{z}{h}+1\right)\frac{x}{h}\right\}\sin\alpha+\left[\left(\frac{z}{h}+1\right)\frac{x}{h}\tan(\chi-\alpha)-\left(\frac{x}{h}\right)^2-\left(\frac{y}{h}\right)^2\right]\cos\alpha\right\}\left\{\left[2\left(\frac{z}{h}+1\right)\tan^2(\chi-\alpha)-2\frac{x}{h}\tan(\chi-\alpha)\right]\right.}{\left.\times\left[\left(\frac{x}{h}\right)^2+\left(\frac{y}{h}\right)^2+\left(\frac{z}{h}+1\right)^2\right]+\left(\frac{z}{h}+1\right)\left\{\left(\frac{x}{h}\right)^2+\left(\frac{y}{h}\right)^2-2\frac{x}{h}\left(\frac{z}{h}+1\right)\tan(\chi-\alpha)+\left[\left(\frac{y}{h}\right)^2+\left(\frac{z}{h}+1\right)^2\right]\tan^2(\chi-\alpha)\right\}\right\}}{\left\{\left(\frac{x}{h}\right)^2+\left(\frac{y}{h}\right)^2-2\frac{x}{h}\left(\frac{z}{h}+1\right)\tan(\chi-\alpha)+\left[\left(\frac{y}{h}\right)^2+\left(\frac{z}{h}+1\right)^2\right]\tan^2(\chi-\alpha)\right\}^2\left[\left(\frac{x}{h}\right)^2+\left(\frac{y}{h}\right)^2+\left(\frac{z}{h}+1\right)^2\right]^{3/2}}\right] \qquad \text{(C51)}$$

Singularities in this equation with $\frac{y}{h}=0$, $\frac{z}{h}=-2n$ $(n\neq 0)$ can be avoided by taking $\frac{x}{h}\neq 2n\tan(\chi-\alpha)$ and $\frac{x}{h}\neq(1-2n)\tan(\chi-\alpha)$. This is easily done except for the condition $\frac{x}{h}=0$, $\tan(\chi-\alpha)=0$.

Reference to equations (C37) to (C47) shows that for the condition $\frac{x}{h}=0$, $\tan(\chi-\alpha)=0$,

$$\phi_0\Big]_{\substack{x=0\\y=0\\\tan(\chi-\alpha)=0}} = M_2\left[\int_0^{h/2}\frac{(z+z_0)dz_0}{\left[(z+z_0)^2\right]^{3/2}}+\int_0^{h/2}\frac{(z+h-z_0')dz_0'}{\left[(z+h-z_0')^2\right]^{3/2}}\right]$$

$$= M_2\left[-\frac{1}{|z+z_0|}+\frac{1}{|z+h-z_0|}\right]_0^{h/2} = M_2\left(\frac{1}{|z|}-\frac{1}{\left|z+\frac{h}{2}\right|}+\frac{1}{\left|z+\frac{h}{2}\right|}-\frac{1}{|z+h|}\right)$$

and

$$\frac{\partial\phi_0}{\partial z}\Big]_{\substack{x=0\\y=0\\\tan(\chi-\alpha)=0}} = M_2\left\{-\frac{z}{(z^2)^{3/2}}+\frac{z+h}{\left[(z+h)^2\right]^{3/2}}\right\} = \frac{Aw_0\cos\alpha}{2\pi\cos(\chi-\alpha)}\left\{\frac{z+h}{\left[(z+h)^2\right]^{3/2}}-\frac{z}{(z^2)^{3/2}}\right\}$$

so that

$$\left.\frac{1}{w_0}\frac{hb}{A}\frac{\partial\phi_0}{\partial z}\right]_{\substack{\frac{x}{h}=0\\ \frac{y}{h}=0\\ \tan(\chi-\alpha)=0}} = \frac{b}{h}\frac{\cos\alpha}{2\pi\cos(\chi-\alpha)}\left\{\frac{\frac{z}{h}+1}{\left[\left(\frac{z}{h}+1\right)^2\right]^{3/2}} - \frac{z/h}{\left[\left(\frac{z}{h}\right)^2\right]^{3/2}}\right\} \tag{C52}$$

For the interference corresponding to the location of a vortex cell at (0,0,0), the potential ϕ_0 has to be modified by subtraction of the potential of a vortex cylinder extending from $s = 0$ to s approaching ∞. Thus for the interference potential in the X,Z plane due to the original vortex cylinder cell, I_1 and I_2 of equation (C48) must be replaced with

$$\left[I_{w_1}\right]_{\substack{y=0\\ n=0}} = -\frac{(M_1x + M_2z)\left[1+\tan^2(\chi-\alpha)\right]}{\left\{(x^2+z^2)\left[1+\tan^2(\chi-\alpha)\right] - \left[z - x\tan(\chi-\alpha)\right]^2\right\}\left[1+\tan^2(\chi-\alpha)\right]^{1/2}}$$

$$+\frac{(M_1x + M_2z)\left\{\left[1+\tan^2(\chi-\alpha)\right]\frac{h}{2} + \left[z - x\tan(\chi-\alpha)\right]\right\}}{\left\{(x^2+z^2)\left[1+\tan^2(\chi-\alpha)\right] - \left[z - x\tan(\chi-\alpha)\right]^2\right\}\left\{x^2+z^2+2\left[z - x\tan(\chi-\alpha)\right]\frac{h}{2} + \left[1+\tan^2(\chi-\alpha)\right]\frac{h^2}{4}\right\}^{1/2}}$$

$$\left[I_{w_2}\right]_{\substack{y=0\\ n=0}} = -\frac{\left[M_2 - M_1\tan(\chi-\alpha)\right]\left\{\left[z - x\tan(\chi-\alpha)\right]\frac{h}{2} + x^2 + z^2\right\}}{\left\{(x^2+z^2)\left[1+\tan^2(\chi-\alpha)\right] - \left[z - x\tan(\chi-\alpha)\right]^2\right\}\left\{x^2+z^2+2\left[z - x\tan(\chi-\alpha)\right]\frac{h}{2} + \left[1+\tan^2(\chi-\alpha)\right]\frac{h^2}{4}\right\}^{1/2}}$$

$$+\frac{\left[M_2 - M_1\tan(\chi-\alpha)\right]\left[z - x\tan(\chi-\alpha)\right]}{\left\{(x^2+z^2)\left[1+\tan^2(\chi-\alpha)\right] - \left[z - x\tan(\chi-\alpha)\right]^2\right\}\left[1+\tan^2(\chi-\alpha)\right]^{1/2}}$$

These quantities are obtained from I_1 and I_2 by changing the limits of integration to $h/2$ and ∞. It follows from these equations and the expressions for I_3 and I_4 that the velocity in the z-direction on the X-axis due to the semi-infinite vortex cylinder extending below the position of the open boundary being subtracted from the image in the open boundary is

APPENDIX C

$$\left[\frac{\partial \phi_{0,w}}{\partial z}\right]_{\substack{y=0\\z=0\\n=0}} = -\frac{M_2\left[x - \frac{h}{2}\tan(\chi-\alpha)\right]\tan(\chi-\alpha) - M_1\left[x + \frac{h}{2}\tan(\chi-\alpha)\right]}{x^2\left\{\left[x - \frac{h}{2}\tan(\chi-\alpha)\right]^2 + \frac{h^2}{4}\right\}^{1/2}} - \frac{\left\{M_1\frac{h}{2} + M_2\left[\frac{h}{2}\tan(\chi-\alpha) - x\right]\right\}\left(\left[2\tan(\chi-\alpha)\right]\left\{\left[x - \frac{h}{2}\tan(\chi-\alpha)\right]^2 + \frac{h^2}{4}\right\} + x\frac{h}{2}\right)}{x^2\left\{\left[x - \frac{h}{2}\tan(\chi-\alpha)\right]^2 + \frac{h^2}{4}\right\}^{3/2}}$$

$$- \frac{M_2\tan^2(\chi-\alpha) + M_1\tan(\chi-\alpha)}{x^2\left[1 + \tan^2(\chi-\alpha)\right]^{1/2}} + \frac{\left[M_1 + M_2\tan(\chi-\alpha)\right]\left[2\tan(\chi-\alpha)\right]}{x^2\left[1 + \tan^2(\chi-\alpha)\right]^{1/2}}$$

$$+ \frac{M_1\left[x - \frac{3}{2}h\tan(\chi-\alpha)\right] + M_2\left[\frac{h}{2}\tan(\chi-\alpha) - x\right]\tan(\chi-\alpha)}{\left[x^2 - 2xh\tan(\chi-\alpha) + h^2\tan^2(\chi-\alpha)\right]\left\{\left[x - \frac{h}{2}\tan(\chi-\alpha)\right]^2 + \frac{h^2}{4}\right\}^{1/2}}$$

$$- \frac{\left[\left\{M_1\left[\frac{h}{2}x - \frac{h^2}{2}\tan(\chi-\alpha)\right] + M_2\left[\frac{h^2}{2}\tan^2(\chi-\alpha) - \frac{3h}{2}x\tan(\chi-\alpha) + x^2\right]\right\}\right.}{\left[x^2 - 2xh\tan(\chi-\alpha) + h^2\tan^2(\chi-\alpha)\right]^2\left\{\left[x - \frac{h}{2}\tan(\chi-\alpha)\right]^2 + \frac{h^2}{4}\right\}^{3/2}}$$

$$\left.\times\left(\left[-2x\tan(\chi-\alpha) + 2h\tan^2(\chi-\alpha)\right]\left\{\left[x - \frac{h}{2}\tan(\chi-\alpha)\right]^2 + \frac{h^2}{4}\right\} + \left[x^2 - 2xh\tan(\chi-\alpha) + h^2\tan^2(\chi-\alpha)\right]\frac{h}{2}\right)\right]$$

$$+ \frac{M_2x\tan(\chi-\alpha) - M_1\left[x - 2h\tan(\chi-\alpha)\right]}{\left[x^2 - 2xh\tan(\chi-\alpha) + h^2\tan^2(\chi-\alpha)\right]\left(x^2 + h^2\right)^{1/2}}$$

$$- \frac{\left\{M_1\left[h^2\tan(\chi-\alpha) - hx\right] + M_2\left[hx\tan(\chi-\alpha) - x^2\right]\right\}\left\{\left[-2x\tan(\chi-\alpha) + 2h\tan^2(\chi-\alpha)\right]\left(x^2 + h^2\right) + h\left[x^2 - 2xh\tan(\chi-\alpha) + h^2\tan^2(\chi-\alpha)\right]\right\}}{\left[x^2 - 2xh\tan(\chi-\alpha) + h^2\tan^2(\chi-\alpha)\right]^2\left(x^2 + h^2\right)^{3/2}}$$

This equation contains singularities for $x = 0$. Since these singularities result from the integration of the part of the vortex cylinder arising from the helicopter rotor, it is convenient to start again from equation (C5) and write (with negative sign because of subtraction of this part) with $y = 0$ the potential at $y = 0$ of the part of the rotor wake outside the position of the open lower boundary as

APPENDIX C

$$\phi_w = -\int_{\frac{h}{2}\sec(\chi-\alpha)}^{\infty} \frac{Aw_0\left[x - s\sin(\chi-\alpha)\right]\sin\alpha + \left[z + s\cos(\chi-\alpha)\right]\cos\alpha}{2\pi r^3}\,ds$$

$$= -M_1\int_{h/2}^{\infty} \frac{\left[x - z_0\tan(\chi-\alpha)\right]dz_0}{\left\{\left[x - z_0\tan(\chi-\alpha)\right]^2 + \left(z + z_0\right)^2\right\}^{3/2}} - M_2\int_{h/2}^{\infty} \frac{(z + z_0)dz_0}{\left\{\left[x - z_0\tan(\chi-\alpha)\right]^2 + \left(z + z_0\right)^2\right\}^{3/2}}$$

Then

$$\left[\frac{\partial\phi_w}{\partial z}\right]_{\substack{x=0\\y=0\\z=0\\n=0}} = M_1\int_{h/2}^{\infty} \frac{\left[z_0\tan(\chi-\alpha)\right](-3z_0)dz_0}{\left[z_0^2\tan^2(\chi-\alpha) + z_0^2\right]^{5/2}} - M_2\int_{h/2}^{\infty} \frac{dz_0}{\left[z_0^2\tan^2(\chi-\alpha) + z_0^2\right]^{3/2}} + M_2\int_{h/2}^{\infty} \frac{(z_0)(3z_0)dz_0}{\left[z_0^2\tan^2(\chi-\alpha) + z_0^2\right]^{5/2}}$$

$$= 3\int_{h/2}^{\infty} \frac{\left[M_2 - M_1\tan(\chi-\alpha)\right]dz_0}{\left[1 + \tan^2(\chi-\alpha)\right]^{5/2}z_0^3} - M_2\int_{h/2}^{\infty} \frac{dz_0}{\left[1 + \tan^2(\chi-\alpha)\right]^{3/2}z_0^3}$$

Consequently, performing the integrations and adding in the terms contributed by I_3 and I_4 at $x = y = z = 0$ yields

$$\left[\frac{\partial\phi_{0,w}}{\partial z}\right]_{\substack{x=0\\y=0\\z=0\\n=0}} = \frac{2}{h^2}\left\{\frac{3\left[M_2 - M_1\tan(\chi-\alpha)\right]}{\left[1 + \tan^2(\chi-\alpha)\right]^{5/2}} - \frac{M_2}{\left[1 + \tan^2(\chi-\alpha)\right]^{3/2}}\right\} - \frac{M_1\left[\frac{3}{2}h\tan(\chi-\alpha)\right] - M_2\left[\frac{h}{2}\tan^2(\chi-\alpha)\right]}{\left[h^2\tan^2(\chi-\alpha)\right]\left\{\frac{h^2}{4}\left[1 + \tan^2(\chi-\alpha)\right]\right\}^{1/2}}$$

$$- \frac{\left\{M_1\left[-\frac{h^2}{2}\tan(\chi-\alpha)\right] + M_2\frac{h^2}{2}\tan^2(\chi-\alpha)\right\}\left\{\left[2h\tan^2(\chi-\alpha)\right]\left[\frac{h^2}{4}\tan^2(\chi-\alpha) + \frac{h^2}{4}\right] + \frac{h^3}{2}\tan^2(\chi-\alpha)\right\}}{h^4\tan^4(\chi-\alpha)\left[\frac{h^2}{4}\tan^2(\chi-\alpha) + \frac{h^2}{4}\right]^{3/2}}$$

$$+ \frac{2M_1h\tan(\chi-\alpha)}{h^3\tan^2(\chi-\alpha)} - \frac{\left\{M_1\left[h^2\tan(\chi-\alpha)\right]\right\}\left[3h^3\tan^2(\chi-\alpha)\right]}{\left(h^2\right)^{7/2}\tan^4(\chi-\alpha)}$$

Similarly,

$$\left[\frac{\partial \phi_w}{\partial x}\right]_{\substack{x=0\\y=0\\z=0\\n=0}} = -M_1 \int_{h/2}^{\infty} \frac{dz_0}{\left[z_0^2\tan^2(\chi-\alpha)+z_0^2\right]^{3/2}} + 3M_1 \int_{h/2}^{\infty} \frac{\left[-z_0\tan(\chi-\alpha)\right]^2 dz_0}{\left[z_0^2\tan^2(\chi-\alpha)+z_0^2\right]^{5/2}} - 3M_2 \int_{h/2}^{\infty} \frac{z_0^2\tan(\chi-\alpha)dz_0}{\left[z_0^2\tan^2(\chi-\alpha)+z_0^2\right]^{5/2}}$$

$$= 3\int_{h/2}^{\infty} \frac{\left[M_1\tan(\chi-\alpha)-M_2\right]\tan(\chi-\alpha)dz_0}{\left[1+\tan^2(\chi-\alpha)\right]^{5/2}z_0^3} - M_1\int_{h/2}^{\infty} \frac{dz_0}{\left[1+\tan^2(\chi-\alpha)\right]^{3/2}z_0^3}$$

and

$$\left[\frac{\partial \phi_{0,w}}{\partial x}\right]_{\substack{x=0\\y=0\\z=0\\n=0}} = \frac{2}{h^2}\left\{\frac{3\left[M_1\tan(\chi-\alpha)-M_2\right]\tan(\chi-\alpha)}{\left[1+\tan^2(\chi-\alpha)\right]^{5/2}} - \frac{M_1}{\left[1+\tan^2(\chi-\alpha)\right]^{3/2}}\right\} + \frac{M_1\frac{h}{2}-3M_2\frac{h}{2}\tan(\chi-\alpha)}{\left[h^2\tan^2(\chi-\alpha)\right]\left[\frac{h^2}{4}\tan^2(\chi-\alpha)+\frac{h^2}{4}\right]^{1/2}}$$

$$+\frac{\left[M_1\frac{h^2}{2}\tan(\chi-\alpha)-M_2\frac{h^2}{2}\tan^2(\chi-\alpha)\right]\left\{-2h\left[\frac{h^2}{4}\tan^2(\chi-\alpha)+\frac{h^2}{4}\right]-\frac{h^3}{2}\tan^2(\chi-\alpha)\right\}\tan(\chi-\alpha)}{\left[h^4\tan^4(\chi-\alpha)\right]\left[\frac{h^2}{4}\tan^2(\chi-\alpha)+\frac{h^2}{4}\right]^{3/2}}$$

$$+\frac{M_2h\tan(\chi-\alpha)-M_1h}{h^3\tan^2(\chi-\alpha)} - \frac{\left[M_1h^2\tan(\chi-\alpha)\right]\left[-2h\tan(\chi-\alpha)\right]}{h^5\tan^4(\chi-\alpha)}$$

In form for computation the velocities corresponding to the image in the open lower boundary with the subtraction of the part of the vortex cylinder outside the test section for $x = y = z = n = 0$ are

$$\frac{1}{w_0}\frac{hb}{A}\left[\frac{\partial \phi_{0,w}}{\partial z}\right]_{\substack{x=0\\y=0\\z=0\\n=0}} = \frac{b}{h}\frac{1}{2\pi\cos(\chi-\alpha)}\left\{\frac{6\left[\cos\alpha-\tan(\chi-\alpha)\sin\alpha\right]}{\left[1+\tan^2(\chi-\alpha)\right]^{5/2}} - \frac{2\cos\alpha}{\left[1+\tan^2(\chi-\alpha)\right]^{3/2}} - \frac{3\sin\alpha-\tan(\chi-\alpha)\cos\alpha}{\left[1+\tan^2(\chi-\alpha)\right]^{1/2}\tan(\chi-\alpha)}\right.$$

$$\left.+\frac{\left[\sin\alpha-\tan(\chi-\alpha)\cos\alpha\right]\left[2\tan^2(\chi-\alpha)+4\right]}{\left[1+\tan^2(\chi-\alpha)\right]^{3/2}\tan(\chi-\alpha)} - \frac{\sin\alpha}{\tan(\chi-\alpha)}\right\} \qquad \text{(C53)}$$

APPENDIX C

$$\frac{1}{w_0}\frac{hb}{A}\left[\frac{\partial \phi_{0,w}}{\partial x}\right]_{\substack{x=0\\y=0\\z=0\\n=0}} = \frac{b}{h}\frac{1}{2\pi\cos(\chi-\alpha)}\left\{\frac{6\left[\tan(\chi-\alpha)\sin\alpha-\cos\alpha\right]\tan(\chi-\alpha)}{\left[1+\tan^2(\chi-\alpha)\right]^{5/2}} - \frac{2\sin\alpha}{\left[1+\tan^2(\chi-\alpha)\right]^{3/2}} + \frac{\sin\alpha-3\tan(\chi-\alpha)\cos\alpha}{\left[1+\tan^2(\chi-\alpha)\right]^{1/2}\tan^2(\chi-\alpha)}\right.$$

$$\left. - \frac{2\left[\sin\alpha-\tan(\chi-\alpha)\cos\alpha\right]\left[1+2\tan^2(\chi-\alpha)\right]}{\left[1+\tan^2(\chi-\alpha)\right]^{3/2}\tan^2(\chi-\alpha)} + \frac{\tan(\chi-\alpha)\cos\alpha-\sin\alpha}{\tan^2(\chi-\alpha)} + \frac{2\sin\alpha}{\tan^2(\chi-\alpha)}\right\} \tag{C54}$$

For $\tan(\chi-\alpha)=0$, the quantity in braces in equation (C53) must be replaced with

$$\cos\alpha \tag{C55}$$

and the quantity in braces in equation (C54) must be replaced with

$$-\frac{7}{2}\sin\alpha \tag{C56}$$

In form for computation, the velocity $\left[\frac{\partial \phi_{0,w}}{\partial z}\right]_{\substack{y=0\\z=0\\n=0}}$ for which equation (C53) is the specialization at $x=0$ is

$$\frac{1}{w_0}\frac{hb}{A}\left[\frac{\partial \phi_{0,w}}{\partial z}\right]_{\substack{y=0\\z=0\\n=0}} = \frac{b}{h}\frac{1}{2\pi\cos(\chi-\alpha)}\left[\frac{\left[\frac{x}{h}+\frac{1}{2}\tan(\chi-\alpha)\right]\sin\alpha-\left[\frac{x}{h}-\frac{1}{2}\tan(\chi-\alpha)\right]\tan(\chi-\alpha)\cos\alpha}{\left(\frac{x}{h}\right)^2\left\{\left[\frac{x}{h}-\frac{1}{2}\tan(\chi-\alpha)\right]^2+\frac{1}{4}\right\}^{1/2}}\right.$$

$$-\frac{\left\{\frac{1}{2}\sin\alpha+\left[\frac{1}{2}\tan(\chi-\alpha)-\frac{x}{h}\right]\cos\alpha\right\}\left(2\tan(\chi-\alpha)\left\{\left[\frac{x}{h}-\frac{1}{2}\tan(\chi-\alpha)\right]^2+\frac{1}{4}\right\}+\frac{1}{2}\frac{x}{h}\right)}{\left(\frac{x}{h}\right)^2\left\{\left[\frac{x}{h}-\frac{1}{2}\tan(\chi-\alpha)\right]^2+\frac{1}{4}\right\}^{3/2}}$$

$$+\frac{\left[\sin\alpha+\tan(\chi-\alpha)\cos\alpha\right]\tan(\chi-\alpha)}{\left(\frac{x}{h}\right)^2\left[1+\tan^2(\chi-\alpha)\right]^{1/2}}+\frac{\left[\frac{x}{h}-\frac{3}{2}\tan(\chi-\alpha)\right]\sin\alpha+\left[\frac{1}{2}\tan(\chi-\alpha)-\frac{x}{h}\right]\tan(\chi-\alpha)\cos\alpha}{\left[\frac{x}{h}-\tan(\chi-\alpha)\right]^2\left\{\left[\frac{x}{h}-\frac{1}{2}\tan(\chi-\alpha)\right]^2+\frac{1}{4}\right\}^{1/2}}$$

$$-\frac{\left[\left\{\left[\frac{1}{2}\frac{x}{h}-\frac{1}{2}\tan(\chi-\alpha)\right]\sin\alpha+\left[\frac{1}{2}\tan^2(\chi-\alpha)-\frac{3}{2}\frac{x}{h}\tan(\chi-\alpha)+\left(\frac{x}{h}\right)^2\right]\cos\alpha\right\}\right.}{\left[\frac{x}{h}-\tan(\chi-\alpha)\right]^4\left\{\left[\frac{x}{h}-\frac{1}{2}\tan(\chi-\alpha)\right]^2+\frac{1}{4}\right\}^{3/2}}$$

$$\left.\times\left(\left[2\tan^2(\chi-\alpha)-2\frac{x}{h}\tan(\chi-\alpha)\right]\left\{\left[\frac{x}{h}-\frac{1}{2}\tan(\chi-\alpha)\right]^2+\frac{1}{4}\right\}+\frac{1}{2}\left[\frac{x}{h}-\tan(\chi-\alpha)\right]^2\right)\right]$$

$$+\frac{\frac{x}{h}\tan(\chi-\alpha)\cos\alpha-\left[\frac{x}{h}-2\tan(\chi-\alpha)\right]\sin\alpha}{\left[\frac{x}{h}-\tan(\chi-\alpha)\right]^2\left[\left(\frac{x}{h}\right)^2+1\right]^{1/2}}$$

$$\left.-\frac{\left\{\left[\tan(\chi-\alpha)-\frac{x}{h}\right]\sin\alpha+\left[\frac{x}{h}\tan(\chi-\alpha)-\left(\frac{x}{h}\right)^2\right]\cos\alpha\right\}\left\{\left[2\tan^2(\chi-\alpha)-2\frac{x}{h}\tan(\chi-\alpha)\right]\left[\left(\frac{x}{h}\right)^2+1\right]+\left[\frac{x}{h}-\tan(\chi-\alpha)\right]^2\right\}}{\left[\frac{x}{h}-\tan(\chi-\alpha)\right]^4\left[\left(\frac{x}{h}\right)^2+1\right]^{3/2}}\right] \tag{C57}$$

Singularities can be prevented by taking $\frac{x}{h} \neq \tan(\chi - \alpha)$. The equations are now at hand for calculating the interference factors defined by equations (3) and (4) in certain parts of the field. In particular, the upwash interference factor $\delta_{R,z}$ can be calculated at $y = 0$ and $z = 0$ and the streamwise interference factor $\delta_{R,x}$ at $x = 0$, $y = 0$, and $z = 0$.

For $x \neq 0$ the upwash interference factor on the tunnel center line $y = 0$, $z = 0$ is

$$\delta_{R,z}\Big]_{\substack{y=0\\z=0}} = \frac{1}{w_0}\frac{hb}{A}\left[\left(\frac{\partial \phi_{0,w}}{\partial z}\right)_{\substack{y=0\\z=0\\n=0}} + \sum_{n\neq 0}(-1)^n \frac{\partial \phi_0\left(\frac{x}{h},0,-2n\right)}{\partial z}\right] + \sum_n (\Delta\delta_{R,z})_{ns} \tag{C58}$$

where the quantities to be summed are calculated according to equations (C30) with (C32) and (C34), (C57), and (C51), and in equation (C51) $\frac{y}{h} = 0$ and $\frac{z}{h} = -2n$.

For $x = 0$, $y = 0$, and $z = 0$, the upwash interference factor is

$$\delta_{R,z}\Big]_{\substack{x=0\\y=0\\z=0}} = \frac{1}{w_0}\frac{hb}{A}\left[\left(\frac{\partial \phi_{0,w}}{\partial z}\right)_{\substack{x=0\\y=0\\z=0\\n=0}} + \sum_{n\neq 0}(-1)^n \frac{\partial \phi_0(0,0,-2n)}{\partial z}\right] + \sum_n \left[(\Delta\delta_{R,z})_{ns}\right]_{x=0} \tag{C59}$$

where the quantities to be summed are calculated from equations (C30) with (C32) and (C34), (C53) with (C55), and (C51) with (C52), with $\frac{x}{h} = 0$, $\frac{y}{h} = 0$; and in equations (C51) and (C52), $\frac{z}{h} = -2n$.

The streamwise interference factor at $x = 0$, $y = 0$, and $z = 0$, obtained as for equation (C59) by use of equations (C29) with (C31) and (C33), (C49) with (C50), and (C54) with (C56), is

$$\delta_{R,x}\Big]_{\substack{x=0\\y=0\\z=0}} = \frac{1}{w_0}\frac{hb}{A}\left[\left(\frac{\partial \phi_{0,w}}{\partial x}\right)_{\substack{x=0\\y=0\\z=0}} + \sum_{n\neq 0}(-1)^n \frac{\partial \phi_0(0,0,-2n)}{\partial x}\right] + \sum_n \left[(\Delta\delta_{R,x})_{ns}\right]_{x=0} \tag{C60}$$

Two further specialized applications of the theory of this appendix are required. The first is the upwash interference velocity on a lifting element centered between two infinite slotted side walls. This interference velocity can be obtained from equation (C22) by replacing the factor $\omega l - \frac{\omega}{\sqrt{\omega^2 + g^2}}$ with $gl - \frac{g}{\sqrt{\omega^2 + g^2}}$. For convenience, n is

assumed to be zero. Also, to correspond with the wing theory, α is assumed to be zero and χ is assumed to be $\pi/2$. Then, the upwash interference velocity is

$$v_s = \frac{\partial(\phi_{ns})}{\partial z}\Bigg]_{\substack{n=0 \\ \alpha=0 \\ \chi=\frac{\pi}{2}}} = \frac{Aw_0\, ds}{4\pi^2} \int_{-\infty}^{\infty}\int_{-\infty}^{\infty} e^{i[\omega(x-s)+gz]} e^{-\frac{b}{2}\sqrt{\omega^2+g^2}}$$

$$\times \frac{g\left(gl - \dfrac{g}{\sqrt{\omega^2+g^2}}\right)}{\cosh\left(\frac{b}{2}\sqrt{\omega^2+g^2}\right) + l\sqrt{\omega^2+g^2}\sinh\left(\frac{b}{2}\sqrt{\omega^2+g^2}\right)} d\omega\, dg$$

The range of integration on s is 0 to ∞ and since for $x \neq 0$

$$\int_0^{\infty} e^{i\omega(x-s)} ds = -\frac{e^{i\omega(x-s)}}{i\omega}\Bigg]_0^{\infty} = \lim_{K\to\infty} \frac{e^{i\omega x} - e^{i\omega(x-K)}}{i\omega} = \frac{e^{i\omega x}}{i\omega} - \lim_{K\to\infty} \frac{e^{-i\omega K}}{i\omega}$$

where K is any large number, it follows that in consideration of the oddness in ω and the evenness in g,

$$v_s = \frac{Aw_0}{\pi^2} \int_0^{\infty}\int_0^{\infty} \left[\frac{\sin \omega x}{\omega} + \lim_{K\to\infty} \frac{\sin \omega K}{\omega}\right] \cos(gz)\, e^{-\frac{b}{2}\sqrt{\omega^2+g^2}}$$

$$\times \frac{g\left(gl - \dfrac{g}{\sqrt{\omega^2+g^2}}\right)}{\cosh\left(\frac{b}{2}\sqrt{\omega^2+g^2}\right) + l\sqrt{\omega^2+g^2}\sinh\left(\frac{b}{2}\sqrt{\omega^2+g^2}\right)} d\omega\, dg$$

Substituting p for $b\omega$ and q for bg and noting that the integrand involving $\lim_{K\to\infty} \frac{\sin \omega K}{\omega}$ contributes to the integral only for ω approaching 0 allows this equation to be written as follows:

$$\frac{b^2 v_s}{Aw_0} = \frac{1}{\pi^2}\int_0^\infty\int_0^\infty \frac{\sin\left(p\frac{x}{b}\right)}{p}\cos\left(q\frac{z}{b}\right)e^{-\frac{1}{2}\sqrt{p^2+q^2}}\frac{q\left(q\frac{l}{b}-\frac{q}{\sqrt{p^2+q^2}}\right)}{\cosh\left(\frac{1}{2}\sqrt{p^2+q^2}\right)+\frac{l}{b}\sqrt{p^2+q^2}\sinh\left(\frac{1}{2}\sqrt{p^2+q^2}\right)}\,dp\,dq$$

$$+\frac{1}{\pi^2}\int_0^\infty \frac{\cos\left(q\frac{z}{b}\right)e^{-\frac{q}{2}}q\left(q\frac{l}{b}-1\right)}{\cosh\frac{q}{2}+\frac{l}{b}q\sinh\frac{q}{2}}\,dq\lim_{K\to\infty}\int_0^\infty\frac{\sin(pK)}{p}\,dp$$

$$=\frac{1}{\pi^2}\int_0^\infty\int_0^\infty \frac{\frac{\sin\left(p\frac{x}{b}\right)}{p}\cos\left(q\frac{z}{b}\right)e^{-\frac{1}{2}\sqrt{p^2+q^2}}q\left(q\frac{l}{b}-\frac{q}{\sqrt{p^2+q^2}}\right)}{\cosh\left(\frac{1}{2}\sqrt{p^2+q^2}\right)+\frac{l}{b}\sqrt{p^2+q^2}\sinh\left(\frac{1}{2}\sqrt{p^2+q^2}\right)}\,dp\,dq+\frac{1}{2\pi}\int_0^\infty\frac{\cos\left(q\frac{z}{b}\right)e^{-\frac{q}{2}}q\left(q\frac{l}{b}-1\right)}{\cosh\frac{q}{2}+\frac{l}{b}q\sinh\frac{q}{2}}\,dq \qquad \text{(C61)}$$

In this equation for p approaching 0, $\dfrac{\sin\left(p\frac{x}{b}\right)}{p}$ approaches x/b. With $p = 0$ and q approaching 0, $\dfrac{q}{\sqrt{p^2+q^2}}$ approaches 1.

The second specialized application of this theory involves simply a modification to permit calculation of the upwash interference factor $\delta_{R,z}$ for skew angle χ approaching $\pi/2$ and with angle of attack α equal to zero. Because of some difficulty with nonuniformity of convergence for χ approaching $\pi/2$, it is necessary to go back to the elementary potentials. With $\alpha = 0$, $y = 0$, and $\chi = \frac{\pi}{2}$, equations (C8) and (C9) become

$$d\phi_n = (-1)^n\frac{Aw_0}{2\pi}\left\{\frac{z-2nh}{\left[\sqrt{(s-x)^2+(z-2nh)^2}\right]^3}\right\}ds$$

and

$$d\phi'_n = (-1)^n\frac{Aw_0}{2\pi}\left(\frac{z-(2n-1)h}{\left\{\sqrt{(s'-x)^2+\left[z-(2n-1)h\right]^2}\right\}^3}\right)ds'$$

To obtain ϕ_n and ϕ'_n, these expressions must be integrated on s and s' from 0 to ∞. The results are

$$\phi_n = (-1)^n\frac{Aw_0}{2\pi}\frac{1}{z-2nh}\left[1+\frac{x}{\sqrt{x^2+(z-2nh)^2}}\right]$$

and

$$\phi'_n = (-1)^n\frac{Aw_0}{2\pi}\frac{1}{\left[z-(2n-1)h\right]}\left\{1+\frac{x}{\sqrt{x^2+\left[z-(2n-1)h\right]^2}}\right\}$$

APPENDIX C

The corresponding velocities in the z-direction at $z = 0$ are

$$\frac{\partial \phi_n}{\partial z} = (-1)^n \frac{Aw_0}{2\pi}\left[\frac{-1}{4n^2h^2}\left(1 + \frac{x}{\sqrt{x^2 + 4n^2h^2}}\right) - \frac{x}{\left(x^2 + 4n^2h^2\right)^{3/2}}\right] \tag{C62}$$

$$\frac{\partial \phi'_n}{\partial z} = (-1)^n \frac{Aw_0}{2\pi}\left\{\frac{-1}{(2n-1)^2h^2}\left(1 + \frac{x}{\sqrt{x^2 + (2n-1)^2h^2}}\right) - \frac{x}{\left[x^2 + (2n-1)^2h^2\right]^{3/2}}\right\} \tag{C63}$$

The upwash interference velocity corresponding to the images in the top and bottom walls is given by the sum of expression (C63) for $n = 0$ and expressions (C62) and (C63) summed over all other integer values of n.

To obtain the upwash interference velocity due to the slotted side walls at $y = z = \alpha = 0$ and $\chi = \frac{\pi}{2}$, expressions like equations (C22) and (C23) except for the replacement of $\omega l - \frac{\omega}{\sqrt{\omega^2 + g^2}}$ and $\omega' l + \frac{\omega'}{\sqrt{\omega'^2 + g'^2}}$ with $gl - \frac{g}{\sqrt{\omega^2 + g^2}}$ and $g'l - \frac{g'}{\sqrt{\omega'^2 + g'^2}}$, respectively, must be integrated on s and s' from 0 to ∞ and summed over all 0, positive, and negative integer values of n. The integration of $e^{-i\omega s}$ gives

$$\int_0^\infty e^{-i\omega s}\, ds = \frac{1}{i\omega} - \lim_{s\to\infty} \frac{e^{-i\omega s}}{i\omega}$$

so that

$$\left.\frac{\partial\left(\phi_{n,s} + \phi'_{n,s}\right)}{\partial z}\right]_{\substack{y=0\\z=0\\\alpha=0\\\chi=\frac{\pi}{2}}} = \frac{(-1)^n Aw_0}{4\pi^2} \int_{-\infty}^{\infty} \int_{-\infty}^{\infty} \left\{e^{i(\omega x - 2nhg)} + e^{i\left[\omega x - (2n-1)hg\right]}\right\} e^{-\frac{b}{2}\sqrt{\omega^2+g^2}}$$

$$\times \frac{g\left(\frac{1}{i\omega} - \lim_{s\to\infty} \frac{e^{-i\omega s}}{i\omega}\right)\left(gl - \frac{g}{\sqrt{\omega^2 + g^2}}\right)}{\cosh\left(\frac{b}{2}\sqrt{\omega^2 + g^2}\right) + l\sqrt{\omega^2 + g^2}\sinh\left(\frac{b}{2}\sqrt{\omega^2 + g^2}\right)}\, d\omega\, dg$$

From considerations of symmetry with substitution of p for ωh and q for gh, this equation can be written

APPENDIX C

$$\left.\frac{\partial\left(\phi_{n,s}+\phi'_{n,s}\right)}{\partial z}\right]_{\substack{y=0\\z=0\\\alpha=0\\\chi=\frac{\pi}{2}}} = \frac{(-1)^n A w_0}{\pi^2 h^2}\int_0^\infty\int_0^\infty\left\{\frac{\sin\left(p\frac{x}{h}\right)}{p} - \lim_{\frac{s}{h}\to\infty}\left[\frac{\cos\left(p\frac{s}{h}\right)\sin\left(p\frac{x}{h}\right)}{p} - \frac{\sin\left(p\frac{s}{h}\right)\cos\left(p\frac{x}{h}\right)}{p}\right]\right\} e^{-\frac{1}{2}\frac{b}{h}\sqrt{p^2+q^2}}$$

$$\times \frac{q\left(q\frac{l}{h} - \frac{q}{\sqrt{p^2+q^2}}\right)\left\{\cos(2nq) + \cos\left[(2n-1)q\right]\right\}}{\cosh\left(\frac{1}{2}\frac{b}{h}\sqrt{p^2+q^2}\right) + \frac{l}{h}\sqrt{p^2+q^2}\sinh\left(\frac{1}{2}\frac{b}{h}\sqrt{p^2+q^2}\right)}\,dp\,dq$$

The integrands involving $\lim_{\frac{s}{h}\to\infty}$ of $\cos\left(p\frac{s}{h}\right)$ and $\sin\left(p\frac{s}{h}\right)$ contribute to the integrals only for $p \to 0$. Moreover, $\lim_{\frac{s}{h}\to\infty}\int_0^\infty \frac{\sin\left(p\frac{s}{h}\right)}{p}\,dp = \frac{\pi}{2}$ and it is easily shown that

$\lim_{\frac{s}{h}\to\infty}\int_0^\infty \frac{\cos\left(p\frac{s}{h}\right)\sin\left(p\frac{x}{h}\right)}{p}\,dp = 0$. Therefore,

$$\left.\frac{\partial\left(\phi_{n,s}+\phi'_{n,s}\right)}{\partial z}\right]_{\substack{y=0\\z=0\\\alpha=0\\\chi=\frac{\pi}{2}}} = \frac{(-1)^n A w_0}{\pi^2 h^2}\int_0^\infty\int_0^\infty \frac{\frac{\sin\left(p\frac{x}{h}\right)}{p}e^{-\frac{1}{2}\frac{b}{h}\sqrt{p^2+q^2}}\,q\left(q\frac{l}{h} - \frac{q}{\sqrt{p^2+q^2}}\right)\left\{\cos(2nq) + \cos\left[(2n-1)q\right]\right\}}{\cosh\left(\frac{1}{2}\frac{b}{h}\sqrt{p^2+q^2}\right) + \frac{l}{h}\sqrt{p^2+q^2}\sinh\left(\frac{1}{2}\frac{b}{h}\sqrt{p^2+q^2}\right)}\,dp\,dq$$

$$+ \frac{(-1)^n A w_0}{2\pi h^2}\int_0^\infty \frac{e^{-\frac{b}{h}\frac{q}{2}}\,q\left(q\frac{l}{h} - 1\right)\left\{\cos(2nq) + \cos\left[(2n-1)q\right]\right\}}{\cosh\left(\frac{b}{h}\frac{q}{2}\right) + \frac{l}{h}q\sinh\left(\frac{b}{h}\frac{q}{2}\right)}\,dq \qquad \text{(C64)}$$

APPENDIX C

Since $\delta_{R,z} = \frac{hb}{Aw_0} v$ where v is the total upwash interference velocity, taking the required sums of expressions (C62), (C63), and (C64) gives

$$\delta_{R,z}\Big]_{\substack{y=0\\z=0\\\alpha=0\\\chi=\frac{\pi}{2}}} = \frac{-1}{2\pi}\frac{b}{h}\left\{1 + \frac{x/h}{\sqrt{\left(\frac{x}{h}\right)^2 + 1}} + \frac{x/h}{\left[\left(\frac{x}{h}\right)^2 + 1\right]^{3/2}}\right\} + \frac{1}{\pi^2}\frac{b}{h}\int_0^\infty\int_0^\infty \frac{\frac{\sin\left(p\frac{x}{h}\right)}{p} e^{-\frac{1}{2}\frac{b}{h}\sqrt{p^2+q^2}} q\left(q\frac{l}{h} - \frac{q}{\sqrt{p^2+q^2}}\right)(1+\cos q)}{\cosh\left(\frac{1}{2}\frac{b}{h}\sqrt{p^2+q^2}\right) + \frac{l}{h}\sqrt{p^2+q^2}\sinh\left(\frac{1}{2}\frac{b}{h}\sqrt{p^2+q^2}\right)} dp\,dq$$

$$+ \frac{1}{2\pi}\frac{b}{h}\int_0^\infty \frac{e^{-\frac{b}{h}\frac{q}{2}} q\left(q\frac{l}{h} - 1\right)(1+\cos q)}{\cosh\left(\frac{b}{h}\frac{q}{2}\right) + \frac{l}{h} q \sinh\left(\frac{b}{h}\frac{q}{2}\right)} dq + \frac{1}{\pi}\frac{b}{h}\sum_{n\neq 0}(-1)^n\left(\frac{1}{2}\left\{-\frac{1}{4n^2}\left[1 + \frac{x/h}{\sqrt{\left(\frac{x}{h}\right)^2 + 4n^2}}\right] - \frac{x/h}{\left[\left(\frac{x}{h}\right)^2 + 4n^2\right]^{3/2}}\right.\right.$$

$$\left. - \frac{1}{(2n-1)^2}\left[1 + \frac{x/h}{\sqrt{\left(\frac{x}{h}\right)^2 + (2n-1)^2}}\right] - \frac{x/h}{\left[\left(\frac{x}{h}\right)^2 + (2n-1)^2\right]^{3/2}}\right\} + \frac{1}{2}\int_0^\infty \frac{e^{-\frac{b}{h}\frac{q}{2}} q\left(q\frac{l}{h} - 1\right)\left\{\cos(2nq) - \cos\left[(2n-1)q\right]\right\}}{\cosh\left(\frac{b}{h}\frac{q}{2}\right) + \frac{l}{h} q \sinh\left(\frac{b}{h}\frac{q}{2}\right)} dq$$

$$\left. + \frac{1}{\pi}\int_0^\infty\int_0^\infty \frac{\frac{\sin\left(p\frac{x}{h}\right)}{p} e^{-\frac{1}{2}\frac{b}{h}\sqrt{p^2+q^2}} q\left(q\frac{l}{h} - \frac{q}{\sqrt{p^2+q^2}}\right)\left\{\cos(2nq) + \cos\left[(2n-1)q\right]\right\}}{\cosh\left(\frac{1}{2}\frac{b}{h}\sqrt{p^2+q^2}\right) + \frac{l}{h}\sqrt{p^2+q^2}\sinh\left(\frac{1}{2}\frac{b}{h}\sqrt{p^2+q^2}\right)} dp\,dq\right) \qquad \text{(C65)}$$

APPENDIX D

APPLICATION OF CONFORMAL TRANSFORMATION IN THE TREFFTZ PLANE FOR CALCULATION OF LIFT INTERFERENCE IN SLOTTED TEST SECTION SYMMETRICAL ABOUT THE VERTICAL AXIS

The disturbance due to the lifting wing is represented by vortices trailing horizontally downstream from the wing tips as in reference 13. The interference velocity is computed in the far-downstream (Trefftz) plane, where the theoretical flow is two-dimensional, by means of the conformal transformation of the rectangular boundary to a circle. This application is limited to slotted configurations symmetrical about the vertical Y-axis and to slot arrangements for which both X- and Y-axes cut only closed portions (panels) of the boundary. The number of slots is then even. The wing is assumed to be mounted with its span horizontal and centered on the Y-axis, but it may be located off the X-axis.

Symbols peculiar to this appendix are as follows:

a_j, b_j real constants to be determined

$F, F_{g,1}, F_{g,2}$ specifically defined functions of θ, $\theta_{g,1}$, and $\theta_{g,2}$, respectively

h height of test section

$\mathfrak{I}$ imaginary part of

$i = \sqrt{-1}$

K quarter-period of Jacobian elliptic functions

K' coperiod corresponding to K

k, k' arguments of K

m, q number of panels or slots

p factor in complex potential determined by slot arrangement

$\mathfrak{R}$ real part of

APPENDIX D

$r_t = |\zeta_t|$

V	tunnel stream velocity
v	upwash interference velocity, positive upward
w	complex potential
X,Y,Z	coordinate axes
x,y	distance along axes
z	complex position in z-plane, $x + iy$
Γ	circulation
δ_w	upwash interference factor for wings
ϵ	small positive quantity near zero
ζ	complex position in ζ-plane, $\xi + i\eta$
ξ	real part of ζ
η	imaginary part of ζ
θ	polar angle
σ	complex argument of exponential as defined in equation (D13))
λ	constant of conformal transformation (see eq. (D2))
ϕ	amplitudes corresponding to arguments of elliptic functions

Subscripts:

g	number designating a slot edge
n,j	index numbers
t	designates position of vortex in right half-plane

Horizontal bar over complex quantity indicates the conjugate. Inclusion between two vertical bars indicates absolute value.

APPENDIX D

For convenience the width of the rectangular test section is taken as unity. Its height is designated h. The conformal transformation which carries the rectangle in the z-plane into the unit circle in the ζ-plane is discussed in reference 13. For convenience and because of the extension required to the development, the procedure of this reference is somewhat modified. The transformation is given by

$$\zeta = \frac{\operatorname{sn}\frac{\lambda z}{2}\operatorname{dn}\frac{\lambda z}{2}}{\operatorname{cn}\frac{\lambda z}{2}} \tag{D1}$$

where with the width of the test section taken as unity,

$$\lambda = 2K = \frac{2K'}{h} \tag{D2}$$

Since for every value of the (quarter) period K of the elliptic functions sn, dn, and cn there exists the corresponding coperiod K', the values of K and K' may be found from the relation

$$\frac{K'}{K} = h \tag{D3}$$

with the aid of tables of the complete elliptic integrals $K(k^2)$ and the relations

$$K' = K(k'^2) \tag{D4}$$

with

$$k'^2 = 1 - k^2 \tag{D5}$$

Note that on the circle

$$\zeta = e^{i\theta} \tag{D6}$$

where θ is the polar angle. Therefore by equation (107) of reference 13 the slot edges θ_g on the circle correspond to the slot edges z_g on the rectangle through

$$e^{2i\theta_g} = \frac{1 - \operatorname{cn}(\lambda z_g)}{1 + \operatorname{cn}(\lambda z_g)} \tag{D7}$$

From the relations of reference 17 (p. 503), it can be shown that with x real $\operatorname{cn}(x - iK') = ik^{-1}\frac{\operatorname{dn} x}{\operatorname{sn} x}$. Therefore, on the lower boundary where $\lambda z_g = \lambda x_g - \frac{i\lambda h}{2} = \lambda x_g - iK'$, it follows that

$$\left.e^{2i\theta_g}\right]_{\text{Lower boundary}} = \frac{1 - ik^{-1}\frac{\operatorname{dn}(\lambda x_g)}{\operatorname{sn}(\lambda x_g)}}{1 + ik^{-1}\frac{\operatorname{dn}(\lambda x_g)}{\operatorname{sn}(\lambda x_g)}} = \frac{k^2\operatorname{sn}^2(\lambda x_g) - \operatorname{dn}^2(\lambda x_g) - 2ik\operatorname{sn}(\lambda x_g)\operatorname{dn}(\lambda x_g)}{k^2\operatorname{sn}^2(\lambda x_g) + \operatorname{dn}^2(\lambda x_g)}$$

so that with positive x_g

$$\theta_g\Big]_{\text{Lower boundary}} = -\frac{1}{2}\sin^{-1}\left[\frac{2k\,\mathrm{sn}(\lambda x_g)\mathrm{dn}(\lambda x_g)}{k^2\mathrm{sn}^2(\lambda x_g) + \mathrm{dn}^2(\lambda x_g)}\right] = -\frac{1}{2}\sin^{-1}\left(2k\sqrt{1 - k^2\sin^2\phi}\,\sin\phi\right) \tag{D8}$$

for values of ϕ corresponding to values of λx_g in tables of elliptic functions with the given values of λ and $K(k^2)$.

Similarly, at the right-hand side boundary $\lambda z_g = \lambda\left(\frac{1}{2} + iy_g\right) = K + i\lambda y_g$ so that

$$e^{2i\theta_g}\Big]_{\text{Right side}} = \frac{1 - \mathrm{cn}(K + i\lambda y_g)}{1 + \mathrm{cn}(K + i\lambda y_g)} = \frac{1 + ik'\dfrac{\mathrm{sn}(\lambda y_g,k')}{\mathrm{dn}(\lambda y_g,k')}}{1 - ik'\dfrac{\mathrm{sn}(\lambda y_g,k')}{\mathrm{dn}(\lambda y_g,k')}}$$

and since

$$\mathrm{dn}^2(\lambda y_g,k') + k'^2\mathrm{sn}^2(\lambda y_g,k') = 1$$

it follows that

$$\theta_g\Big]_{\text{Right side}} = \frac{1}{2}\sin^{-1}\left[2k'\mathrm{sn}(\lambda y_g,k')\mathrm{dn}(\lambda y_g,k')\right] = \frac{1}{2}\frac{y_g}{|y_g|}\sin^{-1}\left(2k'\sqrt{1 - k'^2\sin^2\phi}\,\sin\phi\right) \tag{D9}$$

for values of ϕ corresponding to values of λy_g in tables of elliptic functions with the given values of λ and $K(k'^2)$. Because of the symmetry about the Y-axis of both the rectangular-test-section configuration and the conformal transformation, equations (D8) and (D9) make possible the location of all the slot edges in the transformed plane. Still to be determined are the positions of the vortices trailing from the wing tips.

Let the center of the two-dimensional vortex in the right-hand part of the z-plane be located at (x_t,y_t) so that the complex position is

$$z_t = x_t + iy_t$$

By equation (D1) the location of this vortex in the ζ-plane is

$$\zeta_t = \xi_t + i\eta_t = \mathrm{sn}\left(\frac{1}{2}\lambda z_t\right)\frac{\mathrm{dn}\left(\frac{1}{2}\lambda z_t\right)}{\mathrm{cn}\left(\frac{1}{2}\lambda z_t\right)} \tag{D10}$$

By reference to formulas for expansion of the elliptic functions of complex arguments, it may be shown that if $z = x + iy$, then

$$sn(z) = \frac{sn(x)dn(y) + i\,cn(x)dn(x)sn(y)cn(y)}{cn^2(y) + k^2sn^2(x)sn^2(y)} \tag{D11}$$

and

$$\frac{dn(z)}{cn(z)} = \frac{\left[dn(x)cn(y)dn(y) - ik^2sn(x)cn(x)sn(y)\right]\left[cn(x)cn(y) + i\,sn(x)dn(x)sn(y)dn(y)\right]}{\left[cn(x)cn(y)\right]^2 + \left[sn(x)dn(x)sn(y)dn(y)\right]^2} \tag{D12}$$

In equations (D11) and (D12) the elliptic functions with argument x are taken from tables corresponding to the value of K $\left(\text{or } k^2\right)$ and those with argument y are taken from tables corresponding to the value of K' $\left(\text{or } k'^2\right)$. With $\frac{\lambda}{2}x_t$ in the place of x and $\frac{\lambda}{2}y_t$ in place of y, equations (D11) and (D12) can be used with some complex algebra to calculate ξ_t and η_t from equation (D10) and give the position of the vortex in the right-hand ζ-half-plane. The other vortex is then located at the point $\left(-\xi_t, \eta_t\right)$. If the span lies along the X-axis so that y_t is zero, equation (D10) is easily used directly to calculate $\zeta_t = \xi_t$; or, even more simply in this case, equation (107) of reference 13 gives $\xi_t = \left[\frac{1 - cn\left(\lambda x_t\right)}{1 + cn\left(\lambda x_t\right)}\right]^{1/2}$.

With the configuration in the ζ-plane completely determined, the flow due to the two vortices in the presence of the slotted circular boundary can be investigated. With σ defined by the equation

$$\zeta = e^{i\sigma} \tag{D13}$$

where the complex σ approaches the real variable θ at the circular boundary, it is seen that $\frac{1}{\sqrt{\sin\theta - \sin\theta_g}}$ has singularities, which according to the theory of reference 13 correspond to slot edges, symmetrically arranged with respect to the Y-axis. Since this symmetry has been assumed and since the axes cut only panels, it follows that the basic equation of reference 13 applicable to this analysis is equation (15) of that reference with q equal to the number of panels (or slots) m and p equal to i. However, this equation is specialized to apply only for the span lying along the X-axis. The corresponding equation applicable for the span parallel to but not necessarily lying along the X-axis is

$$\frac{dw}{d\zeta} = \frac{p\zeta \sum_{n=0}^{\frac{m}{2}+1} \left[a_n \cos(n\sigma) + b_n \sin(n\sigma)\right]}{\left(\zeta - \zeta_t\right)\left(\zeta + \bar{\zeta}_t\right)\left(1 - \zeta\bar{\zeta}_t\right)\left(1 + \zeta\zeta_t\right)\prod_{g=1}^{m}\left(\sin\sigma - \sin\theta_g\right)^{1/2}} \tag{D14}$$

where $\zeta = e^{i\sigma}$, $\bar{\zeta}$ is the conjugate of ζ, ζ_t is the position of the vortex in the right-hand half-plane, the a_n and b_n values are constants, w is the complex potential in the ζ-plane, and for this investigation $p \equiv i$. At the circular boundary, where $\zeta = e^{i\theta}$,

$$\left.\frac{dw}{d\zeta}\right]_{\sigma=\theta} = \frac{ie^{-i\theta}\sum_{n=0}^{\frac{m}{2}+1}\left[a_n\cos(n\theta) + b_n\sin(n\theta)\right]}{\left(e^{i\theta} - \zeta_t\right)\left(e^{i\theta} + \bar{\zeta}_t\right)\left(e^{-i\theta} - \bar{\zeta}_t\right)\left(e^{-i\theta} + \zeta_t\right)\prod_{g=1}^{m}\left(\sin\theta - \sin\theta_g\right)^{1/2}}$$

$$= \frac{ie^{-i\theta}\sum_{n=0}^{\frac{m}{2}+1}\left[a_n\cos(n\theta) + b_n\sin(n\theta)\right]}{\left|e^{i\theta} - \zeta_t\right|^2\left|e^{-i\theta} + \zeta_t\right|^2\prod_{g=1}^{m}\left(\sin\theta - \sin\theta_g\right)^{1/2}}$$

Then

$$\left.\frac{dw}{dz}\right]_{\sigma=\pi-\theta} = \frac{ie^{-i(\pi-\theta)}\sum_{n=0}^{\frac{m}{2}+1}\left[a_n\cos(n\pi)\cos(n\theta) - \cos(n\pi)\sin(n\theta)\right]}{\left|e^{i(\pi-\theta)} - \zeta_t\right|^2\left|e^{-i(\pi-\theta)} + \zeta_t\right|^2\prod_{g=1}^{m}\left(\sin\theta - \sin\theta_g\right)^{1/2}}$$

$$= \frac{-ie^{i\theta}\sum_{n=0}^{\frac{m}{2}+1}\left[a_n\cos(n\pi)\cos(n\theta) - b_n\cos(n\pi)\sin(n\theta)\right]}{\left|-e^{-i\theta} - \zeta_t\right|^2\left|-e^{i\theta} + \zeta_t\right|^2\prod_{g=1}^{m}\left(\sin\theta - \sin\theta_g\right)^{1/2}}$$

and it is true as required by the symmetry that

$$\left.\frac{dw}{d\zeta}\right]_{\pi-\theta} = -\left.\frac{d\bar{w}}{d\zeta}\right]_{\theta}$$

provided

$$a_{2j} = 0 \qquad (j = 1, 2, 3, \ldots)$$

$$b_{2j+1} = 0 \qquad (j = 1, 2, 3, \ldots)$$

Consequently, for symmetry about the Y-axis with the axes cutting panels, equation (D14) becomes

$$\frac{dw}{d\zeta} = \frac{i\zeta\left[\sum_{n=0}^{\left[\frac{m}{4}\right]} a_{2n+1}\cos(2n+1)\sigma + \sum_{n=1}^{\left[\frac{1}{2}\left(\frac{m}{2}+1\right)\right]} b_{2n}\sin(2n\sigma)\right]}{\left(\zeta-\zeta_t\right)\left(\zeta+\bar{\zeta}_t\right)\left(1-\zeta\bar{\zeta}_t\right)\left(1+\zeta\zeta_t\right)\prod_{g=1}^{m}\left(\sin\sigma-\sin\theta_g\right)^{1/2}} \tag{D15}$$

where m is the (even) number of slots and $\left[\frac{m}{4}\right]$ is the largest integer less than or equal to $\frac{m}{4}$ and $\left[\frac{1}{2}\left(\frac{m}{3}+1\right)\right]$ is the largest integer less than or equal to $\frac{1}{2}\left(\frac{m}{2}+1\right)$. At the circular boundary, equation (D15) becomes

$$\left.\frac{dw}{d\zeta}\right|_{\sigma=\theta} = \frac{ie^{-i\theta}\left[\sum_{n=0}^{\left[\frac{m}{4}\right]} a_{2n+1}\cos(2n+1)\theta + \sum_{n=1}^{\left[\frac{1}{2}\left(\frac{m}{2}+1\right)\right]} b_{2n}\sin(2n\theta)\right]}{\left|e^{i\theta}-\zeta_t\right|^2\left|e^{-i\theta}+\zeta_t\right|^2\prod_{g=1}^{m}\left(\sin\theta-\sin\theta_g\right)^{1/2}} \tag{D16}$$

Since the real part of w is the potential and its imaginary part is the stream function and since the panel is necessarily a streamline (stream function constant), equation (19) of reference 13 is equivalent to

$$\int_{\text{Panel}} \frac{dw}{d\zeta}\,d\zeta = 0 \tag{D17}$$

At the wall, $\zeta = e^{i\theta}$ and $d\zeta = ie^{i\theta}d\theta$. Moreover, with $\zeta_t = \xi_t + i\eta_t$, it is not difficult to show that

$$\left|e^{i\theta}-\zeta_t\right|^2\left|e^{-i\theta}+\zeta_t\right|^2 = \left(1+r_t^2\right)^2 - 4\xi_t^2 - 4\eta_t\left(1+r_t^2\right)\sin\theta + 4r_t^2\sin^2\theta$$

where $r_t = \left|\zeta_t\right| = \sqrt{\xi_t^2+\eta_t^2}$. With these substitutions the use of equation (D16) in equation (D17) gives, since m is even,

$$\int_{\text{Panel}} \frac{\left[\sum_{n=0}^{\left[\frac{m}{4}\right]} a_{2n+1}\cos(2n+1)\theta + \sum_{n=1}^{\left[\frac{1}{2}\left(\frac{m}{2}+1\right)\right]} b_{2n}\sin(2n\theta)\right]d\theta}{\left[\left(1+r_t^2\right)^2 - 4\xi_t^2 - 4\eta_t\left(1+r_t^2\right)\sin\theta + 4r_t^2\sin^2\theta\right]\prod_{g=1}^{m}\left(\left|\sin\theta-\sin\theta_g\right|\right)^{1/2}} = 0 \tag{D18}$$

APPENDIX D

The limits on the integral of equation (D18) are the values of θ_g at the edges of any panel wholly in the right half-plane. Because of the symmetry about the Y-axis and of the fact that the Y-axis cuts panels, there are $\frac{m}{2} - 1$ independent equations (D18) linear in the constants a_j and b_j. The other two equations needed for determining the $\frac{m}{2} + 1$ constants are obtained from equation (20) of reference 13, where the contour integral is taken about the vortex at ζ_t in the ζ-plane.

Since

$$\sin \sigma = \frac{e^{i\sigma} - e^{-i\sigma}}{2i} = \frac{\zeta - \zeta^{-1}}{2i}$$

and similarly

$$\cos \sigma = \frac{\zeta + \zeta^{-1}}{2}$$

it is evident from equation (D15) that the residue of $dw/d\zeta$ at ζ_t is

$$\frac{i\zeta_t \left\{ \sum_{n=0}^{\left[\frac{m}{4}\right]} a_{2n+1} \left[\frac{\zeta_t^{2n+1} + \zeta_t^{-(2n+1)}}{2} \right] + \sum_{n=1}^{\left[\frac{1}{2}\left(\frac{m}{2}+1\right)\right]} b_{2n} \left(\frac{\zeta_t^{2n} - \zeta_t^{-2n}}{2i} \right) \right\}}{\left(\zeta_t + \bar{\zeta}_t\right)\left(1 - |\zeta_t|^2\right)\left(1 + \zeta_t^2\right) \prod_{g=1}^{m} \left(\frac{\zeta_t - \zeta_t^{-1}}{2i} - \sin \theta_g \right)^{1/2}}$$

Since the value of the contour integral is the product of $2\pi i$ by this residue, equation (20) of reference 13 gives the two relations

$$\mathcal{R}_\pi \left(\frac{\zeta_t \left\{ \sum_{n=0}^{\left[\frac{m}{4}\right]} a_{2n+1} \left[\zeta_t^{2n+1} + \zeta_t^{-(2n+1)} \right] + \sum_{n=1}^{\left[\frac{1}{2}\left(\frac{m}{2}+1\right)\right]} b_{2n} i \left(\zeta_t^{-2n} - \zeta_t^{2n} \right) \right\}}{\left(\zeta_t + \bar{\zeta}_t\right)\left(1 - |\zeta_t|^2\right)\left(1 + \zeta_t^2\right) \left[\prod_{g=1}^{m} \left(\frac{i\zeta_t^{-1} - i\zeta_t}{2} - \sin \theta_g \right) \right]^{1/2}} \right) = \pm 1 \qquad \text{(D19)}$$

and

$$\mathfrak{I}\left(\frac{\zeta_t\left\{\sum_{n=0}^{\left[\frac{m}{4}\right]} a_{2n+1}\left[\zeta_t^{2n+1}+\zeta_t^{-(2n+1)}\right]+\sum_{n=1}^{\left[\frac{1}{2}\left(\frac{m}{2}+1\right)\right]} b_{2n} i\left(\zeta_t^{-2n}-\zeta_t^{2n}\right)\right\}}{\left(\zeta_t+\bar{\zeta}_t\right)\left(1-\left|\zeta_t\right|^2\right)\left(1+\zeta_t^2\right)\left[\prod_{g=1}^{m}\left(\frac{i\zeta_t^{-1}-i\zeta_t}{2}-\sin\theta_g\right)\right]^{1/2}}\right)=0 \qquad \text{(D20)}$$

where $\mathfrak{R}$ and $\mathfrak{I}$ indicate real and imaginary parts, respectively, and the circulation Γ has been taken to be unity.

The sign in equation (D19) is ambiguous because of the two branches of the half power of the Π-product of complex quantities in the denominator. In practice either sign and either branch may be chosen and its correctness easily determined from physical considerations. Because the constant on the right-hand side of equation (D19) is the only nonzero constant appearing on the right of any of the equations in the simultaneous linear set determining the constants a_j and b_j, the choice of sign in this equation determines the signs of any velocities calculated. If these signs are incorrect, they need only be reversed.

Equations (D18), (D19), and (D20) provide the $\frac{m}{2}+1$ linear simultaneous equations for determining the $\frac{m}{2}+1$ constants a_j and b_j. The calculations are best performed by a machine computing system, because for more than about four slots they become too complicated, voluminous, and sensitive to errors of various kinds to be suitable for hand calculation. If the computing system permits use of complex variables, equations (D19) and (D20) may be used directly without the necessity of reduction to real functions of real quantities. It is only necessary to insert the limits on the summations and on the Π-products along with

$$\zeta_t = \xi_t + i\eta_t$$

$$\bar{\zeta}_t = \xi_t - i\eta_t$$

$$\left|\zeta_t\right|^2 = r_t^2 = \xi_t^2 + \eta_t^2$$

and the values of θ_g. The coefficients of the a_j and of the b_j are then easily obtained. Thus, the coefficient of a_3 in equation (D19) is

$$\mathfrak{R}\,\pi\left\{\frac{\zeta_t\left(\zeta_t^3+\zeta_t^{-3}\right)}{\left(\zeta_t+\bar{\zeta}_t\right)\left(1-\left|\zeta_t\right|^2\right)\left(1+\zeta_t^2\right)\left[\prod_{g=1}^{m}\left(\frac{i\zeta_t^{-1}-i\zeta_t}{2}-\sin\theta_g\right)\right]^{1/2}}\right\}$$

The denominator must remain the same in all the expressions for the coefficients of the a_j and b_j in equations (D19) and (D20); that is, the same branch of the Π-product must be used in calculating all the coefficients.

The integrands of the integrals determining the coefficients of the a_j and b_j of equation (D18) have singularities at the limits of the nature of $1/\sqrt{\epsilon}$ for $\epsilon > 0$ as ϵ approaches 0. If the numerical integration routine does not depend on the values of the integrand at the limits, correct values of the coefficients may possibly be obtained by simply ignoring the singularity, since the contribution to the integral of the region within ϵ of either limit is of the order of $\sqrt{\epsilon}$. Otherwise, integrals of the form

$$\int_{\theta_{g,1}}^{\theta_{g,2}} \frac{\begin{pmatrix}\sin\\ \text{or}\\ \cos\end{pmatrix} j\theta \, d\theta}{F(\theta)} \qquad \begin{pmatrix}\theta_{g,2} > \theta_{g,1}\\ j = 1, 2, \ldots\end{pmatrix}$$

may be approximated by

$$\int_{\theta_{g,1}}^{\theta_{g,2}} \frac{\begin{pmatrix}\sin\\ \text{or}\\ \cos\end{pmatrix} j\theta \, d\theta}{F(\theta)} = \int_{\theta_{g,1}+\epsilon}^{\theta_{g,2}-\epsilon} \frac{\begin{pmatrix}\sin\\ \text{or}\\ \cos\end{pmatrix} j\theta \, d\theta}{F(\theta)} + 2\sqrt{\epsilon}\left[\frac{\begin{pmatrix}\sin\\ \text{or}\\ \cos\end{pmatrix} j\theta_{g,2}}{F_{g,2}\left(\theta_{g,2}\right)\sqrt{\cos\,\theta_{g,2}}} + \frac{\begin{pmatrix}\sin\\ \text{or}\\ \cos\end{pmatrix} j\theta_{g,1}}{F_{g,1}\left(\theta_{g,1}\right)\sqrt{\cos\,\theta_{g,1}}}\right]$$

where

$$F(\theta) = \left[\left(1 + r_t^2\right)^2 - 4\xi_t^2 - 4\eta_t\left(1 + r_t^2\right)\sin\theta + 4r_t^2\sin^2\theta\right] \prod_{g=1}^{m} \left(\left|\sin\theta - \sin\theta_g\right|\right)^{1/2}$$

$$F_{g,2}\left(\theta_{g,2}\right) = \left[\left(1 + r_t^2\right)^2 - 4\xi_t^2 - 4\eta_t\left(1 + r_t^2\right)\sin\theta_{g,2} + 4r_t^2\sin^2\theta_{g,2}\right] \prod_{\substack{g=1\\ g\neq g_2}}^{m} \left(\left|\sin\theta_{g,2} - \sin\theta_g\right|\right)^{1/2}$$

$$F_{g,1}\left(\theta_{g,1}\right) = \left[\left(1 + r_t^2\right)^2 - 4\xi_t^2 - 4\eta_t\left(1 + r_t^2\right)\sin\theta_{g,1} + 4r_t^2\sin^2\theta_{g,1}\right] \prod_{\substack{g=1\\ g\neq g_1}}^{m} \left(\left|\sin\theta_{g,1} - \sin\theta_g\right|\right)^{1/2}$$

and ϵ (radians) is a small positive number. Depending on the width of the panel and the number of points in the integration routine, ϵ may be taken to be of the order of 0.0001 to 0.01.

Once the constants a_j and b_j have been obtained, the complex velocity $dw/d\zeta$ can be calculated at any point ζ in the ζ-plane by use of equation (D15), where $\cos(2n + 1)\sigma$, $\sin 2n\sigma$, and $\sin \sigma$ are replaced by their expressions in terms of ζ $(= e^{i\sigma})$. The complex velocity at the corresponding point in the z-plane is then $\frac{dw}{d\zeta}\frac{d\zeta}{dz}$. For this investigation, the point of greatest interest in the z-plane is $z = 0$ and the corresponding point in the ζ-plane is $\zeta = 0$. At this point equation (D15) simplifies by letting ζ approach 0 to

$$\left.\frac{dw}{d\zeta}\right]_{\zeta=0} = \frac{\pm i 2^{\frac{m}{2}-1}\left(a_{\frac{m}{2}+1} + b_{\frac{m}{2}+1}\right)}{r_t^2} \tag{D21}$$

where one of the constants is zero, depending on the value of m. The ambiguity in sign, which corresponds to the ambiguity in sign of the constants, can be settled by noting that for a lifting wing the velocity produced by the vortices at the center of the span is downward (that is, negative) at this point. It is also negative, and purely imaginary, at other points on the Y-axis, where the Y-axis bisects and is normal to the span (displaced to the Trefftz plane), so that for a lifting wing $\rho\left.\frac{dw}{d\zeta}\right]_{\zeta=0}$ is positive.

At $z = \zeta = 0$, $\frac{d\zeta}{dz} = \frac{\lambda}{2}$; thus, the velocity in the z-plane at this point is $-\rho\frac{\lambda}{2}\left.\frac{dw}{d\zeta}\right]_{\zeta=0}$. This velocity is the total velocity due to the vortices in the presence of the slotted walls. The interference velocity at $z = 0$ in the plane of the wing is half the difference between this velocity and that at $z = 0$ in the Trefftz plane due to the vortices in the infinite free field. Thus, the interference velocity is

$$\left.v\right]_{\substack{z=0\\ \Gamma=1}} = \frac{1}{2}\left[-\frac{\lambda}{2}\rho\left.\frac{dw}{d\zeta}\right]_{\zeta=0} + \frac{x_t}{\pi\left(x_t^2 + y_t^2\right)}\right]$$

where the circulation Γ is taken positive for a lifting wing. For $\Gamma \neq 1$, it is only necessary to multiply the right-hand side of this equation by Γ, the negative sign being included if the wing is producing negative lift. Then

$$\left.v\right]_{z=0} = \frac{\Gamma}{2}\left[\frac{x_t}{\pi\left(x_t^2 + y_t^2\right)} - \frac{\lambda}{2}\left|\rho\frac{dw}{d\zeta}\right|_{\zeta=0}\right] \tag{D22}$$

and since

$$C_L S = \frac{4\Gamma x_t}{V}$$

it follows from equation (1) that

$$\delta_w\Big]_{z=0} = \frac{hb}{8x_t}\left[\frac{x_t}{\pi\left(x_t^2 + y_t^2\right)} - \frac{\lambda}{2}\left|\frac{dw}{d\zeta}\right|_{\zeta=0}\right] \tag{D23}$$

where for this appendix $b = 1$. Because it is total induced velocities that are computed and the interference velocity v is the difference between two such total induced velocities the computations must be carried out with second-order accuracy, that is, with such accuracy that the differences are significant.

REFERENCES

1. Wright, Ray H.; Ritchie, Virgil S.; and Pearson, Albin O.: Characteristics of the Langley 8-Foot Transonic Tunnel With Slotted Test Section. NACA Rep. 1389, 1958. (Supersedes NACA RM L51H10 by Wright and Ritchie and RM L51K14 by Ritchie and Pearson.)

2. Heyson, Harry H.: Jet-Boundary Corrections for Lifting Rotors Centered in Rectangular Wind Tunnels. NASA TR R-71, 1960.

3. Heyson, Harry H.: Linearized Theory of Wind-Tunnel Jet-Boundary Corrections and Ground Effect for VTOL-STOL Aircraft. NASA TR R-124, 1962.

4. Heyson, Harry H.; and Grunwald, Kalman J.: Wind-Tunnel Boundary Interference for V/STOL Testing. Conference on V/STOL and STOL Aircraft, NASA SP-116, 1966, pp. 409-434.

5. Cook, Woodrow L.; and Hickey, David H.: Comparison of Wind-Tunnel and Flight-Test Aerodynamic Data in the Transition-Flight Speed Range for Five V/STOL Aircraft. Conference on V/STOL and STOL Aircraft, NASA SP-116, 1966, pp. 447-467.

6. Anscombe, A.; and Williams, J.: Some Comments on High-Lift Testing in Wind Tunnels With Particular Reference to Jet-Blowing Models. Rep. 63, AGARD, North Atlantic Treaty Organization (Paris), Aug. 1956.

7. Rae, William H., Jr.: An Experimental Investigation of the Effect of Test Section Geometry on the Maximum Size Rotor That Can Be Tested in a Closed Throat Wind Tunnel. Paper No. 66-736, Am. Inst. Aeron. Astronaut., Sept. 1966.

8. Theodorsen, Theodore: The Theory of Wind-Tunnel Wall Interference. NACA Rep. 410, 1931.

9. Davis, Don D., Jr.; and Moore, Dewey: Analytical Study of Blockage- and Lift-Interference Corrections for Slotted Tunnels Obtained by the Substitution of an Equivalent Homogeneous Boundary for the Discrete Slots. NACA RM L53E07b, 1953.

10. Coleman, Robert P.; Feingold, Arnold M.; and Stempin, Carl W.: Evaluation of the Induced-Velocity Field of an Idealized Helicopter Rotor. NACA WR L-126, 1945. (Formerly NACA ARR L5E10.)

11. Castles, Walter, Jr.; and De Leeuw, Jacob Henri: The Normal Component of the Induced Velocity in the Vicinity of a Lifting Rotor and Some Examples of Its Application. NACA Rep. 1184, 1954. (Supersedes NACA TN 2912.)

12. Heyson, Harry H.: Wind-Tunnel Wall Effects at Extreme Force Coefficients. Paper presented at International Congress of Subsonic Aeronautics (New York), Apr. 1967.

13. Matthews, Clarence W.: Theoretical Study of the Tunnel-Boundary Lift Interference Due to Slotted Walls in the Presence of the Trailing-Vortex System of a Lifting Model. NACA Rep. 1221, 1955. (Supersedes NACA RM L53A26.)

14. Glauert, H.: Wind-Tunnel Interference on Wings, Bodies and Airscrews. R. & M. No. 1566, British A.R.C., 1933.

15. Staff of the Bateman Manuscript Project, compiler: Tables of Integral Transforms. Vol. I. McGraw-Hill Book Co., Inc., 1954.

16. Lamb, Horace: Hydrodynamics. Sixth ed., Dover Pub., 1945.

17. Whittaker, E. T.; and Watson, G. N.: A Course of Modern Analysis. Cambridge Univ. Press, 1962.